

**PREPARATION AND CHARACTERIZATION OF ALIPHATIC
CYCLOPOLYMER-DERIVED MEMBRANES FOR WATER TREATMENT**

by

NIHAN BİRGÜN

Submitted to the Graduate School of Engineering and Natural Sciences

in partial fulfillment of the requirements for the degree of

Master of Science

SABANCI UNIVERSITY

December 2022

Nihan BİRGÜN 2022©

All Rights Reserved

ABSTRACT

PREPARATION AND CHARACTERIZATION OF ALIPHATIC CYCLOPOLYMER- DERIVED MEMBRANES FOR WATER TREATMENT

NIHAN BİRGÜN

Materials Science and Nano Engineering MSc. Thesis, December 2022

Thesis Advisor: Assist. Prof. Dr. Serkan Ünal

Thesis co-Advisor: Dr. Selda Erkoç İter

Keywords: Reverse osmosis, nanofiltration, cellulose acetate, aliphatic cyclopolymer membranes, acid cyclopolymer thin film composite membranes

The need for clean water is increasing all over the world due to the growth of the population, agricultural activities, and industrial applications. Reverse osmosis (RO) water treatment membrane technology is an emerging technology as it is the most cost-effective way to reach clean water (Yang et al., 2019). Cellulose acetate (CA) and polyamide thin film composite (PA-TFC) membranes are the most common, commercially available RO membranes. CA is an ideal bio-based membrane material with its excellent film-forming ability, cost-effectiveness, biodegradability, and renewability. Compared to aromatic PA-TFC membranes, the main advantages of CA-based RO membranes are ease of manufacture and chlorine resistance. However, flux, fouling resistance, and mechanical strength need to be improved in CA membranes. On the other hand, PA-TFC membranes have excellent separation performance, yet they need improvements in chlorine and fouling resistance. At this point, the development of innovative membrane materials and technologies to obtain potable water is critically important. In this study, *tert*-butyl *alpha*-(hydroxymethyl) acrylate (TBHMA) ether dimer cyclopolymer and its carboxylic acid

functional derivative were synthesized, and for the first time, used as membrane materials for water treatment applications.

Cyclopolymer membranes were produced in two different ways. Firstly, CA/*tert*-butyl cyclopolymer (TBCP) composite membranes were produced by the non-solvent induced phase separation (NIPS) process. For this purpose, TBCP polymers with different molecular weights were synthesized. The effects of TBCP content relative to CA, the molecular weight of TBCP, and the viscosity of the casting solution on the performance of produced membranes were investigated. Secondly, acid cyclopolymer thin film composite (CP-TFC) membranes were produced. CP-TFC membranes were prepared by solution coating of acid cyclopolymers on a polysulfone support layer. Carboxylic acid functional cyclopolymers (ACP) were obtained by the acid hydrolysis of *tert*-butyl ester groups of TBCP and used as membrane materials. The membranes were fabricated from ACPs based on the metal ion crosslinking properties of carboxylic acid groups. Characterization of synthesized cyclopolymers was performed using nuclear magnetic resonance (NMR) spectroscopy, Fourier-transform infrared spectroscopy (FT-IR), thermal gravimetric analysis (TGA), and differential scanning calorimetry (DSC). For the analysis of surface properties and morphology of produced membranes, scanning electron microscope (SEM), water contact angle (WCA), and energy dispersive x-ray spectroscopy (EDS) were used. Flux and salt rejection analyses of produced membranes by both approaches were performed at both RO and nanofiltration levels in a high-pressure membrane filtration system.

Performance analyses showed that the novel CA/TBCP composite membranes present better flux performance compared to CA membranes and can be used as RO and nanofiltration membranes. On the other hand, it was demonstrated that the iron (Fe) ion cross-linked membrane can be used for nanofiltration applications in ionically cross-linked carboxylic acid cyclopolymer TFC membranes.

ÖZET

SU ARITMA İÇİN ALİFATİK SİKLOPOLİMER TÜREVLİ MEMBRANLARIN HAZIRLANMASI VE KARAKTERİZASYONU

Nihan Birgün

Malzeme Bilimi ve Nano Mühendisliği, Yüksek Lisans Tezi, Aralık 2022

Tez Danışmanı: Dr. Öğr. Üyesi Serkan Ünal

Tez Eş-danışmanı: Dr. Selda Erkoç İltter

Anahtar kelimeler: ters osmoz, nanofiltrasyon, selüloz asetat, alifatik siklopolimer membranlar, asit siklopolimer ince film kompozit membranlar

Nüfusun artışı, tarımsal faaliyetler ve endüstriyel uygulamalar nedeniyle temiz suya olan ihtiyaç tüm dünyada artmaktadır. Ters osmoz (RO) su arıtma membran teknolojisi, temiz suya ulaşmanın en uygun maliyetli yolu olduğu için gelişmekte olan bir teknolojidir [1]. Selüloz asetat (CA) ve poliamid ince film kompozit (PA-TFC) membranlar, piyasada bulunan en yaygın RO membranlarıdır. CA, mükemmel film oluşturma yeteneği, maliyet etkinliği, biyolojik olarak parçalanabilirliği ve yenilenebilirliği ile ideal bir biyo-bazlı membran malzemesidir. Aromatik PA-TFC membranlara kıyasla CA bazlı RO membranların başlıca avantajları, üretim kolaylığı ve klor direncidir. Bununla birlikte, CA membranlarında akı, kirlenme direnci ve mekanik mukavemetin iyileştirilmesi gerekmektedir. PA-TFC membranları mükemmel ayrıştırma performansına sahiptir, ancak klor ve kirlenme direncinin iyileştirilmesi gerekmektedir. Bu noktada, içme suyu elde etmek için yenilikçi membran malzemeleri ve teknolojilerinin geliştirilmesi kritik öneme sahiptir. Bu çalışmada, *tert*-bütil alfa-(hidroksimetil) akrilat (TBHMA) eter dimer

siklopolimeri ve karboksilik asit fonksiyonel türevi sentezlenmiş ve ilk kez su arıtma uygulamalarında membran malzemesi olarak kullanılmıştır.

Siklopolimer membranlar iki farklı şekilde üretilmiştir. İlk olarak, CA/*tert*-bütil siklopolimer (TBCP) kompozit membranlar, solventsiz faz ayırma (NIPS) prosesi ile üretilmiştir. Bu amaçla farklı moleküler ağırlıklara sahip TBCP polimerleri sentezlenmiştir. CA membranlara TBCP ilavesinin etkileri, TBCP'nin moleküler ağırlığı ve döküm solüsyonunun viskozitesinin üretilen membranların performansı üzerindeki etkileri araştırılmıştır. İkinci olarak siklopolimer ince film kompozit (CP-TFC) membranlar üretilmiştir. CP-TFC membranları, bir polisülfon destek tabakası üzerine siklopolimerlerin solüsyon kaplamasıyla hazırlanmıştır. TBCP'nin *tert*-bütil ester gruplarının asit hidrolizi ile karboksilik asit fonksiyonel siklopolimerleri (ACP) elde edilmiş ve membran malzemesi olarak kullanılmıştır. Membranlar, karboksilik asit gruplarının metal iyonu çapraz bağlama özelliklerine dayalı olarak ACP'den üretilmiştir. Sentezlenen siklopolimerlerin karakterizasyonu, nükleer manyetik rezonans (NMR) spektroskopisi, fourier dönüşümü kızılötesi spektroskopisi (FT-IR), termal gravimetrik analiz (TGA) ve diferansiyel tarama kalorimetrisi (DSC) kullanılarak yapılmıştır. Üretilen membranların yüzey özelliklerinin ve morfolojilerinin analizi için taramalı elektron mikroskobu (SEM), su temas açısı ölçeri (WCA), enerji dağılımlı x-ışını spektroskopisi (EDS) kullanılmıştır. Her iki yaklaşımla üretilen membranların akı ve tuz reddi analizleri, yüksek basınçlı membran filtrasyon sisteminde hem RO hem de nanofiltrasyon (NF) uygulamaları için gerçekleştirilmiştir.

Performans analizleri, yeni CA/TBCP kompozit membranların, CA membranlara kıyasla daha iyi akı performansı sunduğunu, RO ve nanofiltrasyon membranı olarak kullanılabileceğini göstermiştir. Öte yandan demir (Fe) metal iyonu çapraz bağlı membranın iyonik çapraz bağlı CP-TFC membranlarda, nanofiltrasyon uygulamaları için kullanılabileceği görülmüştür.

ACKNOWLEDGEMENTS

I would like to express my sincere gratitude and appreciation to my thesis advisors Asst. Prof. Dr. Serkan Ünal and Dr. Selda Erkoç İlder for their guidance, encouraging and reassuring support. Their advice has always been invaluable to me, and they have enlightened me with their knowledge and led me throughout my master's thesis. Thanks to Asst. Prof. Dr. Serkan Ünal's experience and academic background, I am sure that I will benefit from the knowledge I have gained from him during my academic career and life. I would like to especially thank Dr. Selda Erkoç İlder, who made this process easier for me with her contributions and supported me with endless understanding and patience in every sense.

Also, I would like to present my appreciation to my jury members, Assoc. Prof. Dr. Bekir Dızman and Assoc. Prof. Dr. Derya Yüksel İmer, for dedicating their time and providing constructive comments for this thesis.

I would like to thank my dear friends Asu Ece Ateşpare, Taha Behroozi Kohlan, and Saeed Salamat Gharamaleki for their encouraging support and help. I was very lucky to have them at my side. My colleagues and friends at Sabancı University Integrated Manufacturing Research and Application Center, Kuray Dericiler, Sina Khalilvandi Behrouzgar, and materials characterization laboratory members also deserve special thanks for their help. I would like to thank the current fellow members of Dr. Ünal's Research Group, especially Dr. Serkan Güçlü, and Ayşe Durmuş Sayar.

Endless thanks to my dear parents, Zöhre and Faruk Birgün, for their unconditional support and trust, my dear brother Osman Birgün, who always guided and supported me my sister-in-law Deniz Birgün and my little nephew Doruk Birgün for motivating me in any condition.

I would like to thank my close friends Simge Benay Köroğlu, Umut Yılmaz, Serdar Bulat, Cihad Taşçı, and Murat Gögen, who have always been by my side, supporting me under all circumstances and making my life enjoyable.

This project was financially supported by The Scientific and Technological Research Council of Turkey (TÜBİTAK) with project number 118Y466.

Dedicated to my beloved family,

TABLE OF CONTENT

ABSTRACT	iv
ÖZET	vi
ACKNOWLEDGEMENTS	viii
LIST OF FIGURES	xiv
LIST OF TABLES	xvii
CHAPTER 1	1
1. INTRODUCTION.....	1
1.1. Motivation.....	1
1.2. Objectives	2
1.3. Outline	2
CHAPTER 2.....	4
2. LITERATURE REVIEW.....	4
2.1. Water Demand and Importance of Freshwater	4
2.2. Water Treatment Membrane Technology	5
2.2.1. Water treatment membrane history	6
2.2.2. Membrane processes	8
2.3. Desalination For Clean Water Production	10
2.4. Reverse Osmosis.....	11
2.5. Commercial Reverse Osmosis Desalination Membranes	12
2.6. Cellulose Acetate Membranes	14
2.7. Cellulose Acetate /Polymer Composite Membranes	17
2.8. Alkyl Alpha-Hydroxymethyl Acrylate (RHMA) Ether Dimer Cyclopolymers as a Potential Membrane Material	18
2.9. Acid Functional Cyclopolymers as a Potential Membrane Material	20
2.10. Acid Functional Polymer Membranes.....	20
2.11. Ionically Crosslinked Membranes.....	21

CHAPTER 3	23
3. CELLULOSE ACETATE / CYCLOPOLYMER COMPOSITE MEMBRANES	23
3.1. Materials and Methods.....	23
3.1.1. Materials.....	23
3.1.2. Experimental	23
3.1.2.1. Synthesis of <i>tert</i> -butyl alpha-hydroxymethyl acrylate (TBHMA) ether dimer monomer	23
3.1.2.2. Synthesis of <i>tert</i> -butyl alpha-hydroxymethyl acrylate (TBHMA) ether cyclopolymers.....	24
3.1.2.3. Fabrication of asymmetric cellulose acetate membranes	25
3.1.2.4. Fabrication of cellulose acetate/cyclopolymer blend composite membranes	26
3.1.3. Characterization	32
3.1.3.1. Nuclear magnetic resonance (NMR) spectroscopy analysis	32
3.1.3.2. Fourier transform infrared (FTIR) spectroscopy analysis	32
3.1.3.3. Differential scanning calorimeter (DSC) analysis.....	32
3.1.3.4. Gel permeation chromatography (GPC) analysis.....	32
3.1.3.5. Scanning electron microscopy (SEM) analysis	33
3.1.3.6. Water contact angle (WCA) analysis	33
3.1.3.7. Thermal gravimetric analysis (TGA)	33
3.1.3.8. Viscosity analysis	33
3.1.4. Membrane Filtration Performance	34
3.1.4.1. Dead-end filtration system	34
3.1.4.2. Desalination performance.....	35
3.1.4.3. Calibration curves of conductivity against NaCl or MgSO ₄ concentrations	35
3.2. Results and Discussion	37
3.2.1. Synthesis of monomer.....	37

3.2.2. Synthesis of <i>tert</i> -butyl cyclopolymer (TBCP)	39
3.2.3. Structural comparison of cellulose acetate and <i>tert</i> -butyl cyclopolymer.....	43
3.2.4. Preparation of cellulose acetate/cyclopolymer composite membranes.....	44
3.2.5. Characterization	44
3.2.6. Desalination performance	52
3.2.6.1. Casting solution viscosity effect on desalination performance	64
3.2.6.2. TBCP molecular weight effect on desalination performance.....	65
3.2.6.3. Stability analysis of the composite membranes.....	66
3.3. Conclusions.....	67
CHAPTER 4.....	69
4. IONICALLY CROSSLINKED CARBOXYLIC ACID FUNCTIONAL CYCLOPOLYMER MEMBRANES	69
4.1. Materials and Methods.....	69
4.1.1. Materials.....	69
4.2. Experimental.....	70
4.2.1.1. Synthesis of carboxylic acid functional cyclopolymers	70
4.2.1.2. Degree of carboxylic acid groups by titration	70
4.2.1.3. Fabrication of ionically crosslinked carboxylic acid cyclopolymer membranes.....	71
4.2.2. Characterization	75
4.2.2.1. Energy Dispersive X-ray Analysis (EDS)	76
4.2.3. Membrane Filtration Performance	76
4.2.3.1. Desalination performance.....	76
4.3. Results and Discussion	76
4.3.1. Synthesis of carboxylic acid functional cyclopolymers.....	76
4.3.2. Preparation of metal ion crosslinked acid cyclopolymer membranes.....	81
4.3.3. Characterization	82
4.3.4. Filtration performance.....	87

4.3.4.1. Desalination	87
4.3.4.2. Stability analysis of the membranes	93
4.4. Conclusions.....	94
REFERENCES	96

LIST OF FIGURES

Figure 1.1 Schematic representing the objectives of this thesis	2
Figure 2.1 Distribution of water resources over the world (<i>Salt Water and Freshwater Distribution on Earth</i> , n.d.).	4
Figure 2.2 Global water demand according to different sectors for 2014 and expectations for 2025 and 2040 years (UNESCO, 2019).....	5
Figure 2.3 Pressure-driven water treatment membrane processes according to their pore size, trans-membrane pressures, and rejected species(Selatile et al., 2018).....	9
Figure 2.4 Desalination capacity and the number of desalination plants over years(Esmaeilion, 2020).	10
Figure 2.5 The contributions of desalination methods all over the world (Esmaeilion, 2020).....	11
Figure 2.6 Representation of reverse osmosis principle (Tomczak & Gryta, 2022).	12
Figure 2.7 Schematic representation of cellulose acetate reverse osmosis membrane structure and chemical structure (Liu et al., 2019).....	13
Figure 2.8 Schematic representation of TFC-PA reverse osmosis membrane structure (Zhao et al., 2021).....	14
Figure 2.9 Cellulose acetate synthesis from natural cellulose.....	15
Figure 2.10 Polymerization mechanisms of alkyl alpha-hydroxymethyl acrylate (RHMA) ether dimers (Erkoc et al., 2006).	18
Figure 2.11 Chemical and structural comparison of CA and TBCP	19
Figure 2.12 Acid hydrolysis of <i>tert</i> -butyl cyclopolymer	20
Figure 2.13 Ionic crosslinking of a polymer containing carboxyl groups (Hunger et al., 2012).....	21
Figure 3.1 The chemical structure of TBHMA ether dimer.....	24
Figure 3.2 Representation of NIPS membrane formation	27
Figure 3.3 Representation of dead-end filtration system.....	34
Figure 3.4 Calibration curve of conductivity against NaCl concentration in aqueous solution.	36
Figure 3.5 Calibration curve of conductivity against MgSO ₄ concentration in aqueous solution.	36
Figure 3.6 Synthesis of <i>tert</i> -butyl alpha-hydroxymethyl acrylate (TBHMA) ether dimer .	37
Figure 3.7 ¹ H NMR spectrum of TBHMA ether dimer (500 MHz, CDCl ₃).....	38

Figure 3.8 ¹³ C NMR spectrum of TBHMA ether dimer (500 MHz, CDCl ₃).....	38
Figure 3.9 FTIR spectrum of TBHMA ether dimer.	39
Figure 3.10 Synthesis of <i>tert</i> -butyl cyclopolymer (TBCP).	40
Figure 3.11 FTIR spectrum of <i>tert</i> -butyl cyclopolymer (TBCP)	40
Figure 3.12 ¹³ C NMR spectrum of TB monomer and TBCP (500 MHz, CDCl ₃).....	42
Figure 3.13 GPC plots of synthesized TB cyclopolymer.....	43
Figure 3.14 TGA results of CA, CTA, TBCP 33K, and TBCP 49K.....	45
Figure 3.15 DSC thermograms. (a), CA; (b), CTA; (c), TBCP 49K; (d), TBCP 33K.....	46
Figure 3.16 Viscosity analysis results of membrane casting solutions. (a) effect of membrane casting solution concentration on viscosity; (b) effect of different molecular weights of TBCP on casting solution viscosity	50
Figure 3.17 Water contact angle results of CA/TBCP composite membranes	51
Figure 3.18 20% (CA+TBCP 49K) membranes NaCl filtration results.....	53
Figure 3.19 25% (CA+TBCP 49K) membranes NaCl filtration results.....	55
Figure 3.20 25% (CA+TBCP 33K) membranes NaCl filtration results.....	56
Figure 3.21 25% (CA+TBCP 65K) membranes NaCl filtration results.....	57
Figure 3.22 20% (CA+TBCP 49K) membranes MgSO ₄ filtration results	59
Figure 3.23 25% (CA+TBCP 49K) membranes MgSO ₄ filtration results	61
Figure 3.24 25 % (CA+TBCP 33K) membranes MgSO ₄ filtration results	62
Figure 3.25 25 % (CA+TBCP 65K) membranes MgSO ₄ filtration results	64
Figure 3.26 Desalination performance comparison of 20% and 25% CA+TBCP 49K (a) 20% CA+TBCP 49K NaCl filtration performance, (b) 25% CA+TBCP 49K NaCl filtration performance, (c) 20% CA+TBCP 49K membranes MgSO ₄ filtration performance, (d) 25 % CA+TBCP 49K membranes MgSO ₄ filtration performance	65
Figure 3.27 Performance comparison of 2000 ppm NaCl filtration 17% CA+ 8% TBCP 33K, 49K, and 65K membrane	66
Figure 3.28 Stability analysis of the CA/TBCP blend composite membranes (15 bar 2000 ppm MgSO ₄ water solution filtration).....	66
Figure 4.1 Acid hydrolysis of <i>tert</i> -butyl cyclopolymer.....	70
Figure 4.2 Synthesis of carboxylic acid cyclopolymer.....	70
Figure 4.3 Schematic diagram of the metal ion coordination crosslinking reaction in carboxylic acid cyclopolymer membrane.....	71
Figure 4.4 Schematic representation of wet technique for the production of ionically crosslinked ACP membranes.....	72

Figure 4.5 Schematic representation of dry technique for the production of ionically crosslinked ACP membranes.....	74
Figure 4.6 Synthesis of carboxylic acid cyclopolymer.....	76
Figure 4.7 Graph of the degree of hydrolysis over time (TFA/ester molar ratio: 5, polymer concentration: 12%, solvent: DCM).....	77
Figure 4.8 ¹³ C NMR spectrum for ACP	78
Figure 4.9 ¹³ C NMR of TBCP.....	78
Figure 4.10 TGA results of ACP and TBCP 49K	79
Figure 4.11 TGA thermogram comparison of carboxylic acid cyclopolymers having different hydrolysis degrees	80
Figure 4.12 FTIR spectrum of TBCP and ACP	81
Figure 4.13 FTIR spectrum of the ionically crosslinked ACP membranes.....	82
Figure 4.14 TGA thermogram of ionically crosslinked ACP membranes	83
Figure 4.15 SEM images of the surface of ionically crosslinked ACP membranes and PSF UF membrane	85
Figure 4.16 Cross-sectional SEM images of the ionically crosslinked ACP membranes and PSF UF membrane	85
Figure 4.17 EDS analysis results of the ionically crosslinked ACP membranes. (a) Fe(dry); (b) Fe (wet); (c) Zn (dry); (d) Al (dry).	86
Figure 4.18 Dry technique metal ion crosslinked ACP membranes 2000 ppm of NaCl aqueous solution filtration performance results.....	88
Figure 4.19 Wet technique metal ion crosslinked ACP membrane 2000 ppm of NaCl aqueous solution filtration performance result comparison with Fe (dry) technique membranes.....	90
Figure 4.20 Dry technique metal ion crosslinked ACP membranes 2000 ppm of MgSO ₄ aqueous solution filtration performance results.....	92
Figure 4.21 Wet technique metal ion crosslinked ACP membrane 2000 ppm of MgSO ₄ aqueous solution filtration performance result comparison with Fe (dry) technique membranes.....	93
Figure 4.22 2000 ppm NaCl solution filtration tests for stability analysis. (a) Fe (dry); (b) Al (dry); (c) Zn (dry); (d) Ca (dry); (e) Co (dry); (f) Fe (wet).	94

LIST OF TABLES

Table 2.1 Historical milestones of the membrane technology (Wang, Lawrence K.; Chen, Jiaping Paul; Hung, Yung-Tse; Shammas, 2011).	7
Table 3.1 Cellulose acetate/cellulose triacetate membrane casting solution composition and membrane preparation parameters.....	25
Table 3.2 Cellulose acetate/ <i>tert</i> -butyl cyclopolymer (20% CA+TBCP 100:1) composite membrane casting solution composition and membrane preparation parameters.....	28
Table 3.3 Cellulose acetate/ <i>tert</i> -butyl cyclopolymer (25% CA+TBCP 100:1) composite membrane casting solution composition and membrane preparation parameters.....	29
Table 3.4 Cellulose acetate/ <i>tert</i> -butyl cyclopolymer (25%CA+TBCP 50:1) composite membrane casting solution composition and membrane preparation parameters.....	30
Table 3.5 Cellulose acetate/ <i>tert</i> -butyl cyclopolymer (25%CA+TBCP 200:1) composite membrane casting solution composition and membrane preparation parameters.....	31
Table 3.6 Technical properties of filtration system.....	34
Table 3.7 Synthesis of TBCP with different [Monomer]: [AIBN] ratios, conversion (%), and theoretical molecular weight.....	41
Table 3.8 GPC analysis results of synthesized TB cyclopolymer	43
Table 3.9 Structural comparison of cellulose acetate and <i>tert</i> -butyl cyclopolymer	44
Table 3.10 TGA results of CA, CTA, TBCP 33K, and TBCP 49K.....	45
Table 3.11 DSC results of CA, CTA, TBCP 59K, and TBCP 33K	47
Table 3.12 SEM images of produced CA/TBCP composite membranes.....	48
Table 3.13 Viscosity analysis results of membrane casting solutions.....	50
Table 3.14 Water contact angle values and drop shapes of CA/TBCP composite membranes.....	51
Table 3.15 20% (CA+TBCP 49K) membranes NaCl filtration results.....	52
Table 3.16 25% (CA+TBCP 49K) membranes NaCl filtration results.....	54
Table 3.17 25% (CA+TBCP 33K) membranes NaCl filtration results.....	55
Table 3.18 25% (CA+TBCP 65K) membranes NaCl filtration results.....	57
Table 3.19 20% (CA+TBCP 49K) membranes MgSO ₄ filtration results.....	58
Table 3.20 25 % (CA+TBCP 49K) membranes MgSO ₄ filtration results.....	60
Table 3.21 25% (CA+TBCP 33K) membranes MgSO ₄ filtration results.....	61
Table 3.22 25% (CA+TBCP 65K) membranes MgSO ₄ filtration results.....	63
Table 4.1 Technical properties of UF PSF membrane.	72

Table 4.2 The composition of the casting solutions prepared in the production of metal ion cross-linked ACP membranes by wet technique and the parameters in membrane production.....	73
Table 4.3 Metal salts used for crosslinking and their molecular weights.....	74
Table 4.4 The composition of the casting solutions prepared in the production of metal ion cross-linked ACP membranes by dry technique and the parameters in membrane production.....	75
Table 4.5 TGA results of ACP and TBCP 49K.....	79
Table 4.6 The composition of the casting solutions and preparation conditions of produced metal ion cross-linked ACP membranes by wet technique and resulting membrane properties	81
Table 4.7 TGA analysis results of ionically crosslinked ACP membranes.....	83
Table 4.8 EDS analysis results as atomic percentages of the elements.....	86
Table 4.9 Dry technique metal ion crosslinked ACP membranes 2000 ppm of NaCl aqueous solution filtration performance results.....	87
Table 4.10 Wet technique metal ion crosslinked ACP membrane 2000 ppm of NaCl aqueous solution filtration performance result	89
Table 4.11 Dry technique metal ion crosslinked ACP membranes 2000 ppm of MgSO ₄ aqueous solution filtration performance results.....	90
Table 4.12 Wet technique metal ion crosslinked ACP membrane 2000 ppm of MgSO ₄ aqueous solution filtration performance result	92

CHAPTER 1

1. INTRODUCTION

1.1. Motivation

The requirement for clean water is increasing all over the world due to the growth of the population, agricultural activities, and industrial applications. It is known that only about 1% of the world's water reserves are usable, and 97% of them consists of saline waters. Therefore, the most effective way to obtain drinking and utility water for human and animal consumption, irrigation, and other industrial uses is desalination, the process of removing dissolved salt and other minerals from saline waters. Desalination with reverse osmosis membrane process is the most dominant technology up to date. Commercially available reverse osmosis membranes are integrally skinned asymmetric cellulose acetate (CA) and polyamide thin film composite (PA-TFC) membranes. While asymmetric CA membranes have low flux, fouling resistance, and mechanical stability, aromatic PA-TFC membranes have low fouling and chlorine resistance. Despite high salt retention, lowering the cost of energy with high flux performance at low pressure is an issue to be developed in the PA-TFC membrane type. All these problems made it necessary to make innovations in the relevant technical field. At this point, the aliphatic cyclopolymers derived from alkyl *alpha*-(hydroxymethyl) acrylate (RHMA) ether dimers are thought to be a potential membrane material because of their structural similarity to cellulose acetate. They have excellent thermal stability, high glass transition temperatures, and low shrinkage. In addition, they can be functionalized and used in chemical or ionic crosslinking reactions to increase membrane stability.

1.2. Objectives

This thesis introduces the use of aliphatic cyclopolymers in the production of water treatment membranes for the first time. Two different types of membranes were produced within the scope of this thesis: CA/TBCP composite membranes and ionically crosslinked carboxylic acid cyclopolymer thin film composite membranes as can be shown in Figure 1.1. The synthesis and characterization of *tert*-butyl cyclopolymers were conducted and innovative cellulose acetate/*tert*-butyl cyclopolymer composite membranes were produced by the phase inversion method. For the ionically crosslinked cyclopolymer membranes, carboxylic acid functional cyclopolymers were synthesized by acid hydrolysis of *tert*-butyl cyclopolymers. After that, novel ionically crosslinked cyclopolymer thin film composite membranes were produced by solution coating on a polysulfone support layer. The performance of produced cyclopolymer membranes was tested for reverse osmosis and nanofiltration membrane applications.

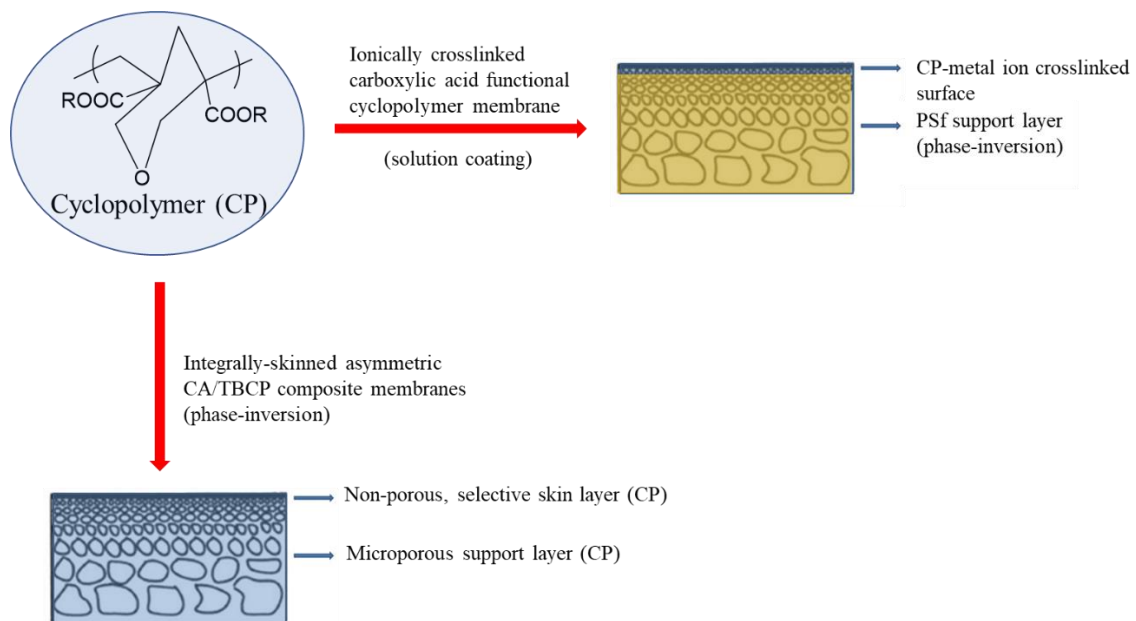


Figure 1.1 Schematic representing the objectives of this thesis

1.3. Outline

This master thesis consists of four chapters. The first chapter explains the motivation and the objective of this thesis with a thesis defense structure. The second chapter provides a literature review of reverse osmosis membrane technology, cellulose acetate (CA)

membranes, *tert*-butyl cyclopolymers and acid functional cyclopolymers as potential membrane material, and ionically crosslinked membranes.

Chapter three covers cellulose acetate/*tert*-butyl cyclopolymer composite membranes with the experimental procedure. Synthesis of *tert*-butyl cyclopolymers (TBCP), fabrication of CA/TBCP composite membranes, structural and morphological characterization, and performance results of produced composite membranes has been discussed in this chapter.

Chapter four focuses on the ionically crosslinked carboxylic acid functional cyclopolymer membranes with the experimental procedure. Synthesis of carboxylic acid functional cyclopolymers (ACP), fabrication of ionically crosslinked ACP membranes, structural and morphological characterization, and performance results of produced membranes have been told in this chapter.

CHAPTER 2

2. LITERATURE REVIEW

2.1. Water Demand and Importance of Freshwater

Water covers approximately 70% of the world's surface area. However, 97.5% of this water is salt water and the remaining 2.5% is freshwater. Around 79% of freshwater is existing as frozen in the glaciers, around 20% of the freshwater is existing as groundwater and 1% is existing in other sources. Figure 2.1 shows the distribution of water resources over the world (El-Dessouky & Ettouney, 2002; *Salt Water and Freshwater Distribution on Earth*, n.d.).

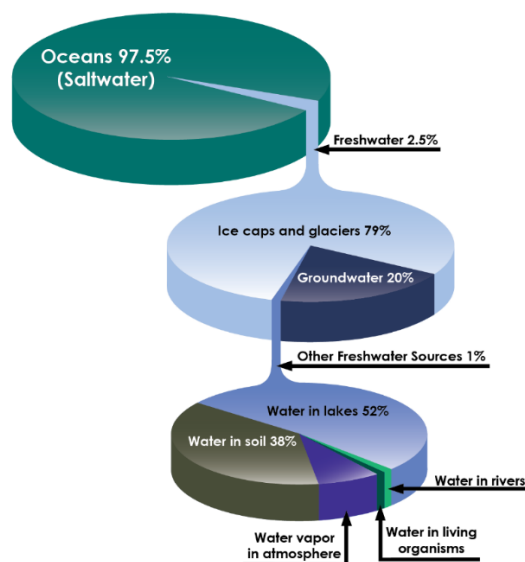


Figure 2.1 Distribution of water resources over the world (*Salt Water and Freshwater Distribution on Earth*, n.d.).

The requirement for clean water is increasing all over the world due to the growth of the population, agricultural activities, and industrial applications. In The United Nations World Water Development Report (2019) they reported that from the 1980s until today water use has increased by 1% per year. And this increment in water consumption is supposed to continue until the 2050s (UNESCO, 2019). One of the activities that consume water resources the most is agricultural irrigation, which constitutes approximately 70% of the total consumption. It is then most required during the cooling process, which is required for water, electricity generation, and steam-based electricity consumption (Koyuncu, 2018). Another thing is that since the world is facing climate change that is causing natural water resources to decrease, the solution for water recovery is increasing demand. Therefore, water re-use, recovery of dirty water, and desalination are promising solutions to this problem (Lee et al., 2011). Figure 2.2 shows the global water demand according to different sectors for 2014 and the amount of water demand expectations for 2025 and 2040 years.

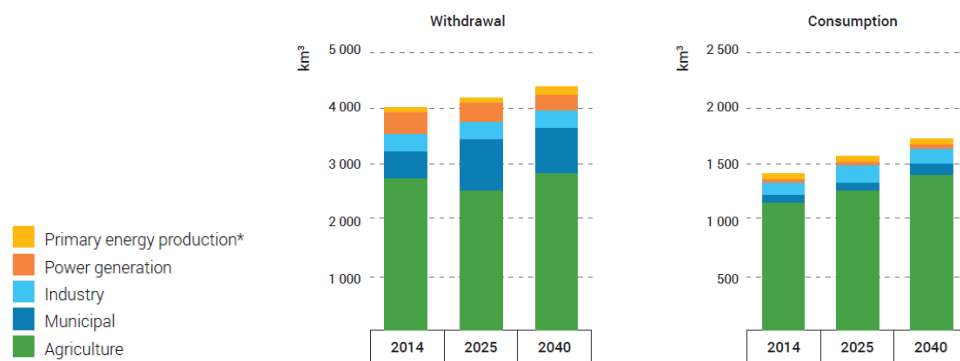


Figure 2.2 Global water demand according to different sectors for 2014 and expectations for 2025 and 2040 years (UNESCO, 2019).

Overall, it is an inevitable fact that the need for clean water has been increasing over the years and strategies are developing in this manner to prevent water scarcity. Two strategies are implemented: wastewater purification and desalinating the saline water. Reverse osmosis membrane technology for desalination and distillation is used for gaining freshwater (Liu et al., 2019).

2.2. Water Treatment Membrane Technology

Water treatment membrane technology is an emerging technology as it is the most cost-effective way to reach clean water (Yang et al., 2019). A membrane can be defined as a

selective barrier between two homogeneous phases while it is allowing one component to pass and the other component to stay by means of selective transportation of a matter, energy, or information. Membrane technology is used in many areas for water treatment such as industrial wastewater treatment, brackish water treatment, and seawater desalination (Drioli & Giorno, 2016; Nicolaisen, 2003). Membrane processes for water treatment are pressure-driven processes and can be classified as microfiltration, ultrafiltration, nanofiltration, and reverse osmosis (Peters, 2010).

2.2.1. Water treatment membrane history

Water treatment membrane history is depending on the way back to the 18th century. In 1748 Abbé Nollet first used osmotic pressure and semi-permeable membrane words by discovering accidentally that animal bladder separated alcohol from the water. In 1855, Fick published the rules of diffusion phenomena which we are currently using for membrane separation, and he worked on semi-permeable membranes. Those firstly studied membranes are made from an alcohol-ether solution of cellulose nitrate called collodion. Thomas Graham then tested dialysis through membranes and made the measurements. He also discovered that the rubber has gas permeabilities so it can be used for gas separation membranes. In 1867 Traube, first made semi-permeable membranes for measuring the osmotic pressure of the solution by Pfeffer (1877), and those led van't Hoff to find the osmotic pressure equation (1887). Later, Nernst (1888) and Plank (1888) developed the flux equations for electrolytes under concentration or electric potential driving forces (Plank, 1888; Nernst, 1888). Donnan worked on the theory of equilibrium and potential on the membrane in the presence of electrolytes in 1911. In 1907-1920 the discovery of microfilters and ultrafilters by Zsigmondy for fine particle or molecular filters. Those were the early discoveries of microfilters and ultrafilters. Then after the 1920s Michaelis (1926), Manegold (1929), and McBrain (1931) studied cellophane or cellulose acetate-nitrate membranes and those were the first models of reverse osmosis membranes. Teorell and Meyer in the 1930s tried electrodialysis membranes and modern membrane electrodes and they studied the transportation mechanisms for neutral or charged membranes. Willem Jhon Kolff accomplished the first successful hemodialysis on a human patient in 1945. In light of this achievement of hemodialysis, membranes started to be used in biomedical applications.

After that in the 1950s microfiltration, electro dialysis, and ion-exchange membranes were explored, and tested in Europe in lab-scale applications and drinking water safety. The practical use of membranes is developed after the 1950s. One of the greatest advances in membrane science and technology has been the production of cellulose acetate-based reverse osmosis asymmetric membranes with high salt retention and flux by Loeb and Sourirajan in 1964. These membranes consisted of an ultrathin selective layer and a thicker permeable microporous support layer. The support layer was providing mechanical strength and the ultrathin layer was providing a selective barrier to the membrane. The greatest improvement in obtaining drinking water from the sea has been experienced in this way. Other membrane production methods were also developed for membrane production with the Loeb-Sourirajan membrane production technique. Later, other polymers such as polyamide, polyacrylonitrile, polyethylene, and polysulfone were used to produce synthetic membranes. With the use of these polymers, an improvement was observed in the mechanical, chemical, and thermal resistance of the membranes. By 1980, reverse osmosis, ultrafiltration, microfiltration, pervaporation, gas separation, and electro dialysis had started to be used in worldwide applications. Also, in the 1980s industrial gas separation membranes are developed for hydrogen, nitrogen carbon dioxide separations. Then in the 2000s nanoparticle-reinforced composite membranes are produced. In the field of membranes, besides membrane production, the emphasis has been on process development, application, and long-term operating experience. Also, reverse osmosis membrane studies have increased over the years. In addition, the use of membrane contactors and membrane reactors has recently started and studies on this subject are increasing. Table 2.1 shows the milestones of the membrane technology (Koyuncu, 2018; Lonsdale, 1982; Mohanty & Purkait, 2011; Wang, Lawrence K.; Chen, Jiaping Paul; Hung, Yung-Tse; Shammas, 2011).

Table 2.1 Historical milestones of the membrane technology (Wang, Lawrence K.; Chen, Jiaping Paul; Hung, Yung-Tse; Shammas, 2011).

Year	Development	Scientist
1748	'Osmosis', permeation of water through animal bladder	Abbé Nollet
1833	The law of diffusion of gases	Thomas Graham
1855	Phenomenological laws of diffusion	Adolf Fick
1860-1880s	Semipermeable membranes: osmotic pressure	M. Traube (1867), W. Pfeffer (1877), J.W. Gibbs (1878), J.H. van't Hoff (1887)

1907-1920	Microporous membranes	R. Zsigmondy
1920s	Prototype of RO	L. Michaelis (1926), E. Manegod (1929), J.W. McBain (1931)
1930s	Electrodialysis membranes, modern membrane electrodes	T. Teorell (1935), K.H. Meyer and J.F. Sievers (1936)
1950s	Electrodialysis, microfiltration, and hemodialysis, ion-exchange membranes	Many
1964	Defect-free, high-flux, anisotropic reverse osmosis membranes	S. Loeb and S. Sourirajan
1968	Basics of pervaporation P. Aptel, and J. Neel Spiral-wound RO module	J. Westmorland
1977	Thin film composite membrane	J. Cadotte
1970–1980	Reverse osmosis, ultrafiltration, microfiltration, electrodialysis	Many
1980s	Industrial membrane gas separation processes	J.M.S. Henis and M.K. Tripodi (1980)
1989	Submerged membrane (bioreactor)	K. Yamamoto

2.2.2. Membrane processes

For water treatment membrane processes, pressure is used as a driving force. The water feed solution is separated by the membrane into permeate which is clean water, and the retentate which is rejected concentrates under pressure (Peters, 2010) (Selatile et al., 2018). The selectivity of a membrane is determined by the pore size of the selective barrier. Membranes can be classified according to their pore size as microfiltration (MF), ultrafiltration (UF), nanofiltration (NF), and reverse osmosis (RO) from bigger pore sizes to smaller (Fikar, 2014; Sagle & Freeman, 2004; Yang et al., 2019). The reason why the pore size differs is that the membrane formation conditions are different from each other. Each type of membrane requires a different amount of pressure which is also called trans-membrane pressure (Sagle & Freeman, 2004; Selatile et al., 2018). Figure 2.3 shows the pressure-driven water treatment membrane processes according to their pore size, working pressure conditions, and the rejected species.

The microfiltration membranes have the biggest pore size with between 10 μm - 0.1 μm . Large particles such as; colloids, bacteria, and soluble macromolecules can be separated from MF membranes (Fikar, 2014; Sagle & Freeman, 2004; Yang et al., 2019). Since MF

membranes are rejecting a wide variety of large molecules they are used in versatile membrane processes for instance; sterilization by bacteria removal, and fruit juice clarification (Anis et al., 2019; Macedonio & Drioli, 2017). The working pressure of this membrane is between 0.2-5 bar. As a membrane material poly(vinylidene fluoride), polysulfone, polyamide, poly(acrylonitrile), cellulose acetate-cellulose nitrate blends, nylons, poly(tetrafluoroethylene), and poly(acrylonitrile)-poly(vinyl chloride) copolymers are used for MF membranes (Sagle & Freeman, 2004).

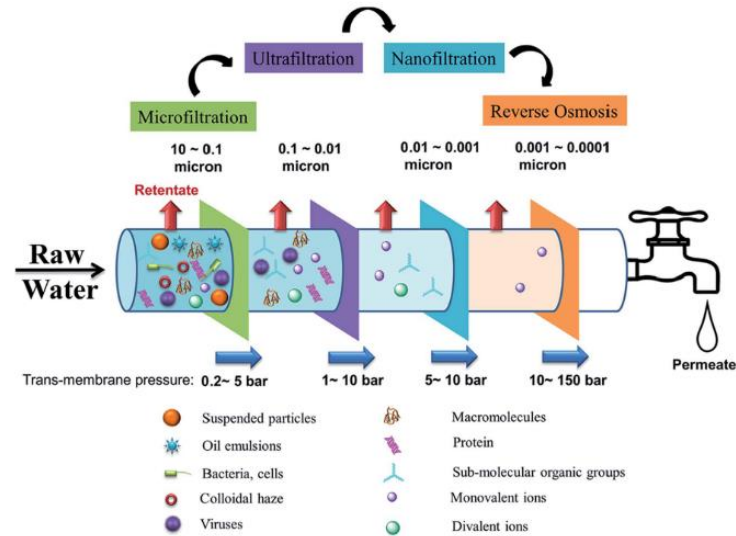


Figure 2.3 Pressure-driven water treatment membrane processes according to their pore size, trans-membrane pressures, and rejected species (Selatle et al., 2018).

Ultrafiltration membranes have smaller pore sizes compared to MF membranes which are between 0.1- 0.01 μm . The performance of UF membranes is represented by molecular weight cut-off (MWCO) expression. MWCO refers to the molecular weight value at which the minimum removal rate is 90%. The pore size also depends on MWCO therefore, when the MWCO decreases the pore size of the membrane decreases. Particles, colloids, bacteria, proteins, and macromolecules can be separated by ultrafiltration membranes. the trans-membrane pressure is between 1-10 bar. Commonly used membrane materials for UF membranes are; poly(ether sulfone), regenerated cellulose, polysulfone, and polyamide. (Anis et al., 2019; Drioli & Giorno, 2016; Mohanty & Purkait, 2011; Nasser, 2020).

The pore size of nanofiltration membranes differs between 0.01- 0.001 μm . Particles, colloids, bacteria, macromolecules, and also divalent ions can be separated by NF membranes (Macedonio & Drioli, 2017). The trans-membrane pressure is between 5-10 bar. As NF membrane material cellulose acetate blends, polyamide composite membranes can be used (Sagle & Freeman, 2004).

Reverse osmosis membranes have the smallest pore size of 0.001-0.0001 μm and are therefore the most selective membranes. Particles, colloids, bacteria, macromolecules, divalent ions, and monovalent ions can be selectively separated by RO membranes. RO membranes are used for seawater desalination, water recycling, and obtaining ultrapure water. The working pressure is between 10-150 bar. The materials used for RO membranes are cellulose acetate, cellulose triacetate, and aromatic polyamides (Macedonio & Drioli, 2017; Mohanty & Purkait, 2011; Nasser, 2020).

2.3. Desalination For Clean Water Production

Seawater or brackish water contains various minerals and salts that are not suitable for direct human consumption. Desalination is a separation process of minerals and salts from these waters to obtain clean water. It is a conversion process of saline water to clean water (Abdelkareem et al., 2018; Lee et al., 2011).

The studies in desalination technologies have been increasing over the years and this is emphasizing the importance of this field. Desalination plants and desalination capacity are also increasing exponentially over the years as demand for freshwater increases. Figure 2.4 represents the number of desalination plants and desalination capacity over the years. This growth is continuing and points out the significance of desalination also membrane technology (Esmaeilion, 2020).

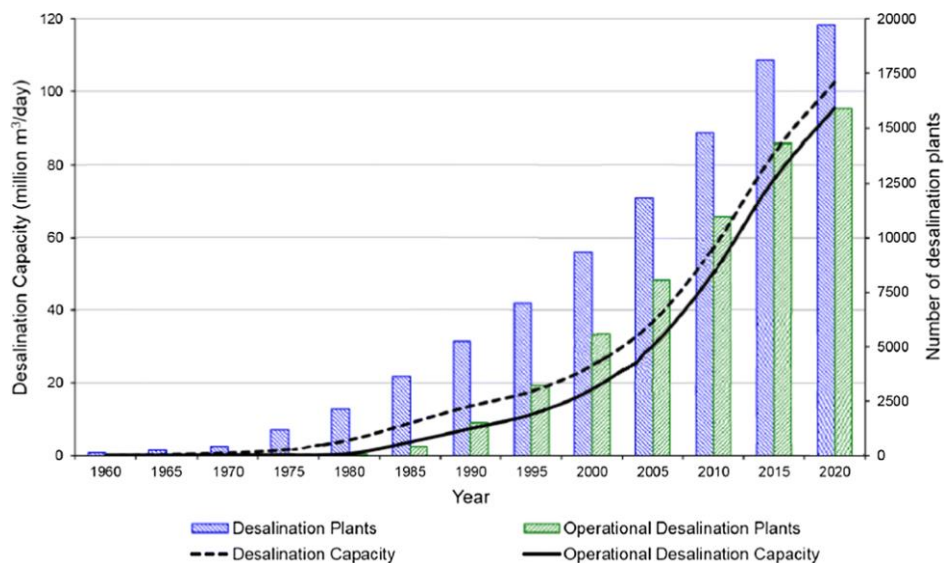


Figure 2.4 Desalination capacity and the number of desalination plants over years (Esmaeilion, 2020).

Desalination processes are examined as two mechanisms: thermal desalination and membrane technologies-based desalination. Thermal desalination methods require higher energy input and higher costs due to the need for thermal energy. Therefore, membrane-based desalination methods are promising with their energy-efficient, lower cost, ease of the process, low space need, and compactness properties (Fritzmman et al., 2007). Reverse osmosis membrane desalination is the most used desalination technology today and it is expected to continue to be used in near future(Lee et al., 2011). Figure 2.5 shows the contributions of desalination methods all over the world. RO membranes have the highest contribution with 69% among the other desalination methods.

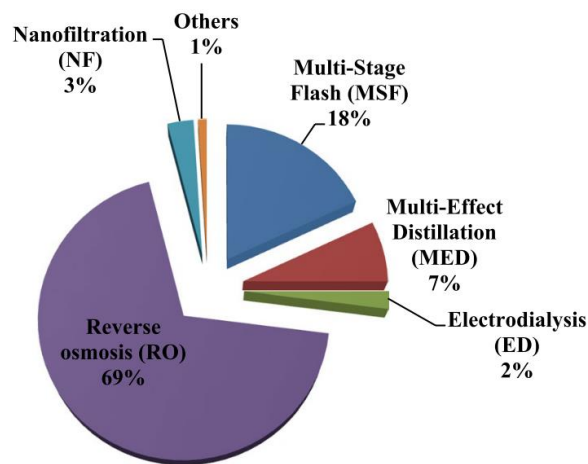


Figure 2.5 The contributions of desalination methods all over the world (Esmaeilion, 2020).

2.4. Reverse Osmosis

Reverse osmosis (RO) is the most used membrane-based water desalination technology as it is a cost-effective way to produce clean water from seawater and brackish water(Lee et al., 2011; Yang et al., 2019).

Osmosis can be defined as the passage of water molecules from low concentration solution to high concentration through a semipermeable membrane. It occurs spontaneously due to differences in chemical potentials between two solutions and continues until the potentials are equaled. In contrast, reverse osmosis is a non-spontaneous process in which pressure is needed as a driving force. Figure 2.6 shows the representation of reverse osmosis membrane technology. With the applied pressure, water molecules pass through the semi-permeable membrane and the salt remains on the other side. Thus, the salt water is purified

by reverse osmosis technology. In the RO process, the water molecules pass from a higher concentration solution to a lower one with the applied external pressure and it is the opposite of osmosis. The working pressure is between 10-150 bar. Reverse osmosis membranes can be used for the rejection of particles, colloids, bacteria, macromolecules, divalent ions, and monovalent ions with their small pore size of 0.001-0.0001 μm . (Greenlee et al., 2009; Macedonio & Drioli, 2017; Mohanty & Purkait, 2011; Nasser, 2020; Shenvi et al., 2015).

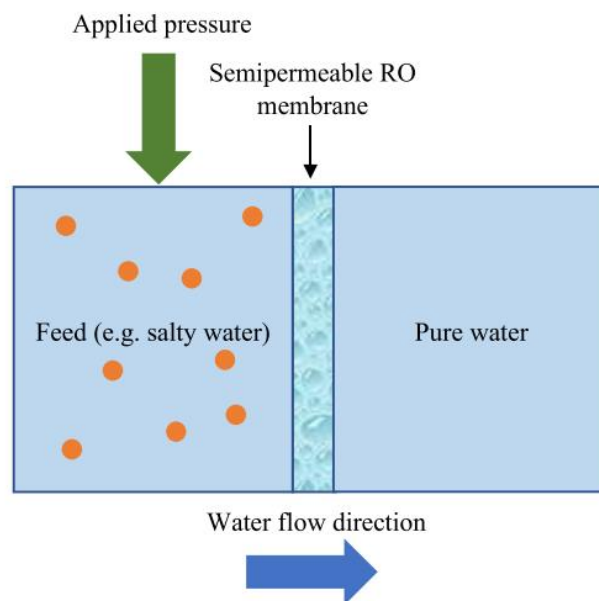


Figure 2.6 Representation of reverse osmosis principle (Tomczak & Gryta, 2022).

The performance of reverse osmosis membranes is evaluated by two parameters; flux and rejection which are dependent on the selected membrane material's chemical composition and structure. Mechanical and thermal stability, high flux performance and rejection of solute, long lifetime, resistance to biological and chemical degradation, fouling resistance, and cost-effectiveness are the looked-for properties of RO membranes. Generally, polymeric materials are used, and according to the chosen polymeric compound, production techniques such as phase inversion, interfacial polymerization, stretching, track-etching, and electrospinning are used (Qasim et al., 2019).

2.5. Commercial Reverse Osmosis Desalination Membranes

Polymer-based reverse osmosis membranes are leading the market with their ease of fabrication, cost-effectiveness, and high membrane performance (Hailemariam et al.,

2020). There are two main types of polymeric membranes used commercially for reverse osmosis, which are cellulose acetate (CA) and thin film composite polyamide (TFC-PA) membranes (Duarte & Bordado, 2016; Greenlee et al., 2009; Sagle & Freeman, 2004).

Firstly, symmetric cellulose acetate membranes were developed in the 1950s by Reid et al. but even though they have good salt rejection, their flux performance was very low and not suitable for practical use (Glater, 1998; Idarraga-Mora et al., 2018; Reid & Breton, 1959; Tomczak & Gryta, 2022). After that asymmetric cellulose acetate membranes were developed by Loeb and Sourirajan in the 1960s with the phase separation method (Duarte & Bordado, 2016; Loeb & Sourirajan, 1963). Asymmetric cellulose acetate membranes consist of a dense layer that provides selectivity and a porous layer for mechanical strength. A non-woven polyester layer (for example polyethylene terephthalate, PET) substrate can also be used to provide mechanical strength (Liu et al., 2019; Qasim et al., 2019). These membranes were started to be used commercially with their high salt rejection and improved water flux performance in the reverse osmosis desalination industry (Lu & Elimelech, 2021; Zhao et al., 2021). Figure 2.7 shows the cellulose acetate RO membrane structure consisting of a cellulose acetate barrier and a PET support layer and a chemical structure of CA (Liu et al., 2019; Ribba et al., 2017).

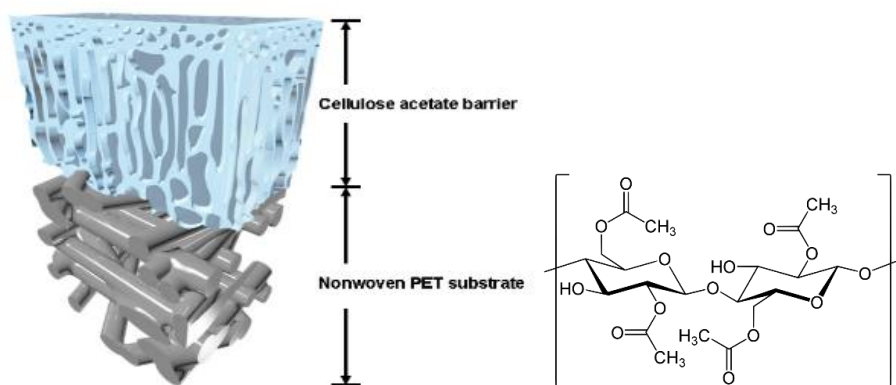


Figure 2.7 Schematic representation of cellulose acetate reverse osmosis membrane structure and chemical structure (Liu et al., 2019).

To increase the water flux performance, durability against pH change and temperature and improve the mechanical strength of CA membranes, thin film composite (TFC) membranes were developed by Cadotte et al. in the 1980s (Cadotte et al., 1980; Sagle & Freeman, 2004). TFC membranes are generally produced by interfacial polymerization of m-phenylenediamine (MPD) and trimesoyl chloride (TMC) and a thin polyamide barrier are formed (Lalia et al., 2013; Lau et al., 2012). TFC membranes consist of three layers; an

active thin polyamide layer that provides selectivity, a porous polysulfone support layer, and a non-woven polyester fabric base (Hailemariam et al., 2020). Figure 2.8 shows the representative structure of TFC-PA reverse osmosis membranes with an ultra-thin polyamide layer, polysulfone support layer, and a polyester nonwoven layer.

Although thin film composite membranes are the most commercially used RO membranes with their high salt rejection and flux performance, their chlorine resistance, and anti-fouling performance need to be improved. Compared to TFC membranes, cellulose acetate membranes (CA) membranes have higher chlorine resistance and higher anti-fouling performance (Sagle & Freeman, 2004; Zhao et al., 2021).

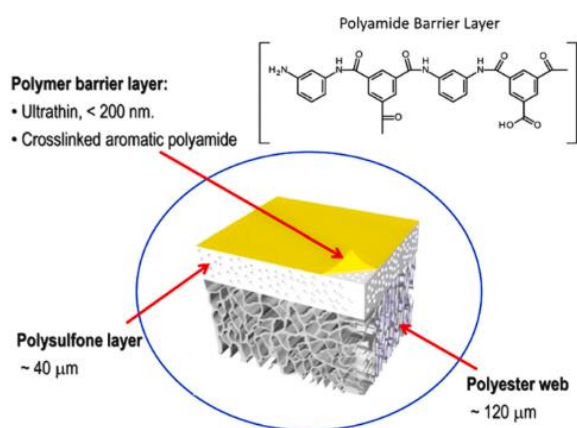


Figure 2.8 Schematic representation of TFC-PA reverse osmosis membrane structure (Zhao et al., 2021).

2.6. Cellulose Acetate Membranes

Cellulose acetate (CA) membranes have versatile usage areas such as nano and microfiltration water treatment membranes, food processing, energy, and the censoring industry (Vatanpour et al., 2022). It is obtained from natural cellulose by the replacement of the hydroxyl group with the acetyl group from natural cellulose (Jazini et al., 2021; Sagle & Freeman, 2004). Figure 2.9 shows the synthesis of CA from natural cellulose. Due to its good film-forming property, elasticity, hydrophilicity that prevents fouling, easy biodegradation, high chlorine resistance, and cost-effectiveness cellulose acetate is used in reverse osmosis water treatment membrane applications (Andrade et al., 2021; Han et al., 2013; Wang et al., 2022).

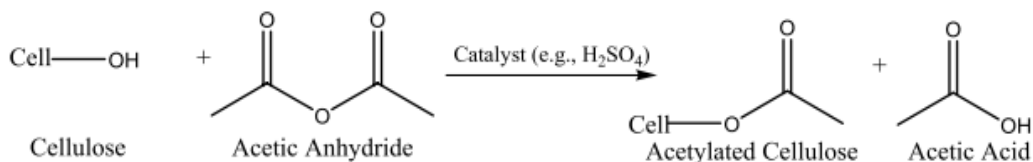


Figure 2.9 Cellulose acetate synthesis from natural cellulose

The asymmetric cellulose acetate membranes are formed of two layers, a dense, and a porous layer. While the very thin, non-porous dense (skin) layer determines the selectivity of the membrane; the porous layer provides mechanical support. The non-woven polyester substrate can be used as membrane backing material to increase the mechanical strength of the membrane (Duarte et al., 2006; Liu et al., 2019). Figure 2.7 shows the cellulose acetate RO membrane structure.

Asymmetric cellulose acetate membranes are generally produced by the non-solvent-induced phase separation (NIPS) method. In the NIPS method, the casting solution is prepared by using the appropriate solvent mixture. After that, the membranes are cast by a film drawing device and waited for the evaporation of the solvent. The dense layer of membrane is formed during the evaporation step. Then the cast films were immersed in a non-solvent coagulation bath (generally cold water) for precipitation and phase inversion. In the coagulation bath due to the exchange of solvent and non-solvent, the porous layer of membrane is formed, and the polymer film becomes solid. The solvent used in the coagulation bath should be insoluble for the polymer but should be miscible with the solvent used in the membrane casting solution. The middle porous layer of cellulose acetate membrane formed during the NIPS process therefore, the pore network of the membrane is highly dependent on the solvent choice, the coagulation bath non-solvent choice, and the exchange rate between them. After the coagulation bath, produced films are annealed in hot water and finger-like voids formed in the porous layer. (Duarte et al., 2006; Guillen et al., 2011; Kahrs & Schwellenbach, 2020; Kunst, 1970; Lalia et al., 2013; Liu et al., 2019; Strathmann et al., 1971).

The performance of reverse osmosis membranes is evaluated by the water flux and salt rejection values. These two parameters are affected by the solvent choice in the casting solution, the evaporation duration, coagulation bath and annealing temperature, and duration and humidity (Duarte et al., 2006; Guillen et al., 2011). The casting solution compositions have been tried to be optimized to achieve the best membrane performance. Asymmetric cellulose acetate membranes were first produced by Loeb and Sourirajan in

the 1960s with the NIPS method. Loeb et al. prepared the casting solution by using CA as a polymer content, acetone as a solvent, and magnesium perchlorate as a swelling agent. They tried to optimize the viscosity of the solution, the casting technique, and the annealing conditions and they achieved a maximum 97.3% salt rejection with 0.38 LMH/bar water flux at room annealing (Glater, 1998)(Loeb & Sourirajan, 1963). After that Kunst et al, used CA as a polymer content, acetone as the solvent, and formamide as a non-solvent at 81°C and reached 98.3% salt rejection with a lower permeation flux of 0.17 LMH/bar (Kunst, 1970). Ghosh et al. prepared another composition containing CA as a polymer, acetone, and dioxane as a solvent, and formamide as non-solvent, and it was seen that by the addition of dioxane on the casting solution, the flux performance improved. They achieved 90% salt rejection with 10.78 L/m²h at 17.2 bar(Ghosh & Sirkar, 1979). The study of Choi et al. also supported that with the addition of dioxane to the membrane casting solution, the permeation flux performance improved (Choi et al., 2016). After that, membrane casting solutions containing both cellulose acetate (CA) and cellulose triacetate (CTA) polymers were prepared for better mechanical strength to compression and better thermal and chemical resistance to biological attack (Shenvi et al., 2015). Cellulose triacetate (CTA) contains more acetyl groups and yields a higher acetylation degree. It was seen that the usage of CA with CTA together, generates a better salt rejection performance, resistance for hydrolysis, and higher mechanical strength but lower permeate flux (Qasim et al., 2019; Sagle & Freeman, 2004; Yang et al., 2019). In their study, Duarte et al. found the optimized membrane solution composition as 4.22 wt.% cellulose triacetate and 9.86 wt.% cellulose diacetate as a polymer content, 45.77 wt.% dioxane, 17.61 wt.% acetone, and 8.45 wt.% acetic acid as the solvents and 14.09 wt. % methanol as the nonsolvent. They reached the 82.7% salt rejection rate with 0.68 LMH/bar permeate flux at 0.5 minutes of evaporation and 85°C annealing condition (Duarte et al., 2006). As can be seen, concluded from the literature review, the evaporation of the solvent in the membrane casting solution determines the dense layer of the membrane and so the selectivity of the membrane(Mohammed Ali et al., 2020). It was seen from the study of Pageau et al., with a higher evaporation time of solvent of more than one-minute decreases the flux performance. By using dioxane in the membrane composition the permeate flux performance increases (Pageau & Sourirajan, 1972). The salt rejection rate increases with the increasing annealing temperature until 85°C, after this temperature the permeate flux performance decreases significantly.

2.7. Cellulose Acetate /Polymer Composite Membranes

Although CA membranes have good chlorine resistance, and high salt rejection, their water flux performance, durability against pH change and temperature, and mechanical strength needed to be improved (Cadotte et al., 1980; Mohammed Ali et al., 2020; Sagle & Freeman, 2004). For this purpose, to achieve the best membrane performance, polymer additives such as polyethylene glycol (PEG), polyvinyl chloride (PVC), and polyvinylpyrrolidone (PVP), have been added to membrane casting composition. These additives can change the surface morphology and increase the hydrophilicity, or some of them can change the void formation and create a sponge-like structure instead of finger-like voids (Guillen et al., 2011).

Polyethylene glycol (PEG) is a frequently used polymer as an additive for membrane production as a plasticizer and pore former (Arthanareeswaran et al., 2004). Different molecular weights of PEG have been added to membrane composition and the effects on the membrane performance and morphology were investigated in the literature. In the studies of Kim et al. it was seen that PEG addition increases the pore size on the surface of the membrane and when the ratio of PEG to NMP is increased, the solution loses its thermodynamic stability (Kim & Lee, 1998). Shieh et al. showed that the hydrophilic character of the membrane increases with PEG addition and so it was thought to be that PEG addition can increase selectivity (Shieh et al., 2001). Arthanareeswaran et al. showed that the low molecular weighted PEG added in the membrane casting solution can increase the permeate flux performance by increasing porosity (Arthanareeswaran et al., 2007).

Polyvinyl chloride (PVC) is another mostly used membrane additive polymer with its flexibility, chemical resistance, and positive effect on increasing hydrophilicity (Qasim et al., 2019). El-Gendi et al. added PVC to the membrane composition, and they observed that the PVC/CA blend membrane containing 16% PVC, 3%CA, and 1% PEG revealed improved mechanical strength (El-Gendi et al., 2017).

Polyvinylpyrrolidone (PVP) was added to the membrane-casting solution composition in many studies. In the study of Saljoughi et al., like the other polymer additives, it was seen that PVP creates macro voids and increases the flux performance (Huang et al., 1983; Qasim et al., 2019). Xu et al. also observed that PVP or PEG as additives caused a morphology change in the membrane and increased the membrane porosity and improve the permeation flux(Xu & Xu, 2002). According to the study of Kumari et al., the thermal

stability, flux, and solute rejection performance are increased until 3w% PVP addition to the casting solution(Kumari et al., 2013).

To conclude, cellulose acetate/polymer composite membranes exhibit superior properties such as higher flux, higher thermal resistance, and higher mechanical strength compared to cellulose acetate membranes.

2.8. Alkyl Alpha-Hydroxymethyl Acrylate (RHMA) Ether Dimer Cyclopolymers as a Potential Membrane Material

Alkyl alpha-hydroxymethyl acrylate (RHMA) ether dimer is synthesized at one step from its corresponding acrylates. There are two different mechanisms involved in the polymerization of RHMA ether dimer monomers. Figure 2.10 shows the polymerization mechanisms of RHMA ether dimer monomers. The first is the formation of cyclopolymers by intramolecular radical addition reaction after radical formation on the double bond in the monomer. These are high molecular weight organic solvent-soluble polymers. The second is the formation of branched or cross-linked polymers by intermolecular addition reactions. Bulky alkyl groups in the monomer (such as *tert*-butyl), ideal polymerization concentration, and high-temperature polymerization lead to intramolecular addition reactions, resulting in the formation of cyclopolymers (Erkoc et al., 2006; Erkoc & Acar, 2008; Tsuda & Mathias, 1994). High monomer concentration, low temperature, and small alkyl groups can lead to the formation of branched or cross-linked polymers.

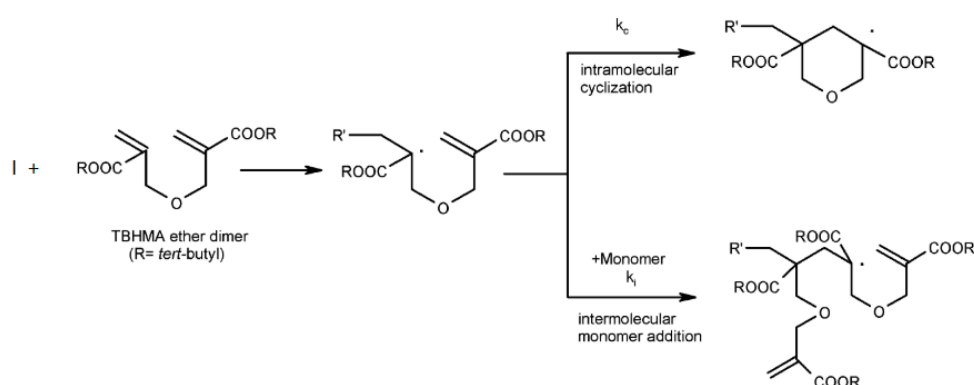


Figure 2.10 Polymerization mechanisms of alkyl alpha-hydroxymethyl acrylate (RHMA) ether dimers (Erkoc et al., 2006).

Cyclopolymers have high glass transition temperature, thermal stability, and low shrinkage properties (Tsuda & Mathias, 1994). Due to these properties, they are thought to be potential membrane materials. Within the scope of this thesis, *tert*-butyl cyclopolymer (TBCP) synthesized from *tert*-butyl alpha-hydroxymethyl acrylate (TBHMA) ether dimer by free radical polymerization according to the literature procedure (Erkoc et al., 2006). TBCP is first used as a cellulose acetate additive polymer for reverse osmosis membranes and CA/TBCP blend composite membranes were produced.

TBCP and CA have essentially the same tetrahydropyran rings. CA has hydroxyl and acetyl groups on the rings, while TBCP has carboxylic acid ester groups. TBCP is a more hydrophobic and amorphous polymer with a rigid structure whereas CA is a more hydrophilic and semi-crystalline polymer (Maheswari et al., 2013). Figure 2.11 shows the chemical and structural comparison of CA and TBCP polymers. Similarities of CA and TBCP in primary structures suggest that secondary structures and aggregation patterns may also be sufficiently similar to facilitate the formation of homogeneous mixtures of the two polymers.

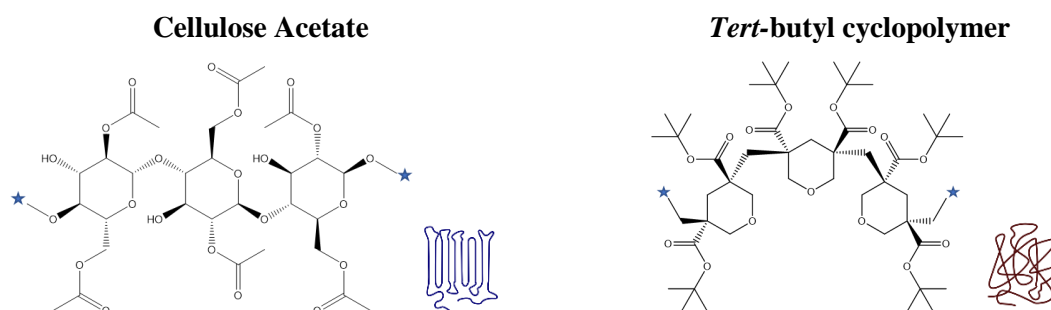


Figure 2.11 Chemical and structural comparison of CA and TBCP

Cao et al. showed in their work that the crystalline structure of the membrane has a high influence on permeation and when the crystallinity increases, the diffusion inside the membrane decreases. Therefore, an amorphous structure gives a better diffusion and so permeation performance (Cao et al., 2000). Rajesh et al. in their study, added poly(amide-imide) (PAI) to the cellulose acetate matrix and produced PAI/CA blend composite membrane. They observed that when the amorphous PAI is added to a semi-crystalline CA matrix, the crystallinity of the CA membrane decreases, and the porosity increased with the addition of PAI. They observed that the flux performance is increased by the addition of amorphous PAI to the semi-crystalline CA matrix (Maheswari et al., 2013). Based on the

studies described, it is expected that the crystallinity decreases with the addition of amorphous TBCP to a semi-crystalline CA matrix, and the flux performance improves. The performance analysis and the structural and morphological analysis of CA/TBCP blend membranes were investigated within the scope of this thesis.

2.9. Acid Functional Cyclopolymers as a Potential Membrane Material

Acid-functional cyclopolymers are synthesized by the acid hydrolysis reaction of *tert*-butyl cyclopolymers. With the hydrolysis reaction of *tert*-butyl alkyl ester groups in trifluoroacetic acid, carboxylic acid functional groups were obtained in the cyclopolymer (Rikkou-Kalourkoti et al., 2012a, 2012b; Tsuda & Mathias, 1994). Figure 2.12 shows the acid hydrolysis reaction of *tert*-butyl cyclopolymer and the chemical structure of carboxylic acid functional cyclopolymer.

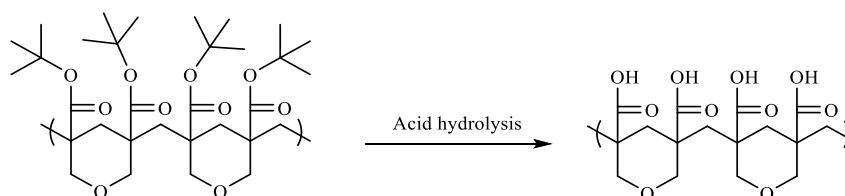


Figure 2.12 Acid hydrolysis of *tert*-butyl cyclopolymer

Carboxylic acid functionalized cyclopolymers are thought to be used in membrane production. Besides being highly hydrophilic, the dissociation of carboxylic acid groups may give a charged character to the membrane (Habert, Huang, et al., 1979).

Within the scope of this thesis, thin film composite (TFC) membranes were produced from carboxylic acid cyclopolymers on polysulfone ultrafiltration membranes by a solution coating method and metal ion crosslinking reactions of carboxylic acid groups.

2.10. Acid Functional Polymer Membranes

Functionalization is applied to membrane polymers to increase membrane properties of fouling resistance, flux performance, and hydrophilicity. Functional groups such as hydroxyl, carboxyl, and amine are formed as a result of chemical functionalization. Functionalization of membrane polymers aims to enhance stability, selectivity, and flux performance (Ashfaq et al., 2020; Ayyavoo et al., 2016; Hunger et al., 2012).

Polyacrylic acid (PAA) based membranes are one of the acid-functional polymer membranes used in water treatment. Because they are hydrophilic and contain carboxylic acid functional groups. These carboxylic acids (-COOH) can dissociate and the membrane can gain a charged character. Upon this charged character, PAA membranes can be used for ionic crosslinking reactions for obtaining metal-ion crosslinked reverse osmosis membranes (Huang et al., 1983).

Carboxyl group functionalized polyimide is another acid-functionalized polymer membrane type. It is synthesized by a polycondensation reaction between durene diamine, diamino benzoic acid (DABA), and 6FDA dianhydride. After the synthesis route, acid-functional polymers can be used for metal ion cross-linked membrane fabrication for nanofiltration applications (Luo et al., 2021).

2.11. Ionically Crosslinked Membranes

Ionic crosslinking is a physical crosslinking that occurs between the charged polymer and an oppositely charged ion. Polymers having a carboxylic acid functional group can form ionic crosslinks with multivalent metal ions like zinc, aluminum, and iron. Figure 2.13 shows the representative ionic crosslinking of polymer containing carboxylic acid groups. Ionically crosslinked membranes can exhibit improved properties such as higher mechanical strength, better thermal stability, and resistance to chemicals. Therefore, their potential for desalination membrane production has been investigated (Everaerts & Clemens, 2002; Huang et al., 1983).

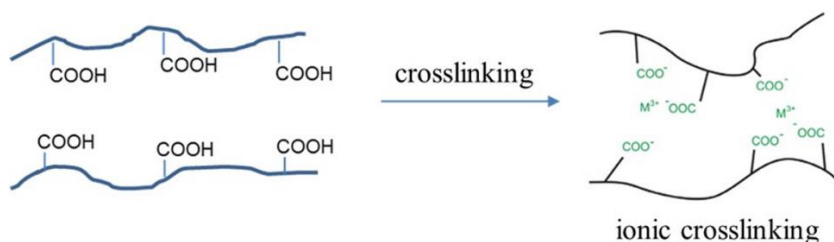


Figure 2.13 Ionic crosslinking of a polymer containing carboxyl groups (Hunger et al., 2012).

Peter et al., produced phenol-selective reverse osmosis membranes from boric acid derivative polyvinyl alcohol (PVA) by ionic crosslinking with polyvalent metal ions. They used $\text{Ba}(\text{OH})_2 \cdot 8\text{H}_2\text{O}$, $\text{Al}(\text{Cl})_3 \cdot 6\text{H}_2\text{O}$, and $\text{KCr}(\text{SO}_4)_2$ as metal salts. These produced

ionically crosslinked membranes resulted in better stability for highly acidic and alkaline environments (Bolto et al., 2009; Peter et al., 1976).

Claudio Habert et al., produced ionically crosslinked poly (acrylic acid) (PAA) membranes with two different methods as dry and wet methods. In the wet method, they first cast the membrane solution onto a surface, then immersed this membrane film into a crosslinking solution containing metal ions (aluminum, zinc, chromium). By the diffusion of metal ions from crosslinking solution to the polymer phase, ionic crosslinking reactions occur between carboxylic groups and metal ions. This way, they produced metal-ion crosslinked PAA membranes for reverse osmosis and they got the best membrane performance with Al^{+3} metal ion (Habert, Huang, et al., 1979). In the dry technique, they prepared the PAA polymer solution and the aluminum metal ion solution, separately. After that, they combined the two solutions and cast them on a glass plate. The prepared membrane film was heated to increase crosslinking density between the carboxylic groups and aluminum metal ions. The produced PAA-Al metal ion crosslinked membrane resulted in 85% NaCl salt rejection and 1250 g/hm^2 flux performance (Habert, Burns, et al., 1979).

Luo et al. produced a metal-ion crosslinked polyimide organic solvent nanofiltration membrane. They synthesized carboxyl functionalized polyamide and conducted metal-ion crosslinking reactions by Ca^{2+} , Mg^{2+} , Fe^{3+} , Zn^{2+} , and Cu^{+2} metal ions in methanol. The produced Cu^{+2} ion crosslinked membrane resulted in good stability against organic solvents like toluene, acetone, and methanol. Also, they observed that the compaction resistance is also improved with the improvement in rigidity of the polymer chain (Luo et al., 2021).

Based on these studies, it was thought that acid-functional cyclopolymers could undergo metal-ion cross-linking reactions and form a metal-ion complex. Since acid cyclopolymers contain carboxylic acid functional groups in their structures like polyacrylic acid, ionic cross-linked PAA membranes have been modeled in ionic cross-linked membrane studies within the scope of this thesis.

CHAPTER 3

3. CELLULOSE ACETATE / CYCLOPOLYMER COMPOSITE MEMBRANES

3.1. Materials and Methods

3.1.1. Materials

Cellulose acetate (average $M_n \approx 30,000$ by GPC), paraformaldehyde (reagent grade, crystalline), 1,4-diazabicyclo[2.2.2]octane (DABCO, $\geq 99.5\%$), *tert*-butyl acrylate, (98%), *tert*-butanol, ($\geq 99.5\%$), 2,2'-azobis(2-methylpropionitrile) (AIBN) (0.2 M toluene solution), toluene ($\geq 99.5\%$), methylene chloride (anhydrous $\geq 99.8\%$), methanol ($\geq 99\%$), acetic acid (glacial, 100%), sodium chloride ($\geq 99.5\%$), magnesium sulfate ($\geq 99\%$), 1,4-dioxane (anhydrous, 99.8%), calcium chloride (anhydrous) were purchased from Sigma-Aldrich (St. Louis, MO, ABD). Acetone (for analysis) was purchased from Merck & Co., Inc. (USA). Hydrochloric acid, (fuming 37%) was purchased from ISOLAB GmbH. RSR-74 type polyethylene terephthalate (PET) non-woven fabrics (thickness: 97 μm) from Teijin Frontier Co., Ltd. (Japan) were used as membrane backing material. All glassware, needles, and stirring bars were dried overnight in an oven at 120 °C. Deionized (DI) water obtained from Merck Millipore Direct-Q 3UV ultrapure water system was used in filtration experiments and analysis.

3.1.2. Experimental

3.1.2.1. Synthesis of *tert*-butyl alpha-hydroxymethyl acrylate (TBHMA) ether dimer monomer

Tert-butyl alpha-hydroxymethyl acrylate (TBHMA) ether dimer is synthesized at one step from its corresponding acrylate, *tert*-butyl acrylate. The formation of TBHMA ether dimer

is conducted with the Baylis-Hillman reaction in the presence of DABCO catalyst and paraformaldehyde. *Tert*-butyl acrylate (128 g, 1 mol), paraformaldehyde (30 g, 1 mol), 1,4-diazabicyclo [2.2.2]-octane (DABCO) (5 g, 0.04 mol), and *tert*-butyl alcohol (10 mL, 0.1 mol) were added to 500 mL four-necked round-bottom flask fitted with a condenser and a magnetic stirring bar. The reaction was stirred at 95°C for 4 days. For the purification of the synthesized monomer, the mixture was diluted with 300 mL of methylene chloride and washed three times with 200 mL of 3% HCl and three times with 200 mL of water. The mixture was dried overnight with CaCl₂ for the removal of water. The crude product was obtained by the removal of methylene chloride by vacuum distillation. Methanol was added to the crude product and the solution was frozen by immersion in liquid nitrogen. With the help of the freezing point difference, the liquid phase including byproducts in methanol was decanted, and pure *tert*-butyl alpha-(hydroxymethyl)acrylate ether dimer (TBHMA) monomer was obtained (Erkoc et al., 2006). The chemical structure of the synthesized monomer was given in Figure 3.1.

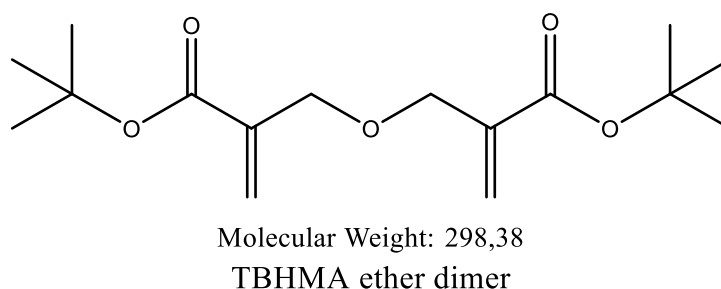


Figure 3.1 The chemical structure of TBHMA ether dimer.

3.1.2.2. Synthesis of *tert*-butyl alpha-hydroxymethyl acrylate (TBHMA) ether cyclopolymers

TBHMA ether dimer cyclopolymer was synthesized by free radical polymerization by using AIBN as an initiator. TBHMA ether dimer monomer (20 mmol, 5.97g) was dissolved in 33 mL of pre-dried toluene in a 100 mL single-neck round-bottom flask fitted with a magnetic stirring bar. The mouth of the reaction flask was closed with a plastic septum and the solution was purged with nitrogen for 45 min. Then, the flask was immersed in a preheated oil bath at 70 °C. 1 mL (0.2 mmol) of 0.2 M solution of 2,2'-Azobis(2-methylpropionitrile) (AIBN) in toluene was transferred to the reaction flask. Polymerization was carried out under nitrogen for 2 hours. Then, the polymer was precipitated in 200 ml of methanol/water (5/1 v/v) mixture and dried in a vacuum oven

overnight (Erkoc & Acar, 2008). TBHMA ether dimer cyclopolymers were synthesized at different molecular weights using different [M]: [AIBN] ratios (200:1, 100:1, 50:1) in the polymerization reactions.

3.1.2.3. Fabrication of asymmetric cellulose acetate membranes

The production of integrally skinned asymmetric cellulose acetate membranes by the non-solvent-induced phase separation (NIPS) method was first demonstrated by Loeb and Sourirajan (Duarte et al., 2006). Asymmetric cellulose acetate membranes were produced for the optimization of the filtration system and the casting solution compositions. According to the literature, the optimized membrane casting solution formulations and preparation conditions were tested as given in Table 3.1. As in the literature, acetone, dioxane, and acetic acid were used as solvents, and formamide and methanol were used as a non-solvent in the membrane casting solution compositions for the fabrication of cellulose acetate RO membranes (Liu et al., 2019).

Table 3.1 Cellulose acetate/cellulose triacetate membrane casting solution composition and membrane preparation parameters.

No	Casting solution composition (w/w %)	Membrane preparation parameters				
		Membr. code	Liquid film thickness/casting speed	Evaporation duration	Coagulation temperature /duration	Annealing temperature / duration
1	CA (25%) Acetone (45%) Formamide (30%)	1a	200 µm, 15 mm/s	40 s	0-4 °C, 2 h	85 °C, 10 min
		1b	200 µm, 15 mm/s	90 s	0-4 °C, 2 h	85 °C, 10 min
2	CA (9.86%) CTA (4.22%) Acetone (17.61%) Dioxane (45.77%) Acetic acid (8.45%) Methanol (14.09%)	2a	100 µm, 25 mm/s	90 s	0-4 °C, 2 h	80-85 °C, 10 min
		2b	254 µm, 25 mm/s	30 s	0-4 °C, 2 h	85 °C, 10 min
		2c	254 µm, 25 mm/s	60 s	0-4 °C, 2 h	85 °C, 10 min
		2d	254 µm, 25 mm/s	90 s	0-4 °C, 2 h	85 °C, 10 min
3	CA (7.04%) CTA (7.04%) Acetone (17.61%) Dioxane (45.77%) Acetic acid (8.45%) Methanol (14.09%)	3a	200 µm, 25 mm/s	30 s	0-4 °C, 2 h	80-85 °C, 10 min
		3b	200 µm, 25 mm/s	60 s	0-4 °C, 2 h	80-85 °C, 10 min
		3c	200 µm, 25 mm/s	90 s	0-4 °C, 2 h	80-85 °C, 10 min
		3d	200 µm, 25 mm/s	120 s	0-4 °C, 2 h	80-85 °C, 10 min

4	CTA (13%) Acetone (22.5%) Dioxane (56.1%) Maleic a. (4.8%) Methanol (3.6%)	4a	200 μm , 30 mm/s	30 s	0-4 $^{\circ}\text{C}$, 2 h	80-85 $^{\circ}\text{C}$, 10 min
		4b	254 μm , 20 mm/s	30 s	0-4 $^{\circ}\text{C}$, 2 h	80-85 $^{\circ}\text{C}$, 10 min
		4c	254 μm , 20 mm/s	60 s	0-4 $^{\circ}\text{C}$, 2 h	80-85 $^{\circ}\text{C}$, 10 min
		4d	254 μm , 20 mm/s	90 s	0-4 $^{\circ}\text{C}$, 2 h	80-85 $^{\circ}\text{C}$, 10 min

All membrane casting solutions were prepared at room temperature. The polymers (CA or CTA) were dissolved in solvents with their respective weight percentages and then non-solvent was added to the casting solutions. The membrane solutions were stirred overnight until a homogenous casting solution was obtained. After degassing the casting solutions, they were poured as a liquid film on a glass plate using a Doctor Blade, having a gap of 254, 200, or 100 μm , at different speeds between 15-30 mm/s in an AB3655-TQC-Sheen Automatic Film Applicator "Compact" with Vacuum bed machine. After casting, the membrane films waited between 30-90 seconds to examine the effect of solvent evaporation time. Then, all the membrane films were coagulated in an ice-water bath at 0-4 $^{\circ}\text{C}$ for 2 hours for the membrane formation by the non-solvent induced phase separation technique. Afterward, the membranes were annealed in a hot water bath at 80-85 $^{\circ}\text{C}$ for 10 minutes to decrease the membrane pore size and increase the mechanical strength. Membranes were produced at least twice at each composition. All membranes were finally kept in a deionized (DI) water bath at room temperature until performance analysis.

3.1.2.4. Fabrication of cellulose acetate/cyclopolymer blend composite membranes

Cellulose acetate/*tert*-butyl cyclopolymer blend composite membranes were fabricated to examine the effect of *tert*-butyl cyclopolymer (TBCP) on membrane performance. *Tert*-butyl cyclopolymer with different molecular weights were obtained by using different [Monomer]: [AIBN] molar ratios (200:1, 100:1, 50:1) in the polymerization reactions. In this way, the effect of molecular weight on membrane performance was also investigated. The optimized casting solution compositions and preparation parameters specified in the studies by Liu et al. were used for the formation of CA/TBCP blend composite membranes (Liu et al., 2019). The casting solutions consist of different weight percentages of CA and TBCP (2%, 4%, 6%, and 8% by weight) and a dioxane-acetone-acetic acid mixture as a solvent and methanol as a non-solvent.

All membranes were prepared under the same preparation conditions. Membranes were cast by “AB3655-TQC-Sheen Automatic Film Applicator "Compact" with Vacuum bed” machine onto a polyester support layer by using Doctor Blade in 200 μm thicknesses with 15 mm/s casting speed. After casting the membrane films, they evaporated for 60 seconds at room temperature. After evaporation, the membrane films were coagulated in an ice-water bath at 0-4°C for 2 hours for the membrane formation by the non-solvent induced phase separation (NIPS) technique. The representation of the NIPS method was shown in Figure 3.2. Membranes were annealed in a hot water bath at 85°C for 10 minutes. Then all membranes were kept in a water bath at room temperature until performance analysis.

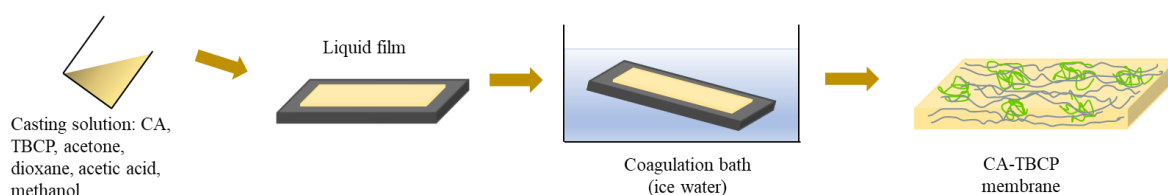


Figure 3.2 Representation of NIPS membrane formation

- CA/TBCP blend composite membranes by TBCPs synthesized with a molar ratio of 100:1 [TB-monomer]: [AIBN]:

For blend composite membranes, firstly, membranes with a polymer content of 20% (CA+TBCP) by weight in the casting solution were produced. TBCP was synthesized according to the procedure given in section 3.1.2.2 with a molar ratio of 100:1 [TB Monomer]: [AIBN]. The membrane containing 20% (w/w) cellulose acetate was produced as the reference membrane. Then, to observe the effect of TBCP content on membrane performance, blend membranes were produced by using polymer mixtures in weight percentages of 20%CA, 18% CA+2% TBCP, 16% CA+4% TBCP, 14% CA+6% TBCP in casting solutions. Membranes were produced according to optimized formulation and preparation conditions in the literature (Liu et al., 2019). The membrane casting solution compositions, and the preparation parameters of the membranes, are given in Table 3.2.

Table 3.2 Cellulose acetate/*tert*-butyl cyclopolymer (20% CA+TBCP 100:1) composite membrane casting solution composition and membrane preparation parameters.

No	Casting solution composition (w/w %)	Membrane preparation conditions				
		Membrane code	Liquid film thickness/casting speed	Evaporation duration	Coagulation temperature/duration	Annealing temperature/duration
5	CA (20%) Acetone (16.9%) Dioxane (42.4%) Acetic acid (7.5%) Methanol (13.2%)	20% CA	200 μ m, 15 mm/s	60 s	0-4 $^{\circ}$ C 2 h	85 $^{\circ}$ C, 10 min
6	CA (18%) TBCP 100:1 (2%) Acetone (16.9%) Dioxane (42.4%) Acetic acid (7.5%) Methanol (13.2%)	18%CA+2% TBCP 100:1	200 μ m, 15 mm/s	60 s	0-4 $^{\circ}$ C 2 h	85 $^{\circ}$ C, 10 min
7	CA (16%) TBCP 100:1 (4%) Acetone (16.9%) Dioxane (42.4%) Acetic acid (7.5%) Methanol (13.2%)	16%CA+4% TBCP 100:1	200 μ m, 15 mm/s	60 s	0-4 $^{\circ}$ C 2 h	85 $^{\circ}$ C, 10 min
8	CA (14%) TBCP 100:1 (6%) Acetone (16.9%) Dioxane (42.4%) Acetic acid (7.5%) Methanol (13.2%)	14%CA+6% TBCP 100:1	200 μ m, 15 mm/s	60 s	0-4 $^{\circ}$ C 2 h	85 $^{\circ}$ C, 10 min

All membrane casting solutions were prepared at room temperature. 20% of the CA or CA/TBCP mixture was dissolved in a solvent mixture containing 42.4% dioxane, 16.9% acetone, 7.5% acetic acid, and 13.2% methanol by weight. Then, the membranes were prepared according to described conditions in Table 3.2 and according to the procedure given in section 3.1.2.1.

To investigate the effect of casting solution viscosity on membrane performance, CA+TBCP blend composite membranes with a polymer content of 25%(CA+TBCP) by weight were produced. The reference membrane was prepared with 25% cellulose acetate polymer content. Likewise, *tert*-butyl cyclopolymer synthesized in a mole ratio of 100:1 [Monomer]: [AIBN] was used with cellulose acetate in the following compositions: 23%

CA+2% TBCP, 21% CA+4% TBCP, 19% CA+6% TBCP, 17% CA+8% TBCP. The membrane casting solution compositions and the preparation parameters are given in Table 3.3.

Table 3.3 Cellulose acetate/*tert*-butyl cyclopolymer (25% CA+TBCP 100:1) composite membrane casting solution composition and membrane preparation parameters.

No	Casting solution composition (w/w %)	Membrane preparation conditions				
		Membrane code	Liquid film thickness/casting speed	Evaporati on duration	Coagulation temperature/d uration	Annealing temperature/ duration
9	CA (25%) Acetone (16%) Dioxane (40%) Acetic acid (7%) Methanol (12%)	25%CA	200 μ m, 15 mm/s	60 s	0-4 $^{\circ}$ C 2 h	85 $^{\circ}$ C, 10 min
10	CA (23%) TBCP (2%) 100:1 Acetone (16%) Dioxane (40%) Acetic acid (7%) Methanol (12%)	23%CA+2% TBCP 100:1	200 μ m, 15 mm/s	60 s	0-4 $^{\circ}$ C 2 h	85 $^{\circ}$ C, 10 min
11	CA (21%) TBCP (4%) 100:1 Acetone (16%) Dioxane (40%) Acetic acid (7%) Methanol (12%)	21%CA+4% TBCP 100:1	200 μ m, 15 mm/s	60 s	0-4 $^{\circ}$ C 2 h	85 $^{\circ}$ C, 10 min
12	CA (19%) TBCP (6%) 100:1 Acetone (16%) Dioxane (40%) Acetic acid (7%) Methanol (12%)	19%CA+6% TBCP 100:1	200 μ m, 15 mm/s	60 s	0-4 $^{\circ}$ C 2 h	85 $^{\circ}$ C, 10 min
13	CA (17%) TBCP (8%) 100:1 Acetone (16%) Dioxane (40%) Acetic acid (7%) Metanol (12%)	17%CA+8% TBCP 100:1	200 μ m, 15 mm/s	60 s	0-4 $^{\circ}$ C 2 h	85 $^{\circ}$ C, 10 min

All the membrane casting compositions were prepared at room temperature. Firstly, cellulose acetate and *tert*-butyl cyclopolymer were dissolved in a solvent mixture

containing 40% dioxane, 16% acetone, 7% acetic acid, and 12% methanol by weight. Then, the membranes were prepared according to described conditions.

- CA/TBCP blend composite membranes by TBCPs synthesized with a molar ratio of 50:1 [TB-monomer]: [AIBN]:

To examine the effect of the molecular weight of TBCPs on composite membrane performance, cyclopolymers with different molecular weights were obtained by changing the molar ratios of [TB-monomer]: [AIBN] (50:1 or 200:1) in polymer syntheses. CA/TBCP blend composite membranes were produced by TBCPs synthesized with a molar ratio of 50:1 [TB-monomer]: [AIBN]. The casting solution compositions and membrane preparation parameters are given in Table 3.4.

Table 3.4 Cellulose acetate/*tert*-butyl cyclopolymer (25%CA+TBCP 50:1) composite membrane casting solution composition and membrane preparation parameters.

No	Casting solution composition (w/w %)	Membrane preparation conditions				
		Membrane code	Liquid film thickness/ casting speed	Evaporation duration	Coagulation temperature/ duration	Annealing temperature/ duration
14	CA (25%) Acetone (16%) Dioxane (40%) Acetic acid (7%) Methanol (12%)	25% CA	200 μ m, 15 mm/s	60 s	0-4 $^{\circ}$ C 2 h	85 $^{\circ}$ C, 10 min
15	CA (23%) TBCP (2%) 50:1 Acetone (16%) Dioxane (40%) Acetic acid (7%) Methanol (12%)	23%CA+2% TBCP 50:1	200 μ m, 15 mm/s	60 s	0-4 $^{\circ}$ C 2 h	85 $^{\circ}$ C, 10 min
16	CA (21%) TBCP (4%) 50:1 Acetone (16%) Dioxane (40%) Acetic acid (7%) Methanol (12%)	21%CA+4% TBCP 50:1	200 μ m, 15 mm/s	60 s	0-4 $^{\circ}$ C 2 h	85 $^{\circ}$ C, 10 min
17	CA (17%) TBCP (8%) 50:1 Acetone (16%) Dioxane (40%) Acetic acid (7%) Metanol (12%)	17%CA+8% TBCP 50:1	200 μ m, 15 mm/s	60 s	0-4 $^{\circ}$ C 2 h	85 $^{\circ}$ C, 10 min

All membrane casting solutions were prepared at room temperature. Firstly, cellulose acetate and *tert*-butyl cyclopolymer were dissolved in a solvent mixture containing 40% dioxane, 16% acetone, 7% acetic acid, and 12% methanol by weight. Then the membranes were prepared according to described conditions.

- CA/TBCP blend composite membranes by TBCPs synthesized with a molar ratio of 200:1 [TB-monomer]: [AIBN]:

CA/TBCP blend composite membranes were produced by TBCPs synthesized with a molar ratio of 200:1 [TB-monomer]: [AIBN]. The membrane casting solution compositions and membrane preparation parameters are given in Table 3.5.

Table 3.5 Cellulose acetate/*tert*-butyl cyclopolymer (25%CA+TBCP 200:1) composite membrane casting solution composition and membrane preparation parameters.

No	Casting solution composition (w/w %)	Membrane preparation conditions				
		Membrane code	Liquid film thickness/casting speed	Evaporation duration	Coagulation temperature/duration	Annealing temperature/duration
18	CA (25%) Acetone (16%) Dioxane (40%) Acetic acid (7%) Methanol (12%)	25% CA	200 μ m, 15 mm/s	60 s	0-4 $^{\circ}$ C 2 h	85 $^{\circ}$ C, 10 min
19	CA (23%) TBCP (2%) 200:1 Acetone (16%) Dioxane (40%) Acetic acid (7%) Methanol (12%)	23%CA+2% TBCP 200:1	200 μ m, 15 mm/s	60 s	0-4 $^{\circ}$ C 2 h	85 $^{\circ}$ C, 10 min
20	CA (21%) TBCP (4%) 200:1 Acetone (16%) Dioxane (40%) Acetic acid (7%) Methanol (12%)	21%CA+4% TBCP 200:1	200 μ m, 15 mm/s	60 s	0-4 $^{\circ}$ C 2 h	85 $^{\circ}$ C, 10 min
21	CA (17%) TBCP (8%) 200:1 Acetone (16%) Dioxane (40%) Acetic acid (7%) Metanol (12%)	17%CA+8% TBCP 200:1	200 μ m, 15 mm/s	60 s	0-4 $^{\circ}$ C 2 h	85 $^{\circ}$ C, 10 min

All membrane casting solutions were prepared at room temperature. Firstly, cellulose acetate and *tert*-butyl cyclopolymer were dissolved in a solvent mixture containing 40% dioxane, 16% acetone, 7% acetic acid, and 12% methanol by weight. Then, the membranes were prepared according to described conditions. All membranes were kept in distilled water at room temperature until permeation and salt rejection performance tests.

3.1.3. Characterization

3.1.3.1. Nuclear magnetic resonance (NMR) spectroscopy analysis

For investigation of the chemical structure of synthesized monomers and cyclopolymers nuclear magnetic resonance spectroscopy (NMR) analysis was applied. Monomer and polymer specimens were prepared as CDCl₃ or DMSO-*d*₆ solutions and ¹H NMR, ¹³C NMR analysis was applied at 500 MHz in Varian NMR spectroscopy.

3.1.3.2. Fourier transform infrared (FTIR) spectroscopy analysis

ThermoScientific Nicolet iS50 FTIR spectrometer was used to examine the bonds in the chemical structure of the synthesized monomer and the polymers prepared for use in the membrane solution. Also, the surface of the fabricated membranes was investigated for surface bonding structure. Measurements were made in transmission mode at a resolution of 32 cm⁻¹ in the wavenumber range of 650 to 4000 cm⁻¹ and an attenuated total reflectance accessory (ATR) was used.

3.1.3.3. Differential scanning calorimeter (DSC) analysis

DSC analysis was applied to synthesized polymers to determine their glass transition temperatures (*T*_g) by Mettler Toledo DSC 3+ instrument. Samples were heated from 25 °C to 250 °C with a 10 °C/min heating rate for the first heating and then cooled down to 25 °C with a 10 °C/min cooling rate. Then the samples were heated again (second heating) from 25 °C to 250 °C with a 10 °C /min heating rate under a nitrogen atmosphere, to determine the glass transition temperatures.

3.1.3.4. Gel permeation chromatography (GPC) analysis

Malvern VISCOTEK GPCmax-Viscotek TDA305 was used to examine the molecular weights and molecular weight distributions of the synthesized cyclopolymers with a D5000-D3000-D1000-DGuard column and refractive index detector. The temperature of the column was 55°C and the injection volume was 100 μL. DMF was used as a solvent at

a flow rate of 0.7 mL/min and MW were calculated using both polymethylmethacrylate standard.

3.1.3.5. Scanning electron microscopy (SEM) analysis

Zeiss LEO Supra 35VP scanning electron microscope at high pressure and low voltage was used to examine the surface morphologies and cross-sectional areas of the membranes. Membranes were cleaned with deionized water and then dried at 40 °C for 2 days to remove the moisture. For cross-sectional images, the membranes were fractured by immersion in liquid nitrogen and the natural cross-sectional area was obtained. Then membranes were coated with Au-Pd at 40mA and under vacuum 3 times for 40 seconds in The Cressington 108 Auto Sputter Coater.

3.1.3.6. Water contact angle (WCA) analysis

Theta Lite Contact Angle Measurement System was used to examine the hydrophilic/hydrophobic characteristics of the produced membranes and to measure the water contact angles. The water drop images were recorded with an optical tensiometer and pictures were taken with a camera. The sessile-drop method was used, and measurements were taken from 5 different areas of each membrane to determine the average contact angle value.

3.1.3.7. Thermal gravimetric analysis (TGA)

For the analysis of the thermal properties of the synthesized polymers, the Mettler Toledo STARe Thermo-Gravimetric Analyzer (TGA) simultaneous thermal weight analyzer was used under nitrogen gas at a heating rate of 10 °C/min, a heating range of 30 °C, and a temperature range of 1000 °C.

3.1.3.8. Viscosity analysis

Viscosity analysis was applied to membrane solutions with Brookfield CAP2000+ Viscometer to examine the viscosity of casting solutions. The viscosity test was applied at room temperature (25°C) and 100 rpm rotating speed.

3.1.4. Membrane Filtration Performance

3.1.4.1. Dead-end filtration system

In a dead-end filtration system, the flow direction of the feed solution is perpendicular to the membrane surface. The feed solution passes through the membrane with the help of applied pressure. The performances of the produced membranes were evaluated with water flux and salt rejection values. These performance tests were performed at room temperature on a Sterlitech, HP4750 stirred-cell dead-end filtration apparatus with an active area of 14.6 cm², under pressure with nitrogen gas. Permeability values were recorded by measuring with a digital scale every 5 minutes and permeation tests were performed for each membrane for 2 hours. The representation and technical properties of the filtration system are given in Figure 3.3 and Table 3.6, respectively.

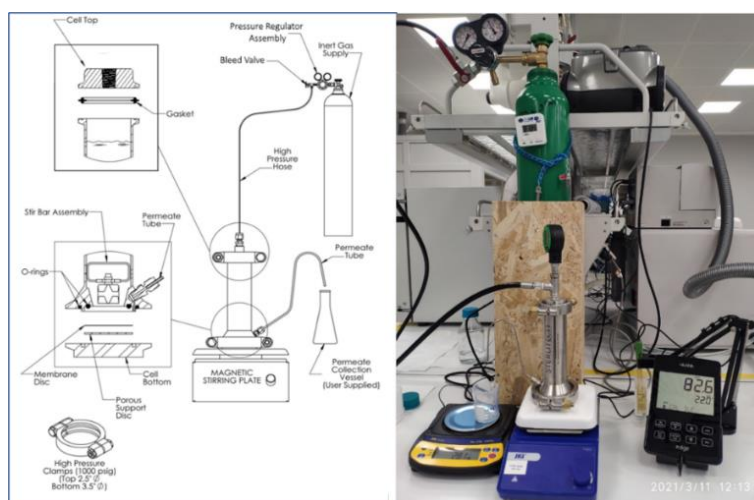


Figure 3.3 Representation of dead-end filtration system.

Table 3.6 Technical properties of filtration system

Parameter	Explanation
Membrane diameter	49 mm
Active membrane area	14.6 cm ²
Maximum working volume	300 mL
Maximum pressure	1000 Psi (69 Bar)
Maximum temperature	121 °C
pH range	Membrane dependent
Body material	316 L stainless steel
Mixer Stick	PTFE
Cell interior dimensions	Diameter:51 cm; height: 19.9 cm

3.1.4.2. Desalination performance

For desalination performance tests, sodium chloride (NaCl), and magnesium sulfate (MgSO₄) aqueous salt solutions were prepared at a concentration of 2000 ppm. In the filtration tests, the samples taken from several different parts of the membranes produced in each composition were tested and the average values of flux and salt rejection were calculated, with their standard deviations. Membranes were washed with deionized water before the filtration tests. For the stability of the system, the values measured in the first 30 minutes were not taken into consideration. The filtration tests were performed for both solutions at room temperature, under nitrogen pressure, for 2.5 hours.

To calculate the salt rejection, the electrical conductivity of the feed and permeate solutions was measured with the HANNA edge® Dedicated Conductivity/TDS/Salinity Meter conductivity meter. By converting the electrical conductivity values to concentration on the calibration curve, the salt rejection percentages were calculated. The formula for the calculation of salt rejection is given below (Nguyen et al., 2013).

$$R = \left(1 - \frac{C_p}{C_f} \right) \times 100$$

R= salt rejection percentage (%), C_p= concentration of permeate, C_f= concentration of the feed.

The desalination performance is also determined by the flux. The volume of the permeate was automatically measured with a digital environment at certain time intervals. The active area of each membrane was 14.6 cm². The flux was calculated by the following formula.

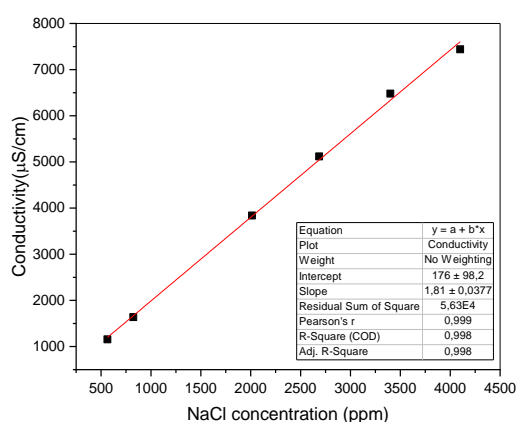
$$J = \frac{M}{A\Delta t}$$

J= flux (L/m².h), M=volume of the permeate (L), A= surface area of the membrane (m²), Δt=filtration duration (h)

3.1.4.3. Calibration curves of conductivity against NaCl or MgSO₄ concentrations

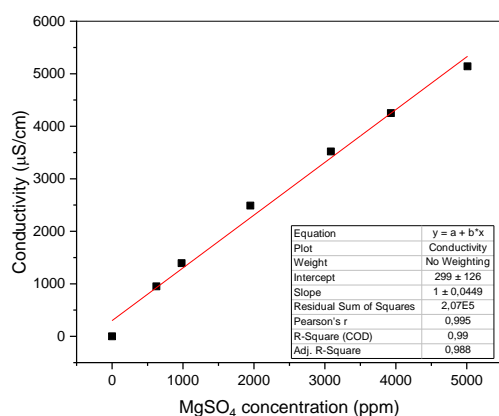
A calibration curve of conductivity against concentration is needed to calculate the salt rejection percentages of the fabricated membranes. The salt rejection percentage was calculated by using concentration values of feed and permeate solutions. First, the conductivity of the solutions was measured by a conductivity meter at room temperature

and then these values were converted to concentration values to calculate the salt rejection percentage. To obtain the calibration curve of sodium chloride and magnesium sulfate, the deionized water solutions of these salts were prepared at 500-1000-2000-3000-4000-5000 ppm concentrations. Conductivity values were measured for each concentration and a calibration curve was obtained from the conductivities as a function of concentration. By using the slope equation of the calibration curve, the conductivity values were converted to concentration values and then the salt rejection (%R) values were calculated. The calibration curves obtained from the conductivities against NaCl and MgSO₄ aqueous solution concentrations were given in Figure 3.4 and Figure 3.5, respectively.



Aqueous salt solution	Electrical conductivity-Salt Concentration equation
NaCl	$y = 1,8118x + 176,43$ $R^2 = 0,9983$

Figure 3.4 Calibration curve of conductivity against NaCl concentration in aqueous solution.



Aqueous salt solution	Electrical conductivity-Salt Concentration equation
MgSO ₄	$y = 1,0046x + 299,16$ $R^2 = 0,9901$

Figure 3.5 Calibration curve of conductivity against MgSO₄ concentration in aqueous solution.

3.2. Results and Discussion

3.2.1. Synthesis of monomer

Tert-butyl alpha-hydroxymethyl acrylate (TBHMA) ether dimer monomer was synthesized according to the procedure in section 3.1.2.1. TBHMA ether dimer was synthesized by a one-pot DABCO-catalyzed Baylis-Hillman reaction followed by dimerization of the Baylis-Hillman adduct at 95 °C (Erkoc et al., 2006). The monomer synthesis reaction was shown in Figure 3.6 .

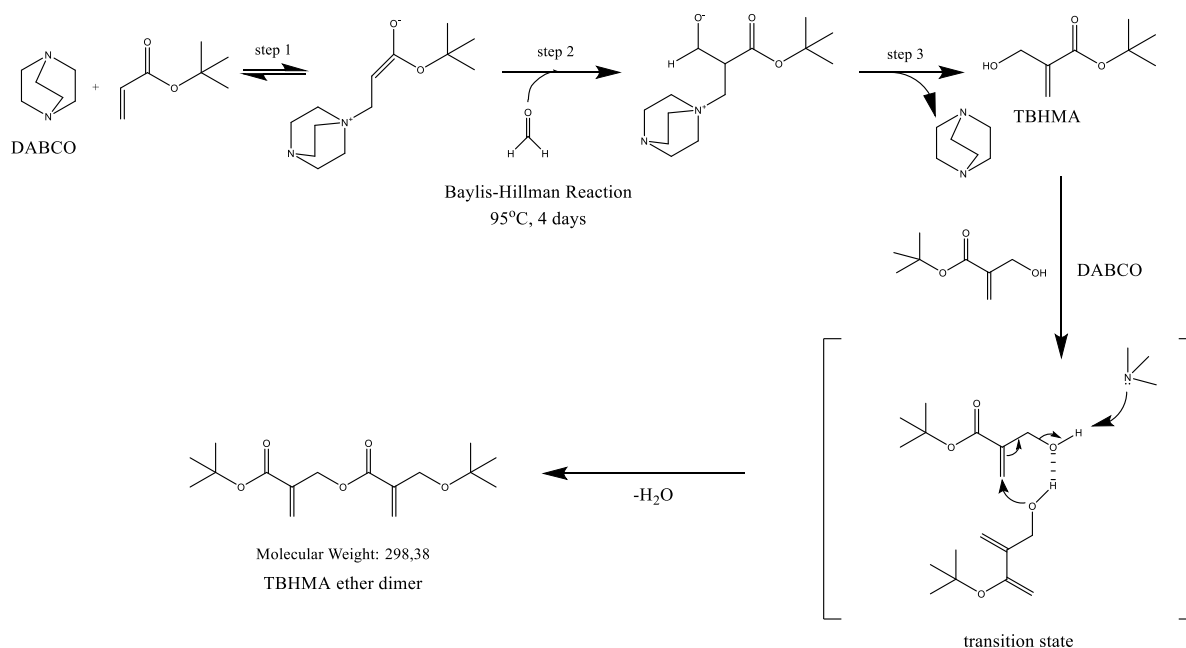


Figure 3.6 Synthesis of *tert*-butyl alpha-hydroxymethyl acrylate (TBHMA) ether dimer

After the synthesis of TBHMA ether dimer, ^1H and ^{13}C NMR analysis was applied to the synthesized monomer in CDCl_3 to confirm the chemical structure.

^1H NMR spectrum of TBHMA ether dimer was shown in Figure 3.7. ^1H NMR (CDCl_3), the peak of a at δ : 1.46 ppm (s, 18H, CH_3), the peak of b at δ : 4.17 ppm (s, 4H, OCH_2), the peak of c at δ : 5.78 ppm (s, 2H, $\text{CH}=\text{C}$), the peak of d at δ : 6.17 ppm (s, 2H, $\text{CH}=\text{C}$) (Tsuda & Mathias, 1994).

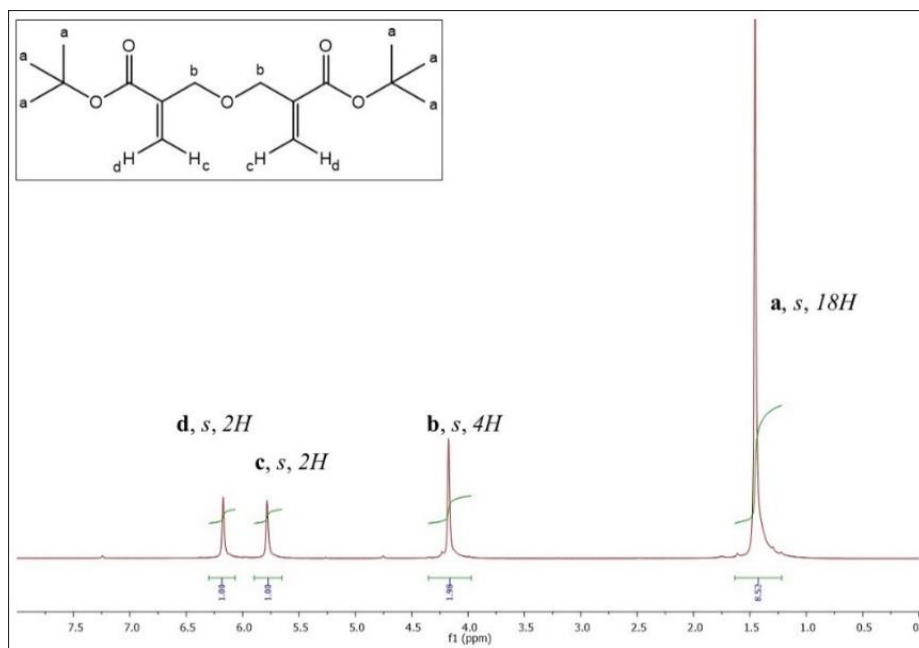


Figure 3.7 ^1H NMR spectrum of TBHMA ether dimer (500 MHz, CDCl_3)

^{13}C NMR spectrum of TBHMA ether dimer was shown in Figure 3.8 ^{13}C NMR (CDCl_3), the peak of a at δ : 28.26 ppm (CH_3), the peak of e at δ : 69.19 ppm (OCH_2), the peak of b at δ : 81.13 ppm ($\text{C}-(\text{CH}_3)_3$), the peak of f at δ : 124.69 ppm ($\text{C}=\text{CH}_2$), the peak of d at δ : 138.83 ppm ($\text{CH}_2=\text{C}$), the peak of c at δ : 165.26 ppm ($\text{C}=\text{O}$) (Tsuda & Mathias, 1994).

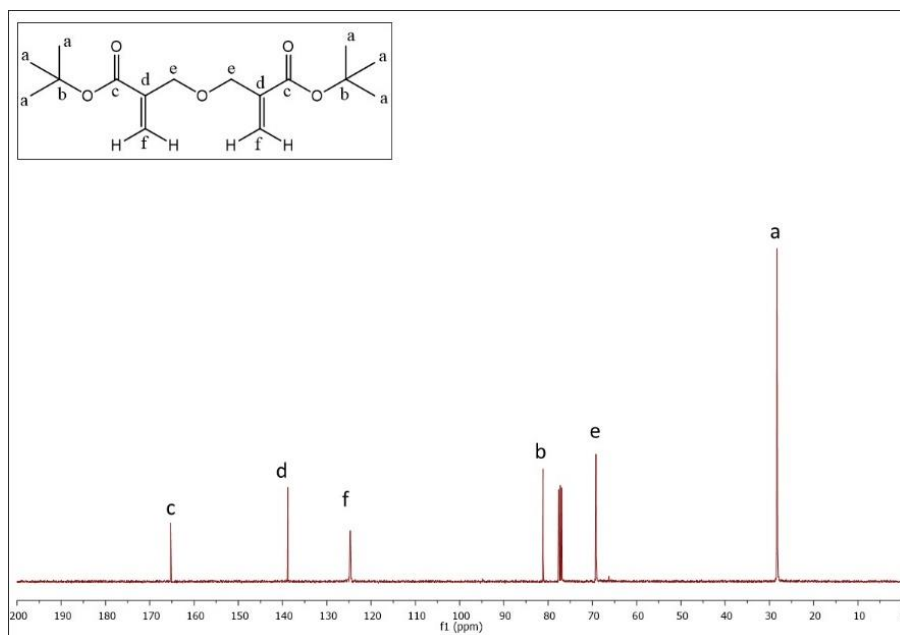


Figure 3.8 ^{13}C NMR spectrum of TBHMA ether dimer (500 MHz, CDCl_3)

The NMR results showed characteristic peaks of the synthesized monomer structure. The integral values of the corresponding peaks in the ^1H NMR spectra confirmed the number of hydrogen atoms.

The chemical bonding structure of the TBHMA ether dimer was also investigated by FTIR spectroscopy. In the FTIR spectrum, around $1100\text{-}1150\text{ cm}^{-1}$ wavenumber, there is strong C-O stretching of ether bonds. There is a carbonyl peak at around 1700 cm^{-1} corresponding C=O bonds. The peak around 1636 cm^{-1} wavenumber corresponds to the C=C alkene bond (Andrews, 1959). The FTIR spectrum of TBHMA was shown in Figure 3.9.

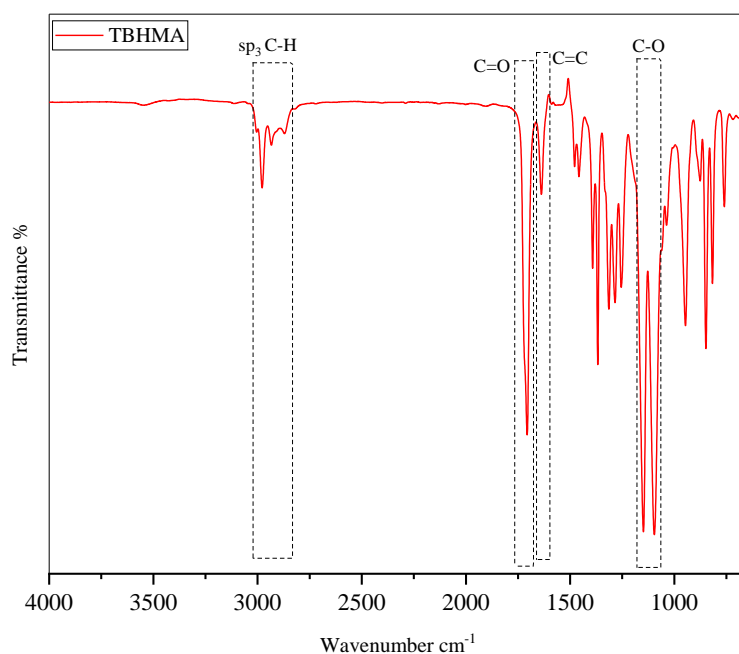


Figure 3.9 FTIR spectrum of TBHMA ether dimer.

3.2.2. Synthesis of *tert*-butyl cyclopolymer (TBCP)

Tert-butyl cyclopolymer was synthesized by free radical polymerization in dry toluene at $70\text{ }^\circ\text{C}$. *N,N'*-azobis(isobutyronitrile) (AIBN) was used as a free radical initiator (Erkoc et al., 2006). The cyclopolymerization reaction was given in Figure 3.10.

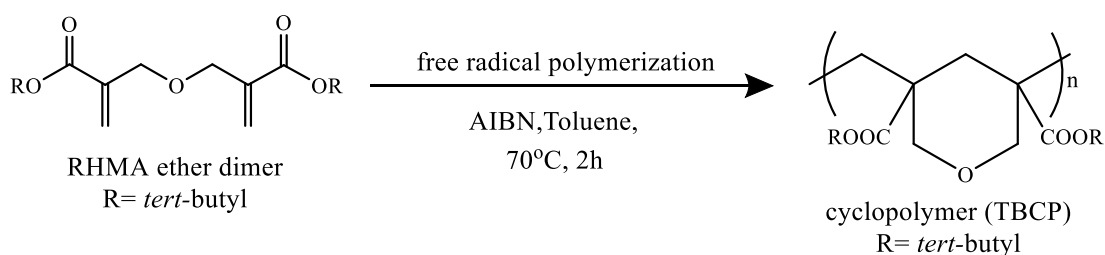


Figure 3.10 Synthesis of *tert*-butyl cyclopolymer (TBCP).

To examine the chemical bonding structure, FTIR spectroscopy was applied to the TBCP. FTIR spectrums of TBHMA ether dimer monomer and TBCP were compared as shown in Figure 3.11. The FTIR spectrum of TBHMA has a carbonyl peak at around 1700 cm^{-1} corresponding to C=O bonds and peaks around 1636 cm^{-1} and 950 cm^{-1} corresponding to the C=C alkene bond (Andrews, 1959). The intensity of these peaks in the FTIR spectrum of TBCP was decreased due to cyclopolymerization and loss of double bonds.

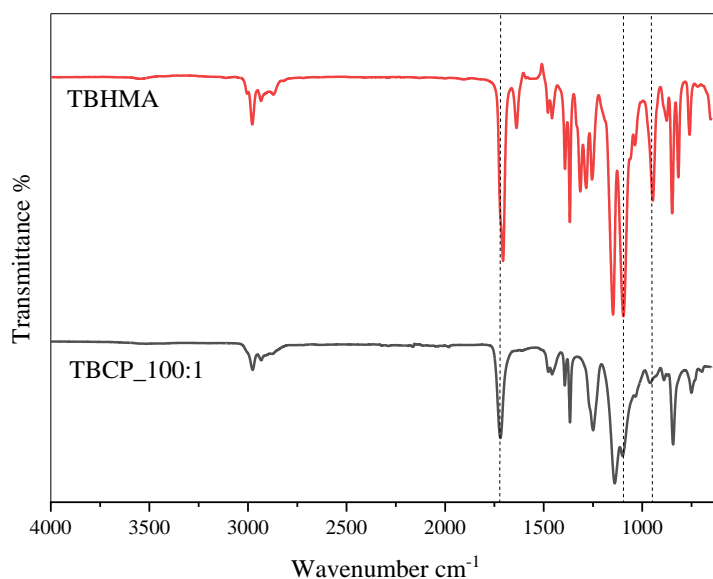


Figure 3.11 FTIR spectrum of *tert*-butyl cyclopolymer (TBCP)

The molar ratio of [TB monomer]: [AIBN] was changed to 200:1, 100:1, and 50:1 in free radical cyclopolymerization reactions to obtain *tert*-butyl cyclopolymers with different molecular weights. The duration of cyclopolymerization was changed to 4h, 2h, and 1h, respectively. Table 3.7 shows the conversion (%) and theoretical molecular weight in TB cyclopolymers synthesized with different polymerization conditions such as [TB monomer]: [AIBN] molar ratio, the molarity of monomer [M], temperature, and time.

Table 3.7 Synthesis of TBCP with different [Monomer]: [AIBN] ratios, conversion (%), and theoretical molecular weight.

No	Monomer	[Monomer]:[I nitator]	[M] (mol/L)	Temp	Duration (h)	Conversion (%)	$M_{n,teo}$ (10^3 g/mol)
1	TBHMA	100:1	0.5	80	2	79.73	23.75
2	TBHMA	100:1	1.0	80	1	71.85	21.41
3	TBHMA	100:1	0.5	70	2	74.19	22.10
4	TBHMA	100:1	0.5	70	2	82.91	24.70
5	TBHMA	50:1	0.5	70	1	14.40	2.14
6	TBHMA	100:1	0.5	70	2	63.31	18.86
7	TBHMA	50:1	0.5	70	1,5	32.32	4.81
8	TBHMA	100:1	0.5	70	2	49.74	14.82
9	TBHMA	50:1	0.5	70	1	69	10.29
10	TBHMA	100:1	0.5	70	2	49.74	14.84
11	TBHMA	100:1	0.5	70	2	82.91	24.74
12	TBHMA	200:1	0.5	70	4	72.5	43.28

Theoretical molecular weight was calculated by the below formula:

$$M_n = (M_{w,tb\ monomer}) \times (\%conv.) \times ([M]:[I])$$

For the free radical cyclopolymerization of TBHMA ether dimer, polymerization solutions with different monomer concentrations, 0.5 M and 1.0 M, were first tried at 80°. Since the intermolecular addition reactions could not be controlled at high monomer concentrations such as 1.0 M, the polymerization reactions ended in a short time with uncontrolled intermolecular addition reactions leading to pendent double bonds. 0.5M monomer concentration gives organic soluble cyclopolymers with no double bonds. (Erkoc et al., 2006). After the cyclopolymerization, all synthesized polymers dissolved in an organic solvent, methylene chloride, which shows that cyclization was efficient, and cross-linking was prevented.

The ^{13}C NMR spectroscopy was applied to TBCP to confirm the chemical structure and observe the cyclization efficiency. Spectrum results of TB monomer and TBCP in CDCl_3 at 500 MHz were compared in Figure 3.12. ^{13}C NMR of TBCP, the peak of a at δ : 28.1 ppm ($\text{OC}(\text{CH}_3)_3$), the peak of g at δ : 45.3 ppm (backbone C_q), the peak of e at δ : 71.0 ppm (OCH_2C_q), the peak of b at δ : 82.1 ppm ($\text{OC}(\text{CH}_3)_3$), the peak of c at δ : 174.2 ppm ($\text{C}_q\text{COOC}(\text{CH}_3)_3$) (Erkoc & Acar, 2008). The peaks of f at δ : 124.69 ppm ($\text{C}=\text{CH}_2$) and d at δ : 138.83 ppm ($\text{CH}_2=\text{C}$) in the ^{13}C NMR spectrum of TB monomer belong to double bonds. These peaks disappeared due to cyclization at ^{13}C NMR spectrum of TBCP. This indicates that cyclization occurred efficiently.

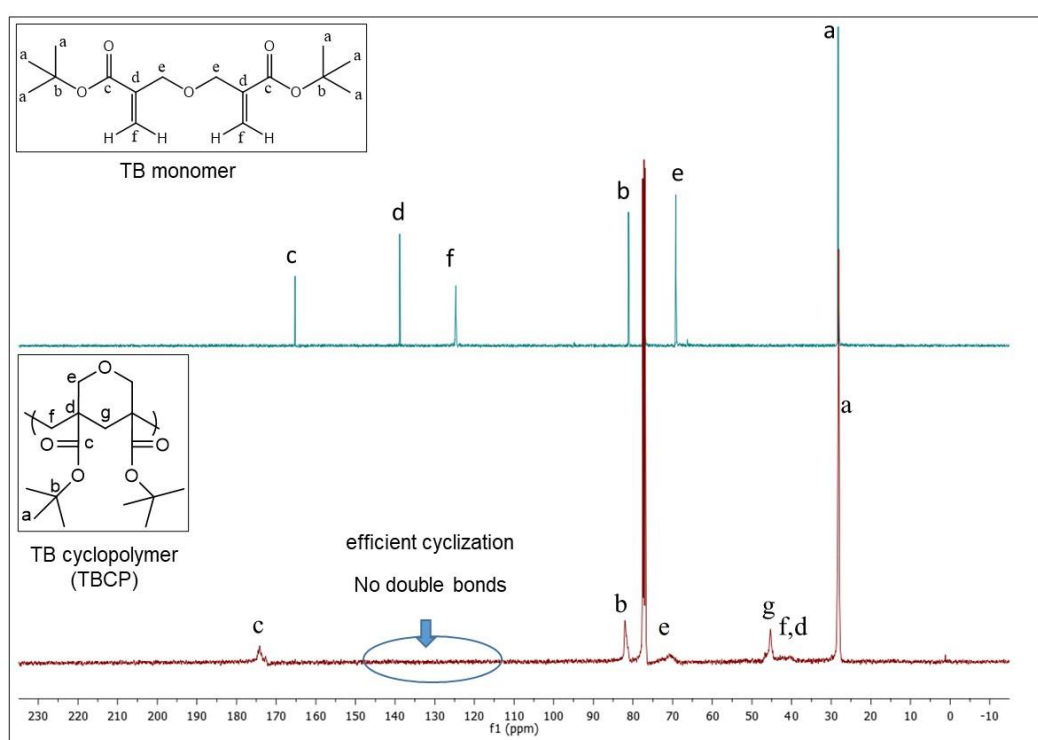


Figure 3.12 ^{13}C NMR spectrum of TB monomer and TBCP (500 MHz, CDCl_3)

Gel permeation chromatography was applied to cyclopolymers synthesized in molar ratios of 200:1, 100:1, 50:1 [TB monomer]: [AIBN] to record their molecular weights and polydispersity values using poly (methyl methacrylate) PMMA standards. As can be seen from Figure 3.13 and Table 3.8, it was observed that the molecular weight distributions were uniform and the PDI values were between 2.2 and 2.4. As expected, the TBCP synthesized with 200:1 molar ratio had the highest molecular weight with 157.4 kDa, while the TBCP synthesized with 50:1 molar ratio had the lowest molecular weight with 77.4 kDa. The molecular weight of cyclopolymers were compared with that of cellulose acetate

(CA) and it was seen that the TBCP synthesized with 200:1 molar ratio had the M_w closest to that of CA.

TB cyclopolymers synthesized with monomer initiator mol ratios of 50:1, 100:1, and 200:1 was named TBCP 33K, TBCP 49K, and TBCP 65K, respectively, according to their number average molecular weights.

Table 3.8 GPC analysis results of synthesized TB cyclopolymers

No	Polymer	M_n (kDa)	M_w (kDa)	PDI
1	CA	72.3	150.9	2.1
2	TBCP 33K	33.2	77.4	2.3
3	TBCP 49K	49.1	112.1	2.2
4	TBCP 65K	65.2	157.4	2.4

The temperature of the GPC column was 55°C and the injection volume was 100 μ L. DMF was used as a solvent at a flow rate of 0.7 mL/min and MWs were calculated using the polymethylmethacrylate standard.

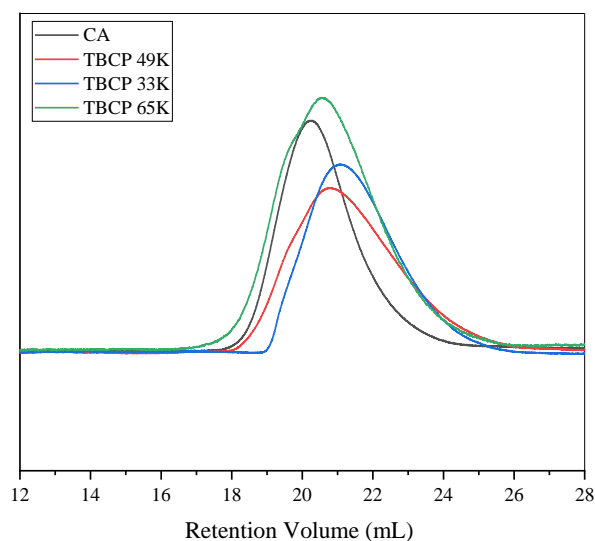


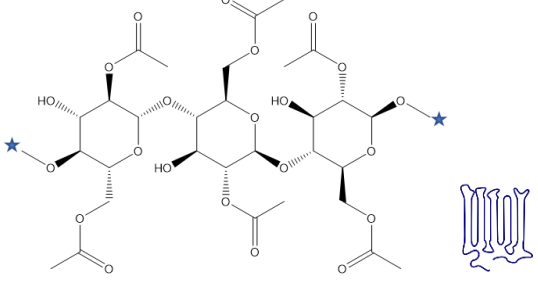
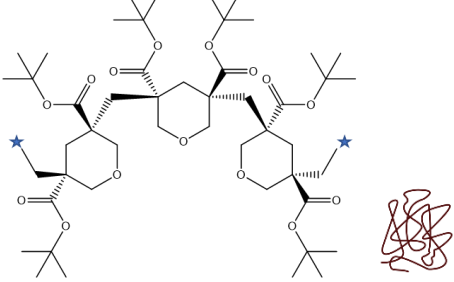
Figure 3.13 GPC plots of synthesized TB cyclopolymers

3.2.3. Structural comparison of cellulose acetate and *tert*-butyl cyclopolymer

When the chemical structures of CA and TBCP are compared, it is seen that both polymers basically have repeating tetrahydropyran rings. CA polymer has interring bonds over C1 and C4 on the rings, while TBCP has interring bonds over C2 and C4. CA has ether bonds between the rings, while TBCP has $-CH_2-$ bonds. TBCP is more hydrophobic than CA.

While CA is a semi-crystalline polymer and has acetyl and hydroxyl groups on the rings, TBCP is an amorphous polymer and has carboxylic acid ester groups on the rings (Maheswari et al., 2013). The structural comparison of cellulose acetate and *tert*-butyl cyclopolymer were given in Table 3.9.

Table 3.9 Structural comparison of cellulose acetate and *tert*-butyl cyclopolymer

Cellulose Acetate	<i>Tert</i> -butyl cyclopolymer
	
<ul style="list-style-type: none"> • Tetrahydropyran repeating unit rings • C1-C4 linkages • Ether (-O-) linkages between rings • Acetal (-O-CO-R) and hydroxyl (-OH) groups • More hydrophilic • Semi-crystalline polymer 	<ul style="list-style-type: none"> • Tetrahydropyran repeating unit rings • C2-C4 linkages • -CH₂- linkages between rings • Carboxylic acid ester (-CO-O-R) groups • More hydrophobic • Amorphous polymer

3.2.4. Preparation of cellulose acetate/cyclopolymer composite membranes

In section 3.1.2.4. preparation of cellulose acetate/cyclopolymer composite membranes has been explained in detail. All membranes were fabricated by the non-solvent-induced phase separation (NIPS) method. The prepared casting solutions were poured onto nonwoven polyester support layers at room temperature. The liquid films were evaporated for the formation of selective/active layer on the surface. Then the liquid films were immersed in a coagulation bath for membrane formation.

3.2.5. Characterization

Thermal gravimetric analysis (TGA) of the TBCPs was performed to determine the thermal stability of the polymers and the results were compared with cellulose acetate and cellulose triacetate. In *tert*-butyl cyclopolymer (TBCP), the initial thermal decomposition temperature is seen to be 180-200 °C. It is known that tertiary-alkyl ester groups generally dissociate olefinically when heated to this temperature(Mathias et al., 1991). The basic

decomposition starts around 350 °C and continues up to 500 °C, which is caused by the decomposition of carbonyl (-COO-) and cyclic structures (depolymerization). Thermal degradation of cellulose acetate entails the dissociation of the polymer chain into glycosidic bonds, depolymerization, dehydration, and cleavage of acetate groups. The thermal decomposition temperatures of cellulose acetate and cellulose triacetate polymers start at about 280 °C and continue up to 430 °C (Barud et al., 2007; Wu et al., 2014). TGA analysis results are given in Figure 3.14 and Table 3.10.

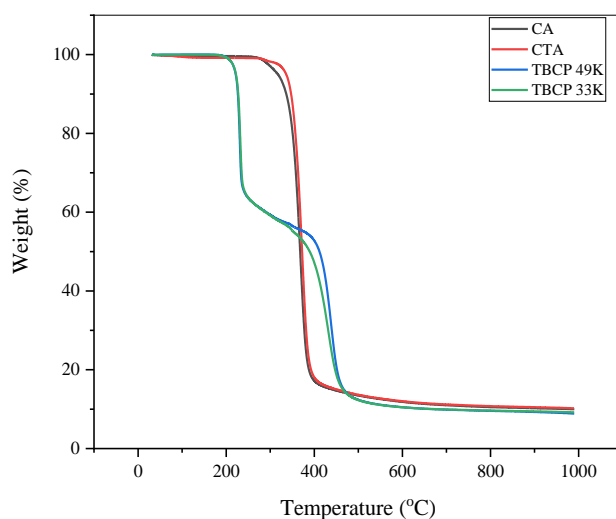


Figure 3.14 TGA results of CA, CTA, TBCP 33K, and TBCP 49K

Table 3.10 TGA results of CA, CTA, TBCP 33K, and TBCP 49K

Sample	T _{d, onset} (°C)	T _d (°C) 5%	The residue (%)
CA	275	316	11
CTA	254	335	11
TBCP 49K	180 (T _{d1}) 280 (T _{d2})	221	9
TBCP 33K	180 (T _{d1}) 280 (T _{d2})	222	9

A thermal weight analyzer was used under nitrogen gas at a heating rate of 10 °C/min, a heating range of 30 °C, and a temperature range of 1000 °C.

DSC curves and estimated glass transition temperature (T_g) and melting temperature (T_m) values of cellulose acetate (CA), cellulose triacetate (CTA), and tertiary-butyl cyclopolymers (TBCP 33K and TBCP 49K) were shown in Figure 3.15 and Table 3.11.

The first endothermic peak at 190 °C in the DSC curve of cellulose acetate gives the T_g value of cellulose acetate. The second endothermic peak at approximately 222 °C indicates the T_m value of cellulose acetate. T_g and T_m values of cellulose triacetate are 162 °C and 285 °C, respectively. The presence of T_g and T_m values indicates that cellulose acetate is a semicrystalline polymer. When the DSC thermogram of *tert*-butyl cyclopolymers (49 K and 33K) were examined, it was seen that only T_g values were detected around 153 °C. The absence of T_m values of the cyclopolymers indicates that, unlike cellulose acetate, these cyclopolymers are amorphous rather than semi-crystalline.

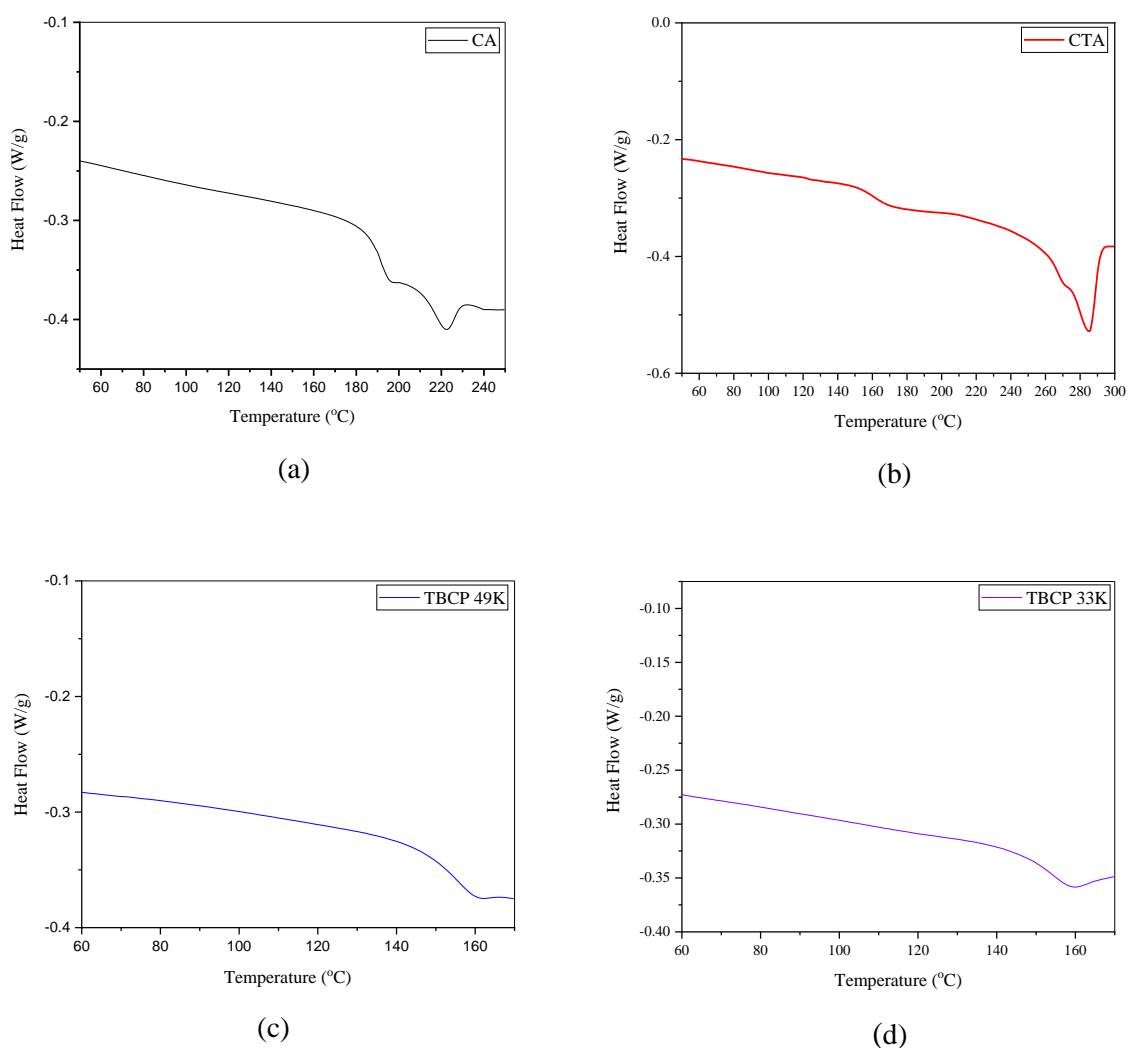


Figure 3.15 DSC thermograms. (a), CA; (b), CTA; (c), TBCP 49K; (d), TBCP 33K.

Table 3.11 DSC results of CA, CTA, TBCP 59K, and TBCP 33K

Polymer	T _g (°C)	T _m (°C)
CA	190.0	221.9
CTA	162.4	285.1
TBCP 49K	153.2	-
TBCP 33K	152.5	-

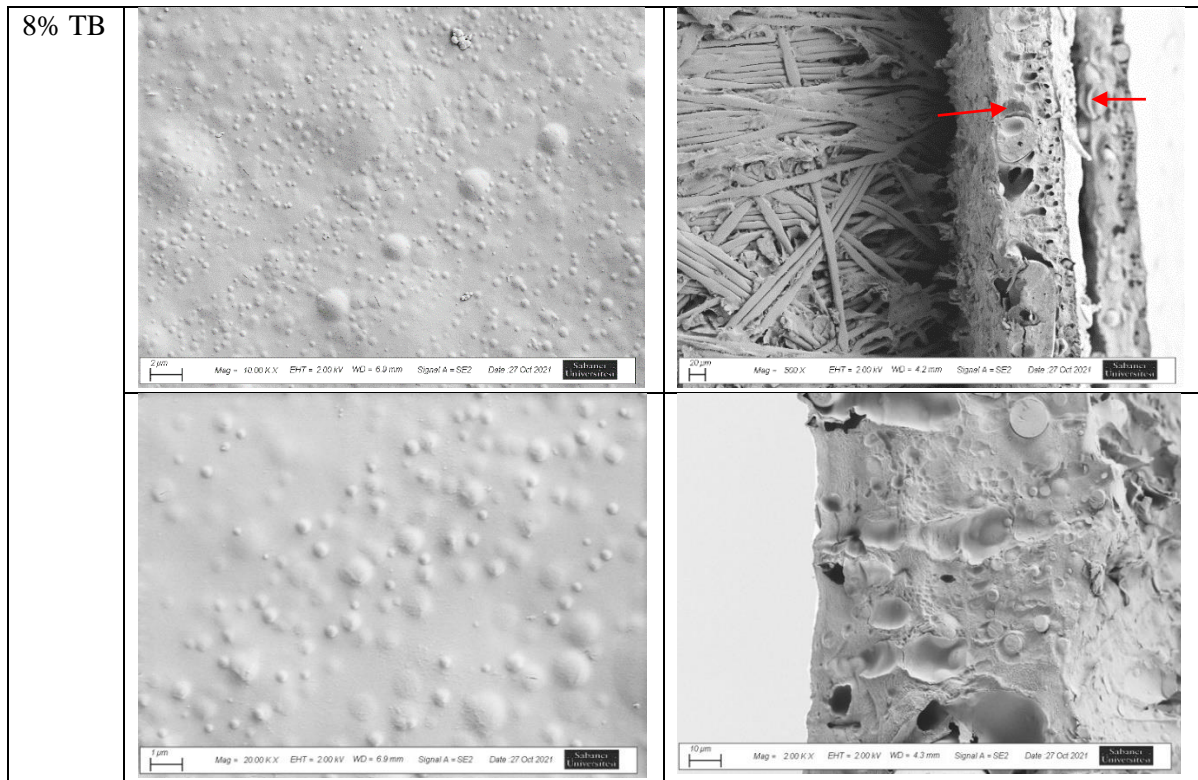
Samples were heated from 25 °C to 250 °C with a 10 °C/min heating rate. Second heating thermograms were considered.

Scanning electron microscopy (SEM) was used for cross-sectional and active surface morphology analysis of produced control CA and cellulose acetate/cyclopolymer composite membranes. When the SEM images of the active (top) surface of the membranes were examined, it was seen that the active surface of the 25% CA-containing control membrane has a smooth, uniform, and non-porous membrane morphology, which is a general feature of CA RO membranes (Liu et al., 2019; Zhou et al., 2016). On the other hand, the active surfaces of the membranes containing 2% and 8% TBCP were rougher. Homogeneously dispersed circular bump structures were observed on the active surfaces of the modified composite membranes. By increasing the amount of TBCP from 2wt% to 8wt%, the circular size of the bumps increased.

When the cross-sectional morphology of the membranes was examined, it was observed that they had an integrally asymmetrical structure characterized by a very thin and dense active skin layer at the top and a thicker, porous layer at the bottom. The utilization of semi-crystalline polymers like cellulose acetate in membranes results in less permeable membranes as they form a more compact and tortuous path across the porous layer. In contrast, amorphous polymers are loosely packed and create free volume in the membrane cross-section (Maheswari et al., 2013). With the addition of amorphous TBCP to the semi-crystalline CA matrix, it was observed that the tortuous path of CA decreased, and macrovoids were formed in the bottom structure of the resulting membranes. It was also observed that when the TBCP concentration was increased from 2% to 8% the number of voids in the porous layer increased. These voids are thought to be explained by the improvement of the flux performance with an increasing amount of TBCP in the casting solution. SEM images were shown in Table 3.12.

Table 3.12 SEM images of produced CA/TBCP composite membranes

Sample	Surface	Cross-section
CA		
2% TB		



Viscosity analysis was performed for the membrane casting solutions to compare the effect of different molecular weight cyclopolymers on the membrane composition and fabrication process. The test was applied to membrane casting compositions prepared with the same weight percentage of polymer blends such as 4% TBCP and 21% CA, but different molecular weights of TBCP. In addition, to investigate the effect of membrane casting solution concentration, 20% (CA+TBCP 49K) and 25% (CA+TBCP 49K) casting solutions were compared. According to the viscosity analysis results shown in Figure 3.16 and Table 3.13, the membrane casting solution consisting of a polymer mixture of 20% (CA+TBCP 49K) by weight had a lower viscosity than the membrane consisting of 25% (CA+TBCP 49K). When we compare the effect of different molecular weights on casting solution viscosity, we can see that the lowest molecular weight TBCP 33K polymer gave the lowest viscosity and the highest molecular weight TBCP 65K polymer gave the highest viscosity. Higher molecular weight polymers with longer polymer chains and more entanglements are expected to yield higher solution viscosities.

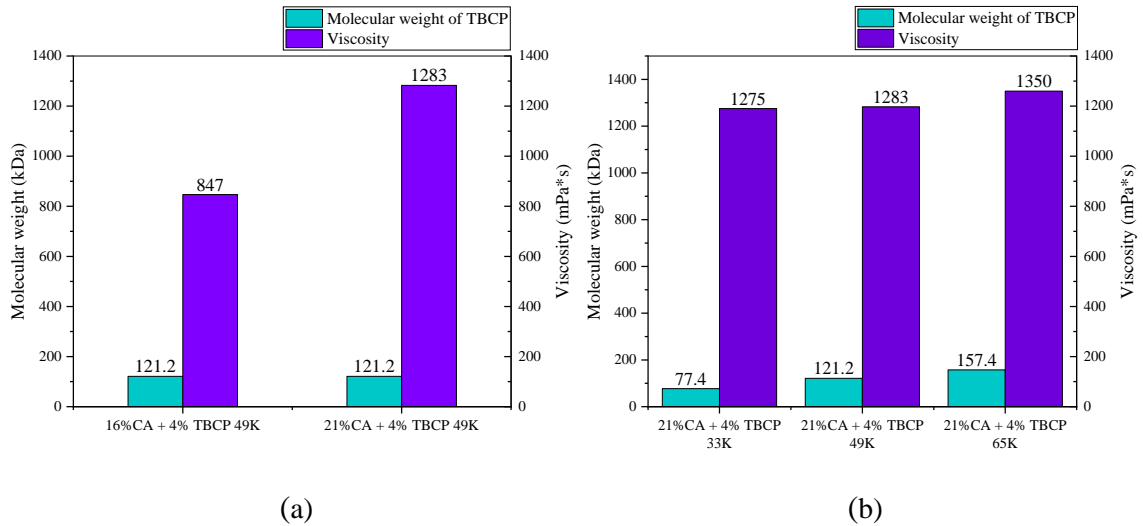


Figure 3.16 Viscosity analysis results of membrane casting solutions. (a) effect of membrane casting solution concentration on viscosity; (b) effect of different molecular weights of TBCP on casting solution viscosity

Table 3.13 Viscosity analysis results of membrane casting solutions

Sample	Molecular Weight of TBCP (kDa)	Viscosity (mPa*s)
16%CA + 4% TBCP 49K	121.2	847
21%CA + 4% TBCP 49K	121.2	1283
21%CA + 4% TBCP 33K	77.4	1275
21%CA + 4% TBCP 65K	157.4	1350

The liquid-membrane interactions also referred to as the wettability of a membrane were examined by water contact angle analysis. To examine the hydrophobic/hydrophilic characteristics of the CA/TBCP blend composite membranes, water contact angles (WCA) of membranes were measured. As can be seen from Figure 3.17 and Table 3.14 with WCA analysis, it was observed that contact angles on fabricated membranes increased with the increasing amount of TBCP in the membrane composition. These results were attributed to the hydrophobic nature of TBCP, increasing the water contact angle of resulting membranes with the addition of TBCP from 2% to 8%.

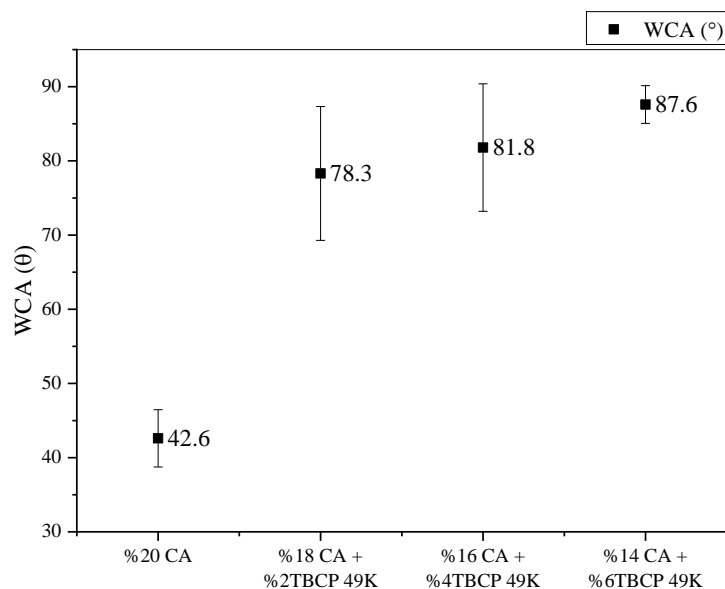


Figure 3.17 Water contact angle results of CA/TBCP composite membranes

Table 3.14 Water contact angle values and drop shapes of CA/TBCP composite membranes

Membrane	Water contact angle (degree)	Standard Deviation	Drop shape analysis
20% CA	42.6	±3.86	
18% CA + 2%TBCP 49K	78.3	±9.02	
16% CA + 4%TBCP 49K	81.8	±8.59	
14% CA + 6%TBCP 49K	87.6	±2.54	

Choo and Lee (1996) have reported that among polyvinylidene fluoride (PVDF), polysulfone(PSF), and cellulose acetate(CA) membranes, PVDF has the most hydrophobic character and lowest fouling tendency (Chen et al., 2012). Therefore, increased hydrophobic character, with the addition of TBCP may decrease the fouling tendency of CA membranes.

3.2.6. Desalination performance

The desalination performance of membranes was analyzed by their flux and salt rejection tests. 2000 ppm NaCl and MgSO₄ salts of deionized water solutions were used for desalination performance tests in a dead-end filtration system at room temperature, 15 bar trans-membrane pressure, under nitrogen gas.

In order to investigate the effect of casting solution concentration on the membrane performance, membrane casting solutions with different concentrations were prepared. In addition, the performance of membranes produced from TBCPs with different molecular weights was also compared to examine the effect of TBCP molecular weight on the final CA/TBCP membrane performance.

2000 ppm NaCl filtration tests:

- 20% CA+TBCP 49K membranes:

Membrane casting solutions were prepared with a 20% (w/w) total polymer content (CA + TBCP 49K). While 2%, 4% and 6% TBCP 49K was added to the casting solutions of composite membranes, the control membrane was prepared from the casting solution containing 20% CA. As shown in Table 3.15 and Figure 3.18 in detail, the flux values of CA/TBCP composite membranes increased compared to the control membrane that is solely based on CA as the polymeric component. It can be thought that the increase in flux values was due to the macro voids that TBCP formed in the sub-layers of the membrane. On the other hand, the salt rejection values slightly decreased. The best salt rejection performance was observed in 16%CA+4%TB 49K membrane with 93.26% salt rejection and 3 L/m²h flux. While the flux value of the CA membrane was 2.91 L/m²h, the flux value of the membrane containing 6% (w/w) TBCP was 5.3 L/m²h. The flux value increased by 82% whereas the salt rejection value decreased by 9%. It is expected that when the flux increases generally the salt rejection decreases.

Table 3.15 20% (CA+TBCP 49K) membranes NaCl filtration results

No	Casting soln. composition	Membrane code	15 Bar 2000 ppm NaCl soln. filtration	
			Flux, <i>J</i> (L/m ² h)	Salt Rejection R (%)
5	CA (20%) Acetone (16.9%) Dioxane (42.4%) Acetic acid (7.5%) Methanol (13.2%)	20% CA	2.91 ± 0.29	98.09 ± 2.35

6	CA (18%) TBCP 49K (2%) Acetone (16.9%) Dioxane (42.4%) Acetic acid (7.5%) Methanol (13.2%)	18%CA+2%TBCP 49K	3.88 ±0.23	91.90 ± 0.73
7	CA (16%) TBCP 49K (4%) Acetone (16.9%) Dioxane (42.4%) Acetic acid (7.5%) Methanol (13.2%)	16%CA+4%TBCP 49K	3.0 ± 0.08	93.26 ± 3.62
8	CA (14%) TBCP 49K (6%) Acetone (16.9%) Dioxane (42.4%) Acetic acid (7.5%) Methanol (13.2%)	14%CA+6%TBCP 49K	5.3 ± 0.05	84.07 ± 4.97

2000 ppm NaCl salt of deionized water solutions were prepared, and desalination performance tests were applied at room temperature in the dead-end filtration system under 15 bar pressure nitrogen gas.

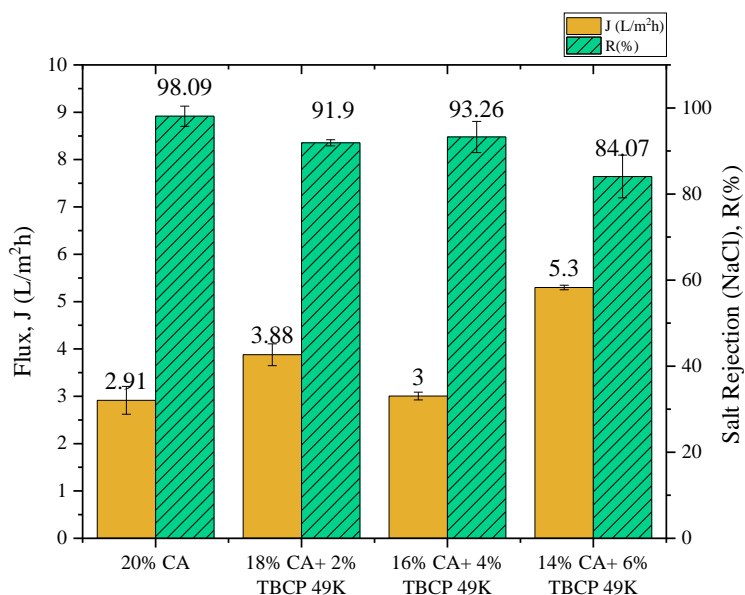


Figure 3.18 20% (CA+TBCP 49K) membranes NaCl filtration results

- 25% CA+TBCP 49K membranes:

The total polymer content (CA + TBCP 49K) in the casting solutions was increased to 25% (w/w) and these membranes were tested for desalination performance analysis. While 2%, 4%, 6%, and 8% TBCP 49K was added to the casting solutions of composite membranes, the control membrane was prepared from the casting solution containing 25% CA. Desalination performance results for the fabricated membranes were given in Table 3.16 and Figure 3.19. The flux value of the membrane consisting of only 25% CA polymer by

weight was determined as 0.68 (L/m²h). It was observed that with the addition of TBCP 49K, the flux values increased significantly. For instance, the flux of 21%CA+4%TB 49K membrane was determined as 1.77± 0.06 (L/m²h) which corresponds to an increase of 160% compared to the CA membrane without any detrimental effect in the salt rejection. 23%CA+2%TB 49K and 21%CA+4%TB 49K membranes salt rejection values were calculated as 95 ±3.77 % and 96.32 ± 0.71% respectively. Although the salt rejection value decreased slightly in the case of TBCP contents above 4%, the membranes' salt rejection values prepared with up to 4% TBCP in the casting composition were at acceptable levels for RO desalination membranes with significantly increased flux values.

Table 3.16 25% (CA+TBCP 49K) membranes NaCl filtration results

No	Casting soln. composition	Membrane code	15 Bar 2000 ppm NaCl soln. filtration	
			Flux, <i>J</i> (L/m ² h)	Salt Rejection R (%)
9	CA (25%) Acetone (16%) Dioxane (40%) Acetic acid (7%) Methanol (12%)	25% CA	0.68 ± 0.25	96.66 ± 0.81
10	CA (23%) TBCP (2%) 49K Acetone (16%) Dioxane (40%) Acetic acid (7%) Methanol (12%)	23% CA+2%TBCP 49K	0.97±0.12	95 ±3.77
11	CA (21%) TBCP (4%) 49K Acetone (16%) Dioxane (40%) Acetic acid (7%) Methanol (12%)	21%CA+4%TBCP 49K	1.77± 0.06	96.32 ± 0.71
12	CA (21%) TBCP (6%) 49K Acetone (16%) Dioxane (40%) Acetic acid (7%) Methanol (12%)	19%CA+6%TBCP 49K	1.21± 0.08	92.98± 1.45
13	CA (17%) TBCP (8%) 49K Acetone (16%) Dioxane (40%) Acetic acid (7%) Metanol (12%)	17%CA+8%TBCP 49K	1.97±0.64	74.68±2.27

2000 ppm NaCl salt of deionized water solutions were prepared, and desalination performance tests were applied at room temperature in the dead-end filtration system under 15 bar pressure nitrogen gas.

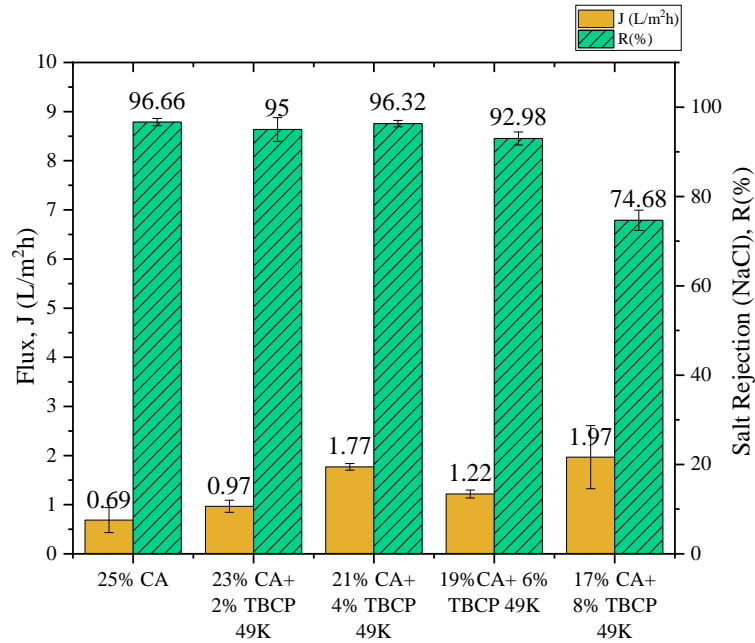


Figure 3.19 25% (CA+TBCP 49K) membranes NaCl filtration results

- 25% CA+TBCP 33K membranes:

As shown in Table 3.17 and Figure 3.20, desalination tests of the membranes prepared from CA and different molecular weight TBCPs were conducted. Similar to other CA+TBCP 49K membranes, in CA + TBCP 33K membranes, when compared to the control CA membrane, it was observed that the flux values increased, and salt rejection values decreased with the addition of TBCP 33K to the casting solutions.

Table 3.17 25% (CA+TBCP 33K) membranes NaCl filtration results

No	Casting soln. composition	Membrane code	15 Bar 2000 ppm NaCl soln. filtration	
			Flux, <i>J</i> (L/m ² h)	Salt Rejection <i>R</i> (%)
14	CA (25%) Acetone (16%) Dioxane (40%) Acetic acid (7%) Methanol (12%)	25%CA	0.68 ± 0.25	96.66 ± 0.81
15	CA (23%) TBCP (2%) 33K Acetone (16%) Dioxane (40%) Acetic acid (7%) Methanol (12%)	23%CA+2%TBCP 33K	1.21±0.91	94.45± 5.82

16	CA (21%) TBCP (4%) 33K Acetone (16%) Dioxane (40%) Acetic acid (7%) Methanol (12%)	21%CA+4%TBCP 33K	3.15 ± 1.68	82.1 ± 1.94
17	CA (17%) TBCP (8%) 33K Acetone (16%) Dioxane (40%) Acetic acid (7%) Metanol (12%)	17%CA+8%TBCP33K	2.68 ± 0.24	82.6 ± 0.8

2000 ppm NaCl salt of deionized water solutions were prepared, and desalination performance tests were applied at room temperature in the dead-end filtration system under 15 bar pressure nitrogen gas.

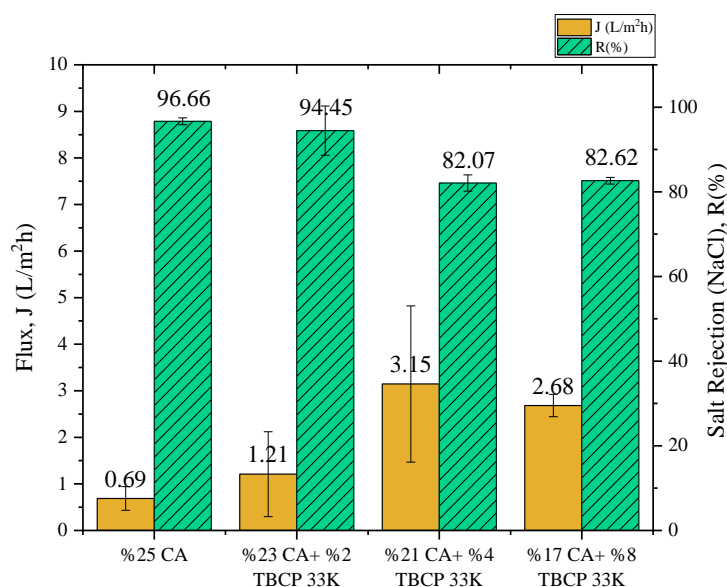


Figure 3.20 25% (CA+TBCP 33K) membranes NaCl filtration results

- 25% CA+TBCP 65K membranes:

A higher molecular weight of TBCP (65K) was synthesized with a 200:1 [Monomer]: [AIBN] mole ratio and incorporated into the membranes for the comparison of the molecular weight effect on the membrane performance. Similar to the membranes produced using TBCP with lower molecular weights, it was observed that the flux value increased with increasing the TBCP ratio in the casting composition. The NaCl filtration performance results of 25% CA+TBCP 65K are given in Table 3.18 and Figure 3.21.

Table 3.18 25% (CA+TBCP 65K) membranes NaCl filtration results

No	Casting soln. composition	Membrane code	15 Bar 2000 ppm NaCl soln. filtration	
			Flux, J (L/m ² h)	Salt Rejection, R (%)
18	CA (25%) Acetone (16%) Dioxane (40%) Acetic acid (7%) Methanol (12%)	25% CA	0.68 ± 0.25	96.66 ± 0.81
19	CA (23%) TBCP (2%) 65K Acetone (16%) Dioxane (40%) Acetic acid (7%) Methanol (12%)	23%CA+2%TBCP 65K	2.39 ± 0.17	85.08 ± 0.14
20	CA (21%) TBCP (4%) 65K Acetone (16%) Dioxane (40%) Acetic acid (7%) Methanol (12%)	21%CA+4%TBCP 65K	2.56 ± 0.23	92.84 ± 0.23
21	CA (17%) TBCP (8%) 65K Acetone (16%) Dioxane (40%) Acetic acid (7%) Metanol (12%)	17%CA+8%TB 65K	3.7 ± 0.08	74.9 ± 2.66

2000 ppm NaCl salt of deionized water solutions were prepared, and desalination performance tests were applied at room temperature in the dead-end filtration system under 15 bar pressure nitrogen gas.

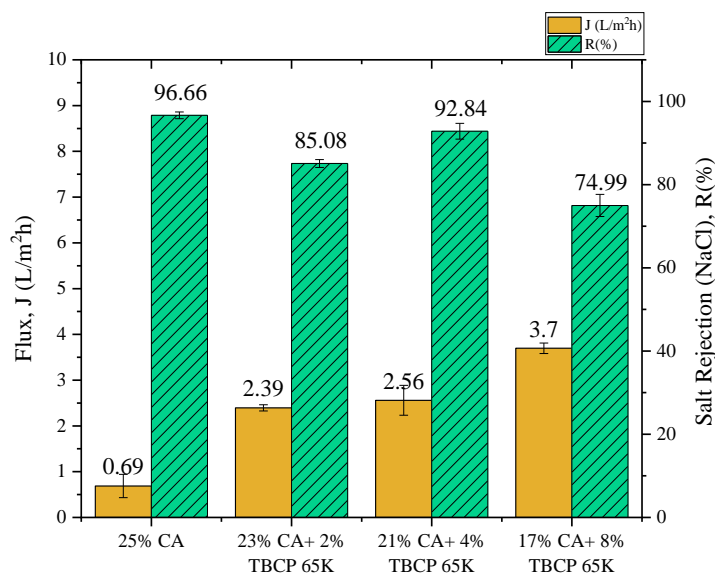


Figure 3.21 25% (CA+TBCP 65K) membranes NaCl filtration results

2000 ppm MgSO₄ filtration tests:

- 20% CA+TBCP 49K membranes:

In order to investigate the CA/TBCP composite membranes in nanofiltration applications, 2000ppm MgSO₄ aqueous solution filtration tests were conducted. Similar to the NaCl filtration results of CA/TBCP composite membranes, it was observed that in general, flux values increased with increasing TBCP content in the casting solution. As shown in Table 3.19 and Figure 3.22, while the flux value of the membrane produced only with CA was 2.23 L/m²h, the flux value of the 18%CA+2%TBCP membrane increased by 85% to 4.13 L/m²h with the 100% salt rejection value. Likewise, the flux value of the 16%CA+4%TBCP 49K membrane increased by approximately 60%, while the salt rejection value remained the same as 100%. The flux value of the 14%CA+6%TB 49K membrane increased by 242% compared to the membrane produced from CA only, while the salt rejection value was 96.8%. As a result of 2000 ppm MgSO₄ filtration tests, it can be concluded that the addition of TBCP until 8% increases the flux performance without deteriorating the salt rejection performance. Such membranes offer great potential in nanofiltration applications.

Table 3.19 20% (CA+TBCP 49K) membranes MgSO₄ filtration results

No	Casting soln. composition	Membrane code	15 Bar 2000 ppm MgSO ₄ soln. filtration	
			Flux, <i>J</i> (L/m ² h)	Salt Rejection, <i>R</i> (%)
5	CA (20%) Acetone (16.9%) Dioxane (42.4%) Acetic acid (7.5%) Methanol (13.2%)	20%CA	2.23±0.4	100
6	CA (18%) TBCP 49K (2%) Acetone (16.9%) Dioxane (42.4%) Acetic acid (7.5%) Methanol (13.2%)	18%CA+2%TBCP 49K	4.13±1.2	100
7	CA (16%) TBCP 49K (4%) Acetone (16.9%) Dioxane (42.4%) Acetic acid (7.5%) Methanol (13.2%)	16%CA+4%TBCP 49K	3.55±0.2	100
8	CA (14%) TBCP 49K (6%) Acetone (16.9%) Dioxane (42.4%) Acetic acid (7.5%) Methanol (13.2%)	14%CA+6%TBCP 49K	7.63±0.9	96.8 ± 4.5

2000 ppm MgSO_4 salt of deionized water solutions were prepared, and desalination performance tests were applied at room temperature in the dead-end filtration system under 15 bar pressure nitrogen gas.

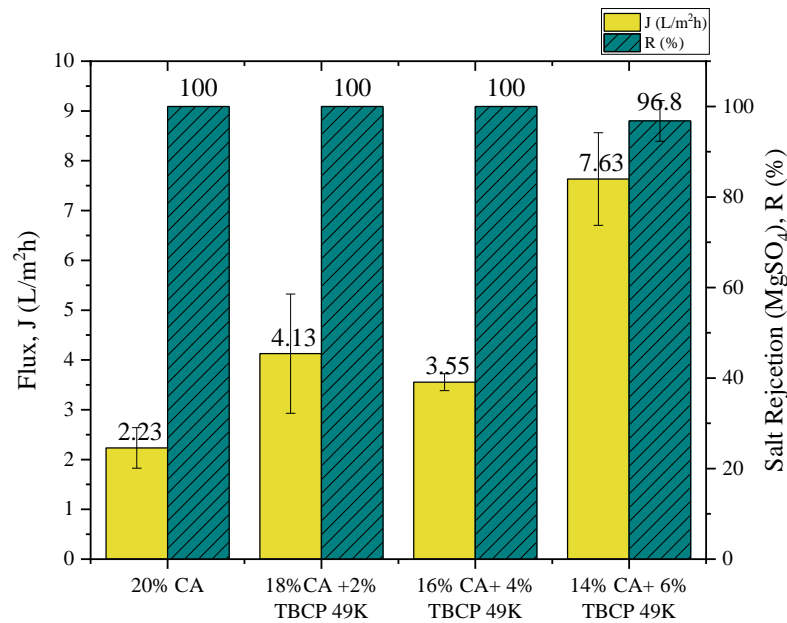


Figure 3.22 20% (CA+TBCP 49K) membranes MgSO_4 filtration results

- 25% CA+TBCP 49K membranes:

The polymer content (CA+TBCP) in the casting solution was increased to 25% (w/w%) and these membranes were analyzed for their nanofiltration performance in 2000 ppm MgSO_4 filtration tests. Similar to the nanofiltration performance of CA/TBCP composite membranes, it was observed that the flux performance increased with the addition of TBCP to the casting solution. As summarized in Table 3.20 and Figure 3.23, when the membrane performances were compared with the control membrane made of only 25% CA, it was seen that the salt rejection performance remained unaffected at 100% until the addition of 6% TBCP, while the flux performance increased up to 116% (for 21%CA+4%TBCP 49K). The salt rejection value for the 17%CA+8% TBCP 49K membrane was determined as 97.12%, while the flux value increased by 200% compared to the 25% CA membrane. Compared to 20% CA+TBCP 49K membranes, in general, the effect of the TBCP incorporation in the increase of flux while preserving salt rejection at 100% was more pronounced in the case of 25% CA+TBCP 49K membranes. Yet, control membranes produced from 25% casting solutions using CA only were more compact, as evidenced by

significantly lower flux values, 0.8 L/m²h, compared to 2.23 L/m²h in the case of control CA membranes produced from 20% CA containing casting solutions.

Table 3.20 25 % (CA+TBCP 49K) membranes MgSO₄ filtration results

No	Casting soln. composition	Membrane code	15 Bar 2000 ppm MgSO ₄ soln. filtration	
			Flux, <i>J</i> (L/m ² h)	Salt Rejection, <i>R</i> (%)
9	CA (25%) Acetone (16%) Dioxane (40%) Acetic acid (7%) Methanol (12%)	25% CA	0.8 ± 0.45	100
101	CA (23%) TBCP (2%) 49K Acetone (16%) Dioxane (40%) Acetic acid (7%) Methanol (12%)	23%CA+2%TBCP 49K	0.94±0.02	100
11	CA (21%) TBCP (4%) 49K Acetone (16%) Dioxane (40%) Acetic acid (7%) Methanol (12%)	21%CA+4%TBCP 49K	1.73± 0.23	100
12	CA (21%) TBCP (6%) 49K Acetone (16%) Dioxane (40%) Acetic acid (7%) Methanol (12%)	19%CA+6%TBCP 49K	1.3 ± 0.12	100
13	CA (17%) TBCP (8%) 49K Acetone (16%) Dioxane (40%) Acetic acid (7%) Metanol (12%)	17%CA+8%TBCP 49K	2.4	97.12

2000 ppm MgSO₄ salt of deionized water solutions were prepared, and desalination performance tests were applied at room temperature in the dead-end filtration system under 15 bar pressure nitrogen gas.

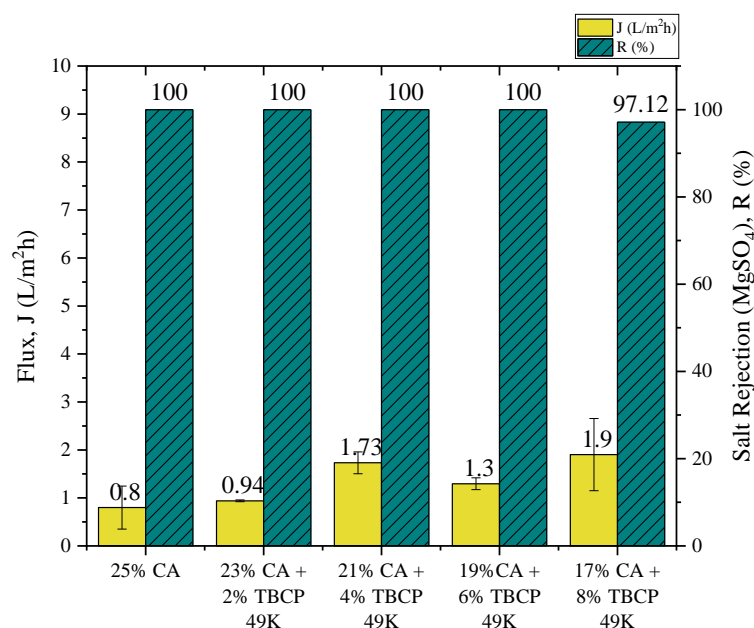


Figure 3.23 25% (CA+TBCP 49K) membranes MgSO₄ filtration results

- 25% CA+TBCP 33K membranes:

MgSO₄ filtration tests of the membranes prepared from CA and lower molecular weight TBCP were also conducted for the membranes prepared from 25% polymer containing casting solutions. As summarized in Table 3.21 and Figure 3.24, similar to CA+TBCP 49K membranes, it was observed that the flux value increased, and the salt rejection value decreased for CA+TBCP 33K membranes. The incorporation of lower molecular weight TBCP had a more pronounced effect on the flux increase at 100% salt rejection, compared to the analogue's membrane TBCP 49K.

Table 3.21 25% (CA+TBCP 33K) membranes MgSO₄ filtration results

No	Casting soln. composition	Membrane code	15 Bar 2000 ppm MgSO ₄ soln. filtration	
			Flux, J (L/m ² h)	Salt Rejection, R (%)
14	CA (25%) Acetone (16%) Dioxane (40%) Acetic acid (7%) Methanol (12%)	25%CA	0.8 ± 0.45	100
15	CA (23%) TBCP (2%) 33K Acetone (16%) Dioxane (40%) Acetic acid (7%) Methanol (12%)	23%CA+%2TBCP 33K	2.04±0.03	100

16	CA (21%) TBCP (4%) 33K Acetone (16%) Dioxane (40%) Acetic acid (7%) Methanol (12%)	21%CA+4%TBCP 33K	1.81 ± 0.53	92.29 ± 0.46
17	CA (17%) TBCP (8%) 33K Acetone (16%) Dioxane (40%) Acetic acid (7%) Metanol (12%)	17%CA+8%TBCP 33K	1.6	100

2000 ppm $MgSO_4$ salt of deionized water solutions were prepared, and desalination performance tests were applied at room temperature in the dead-end filtration system under 15 bar pressure nitrogen gas.

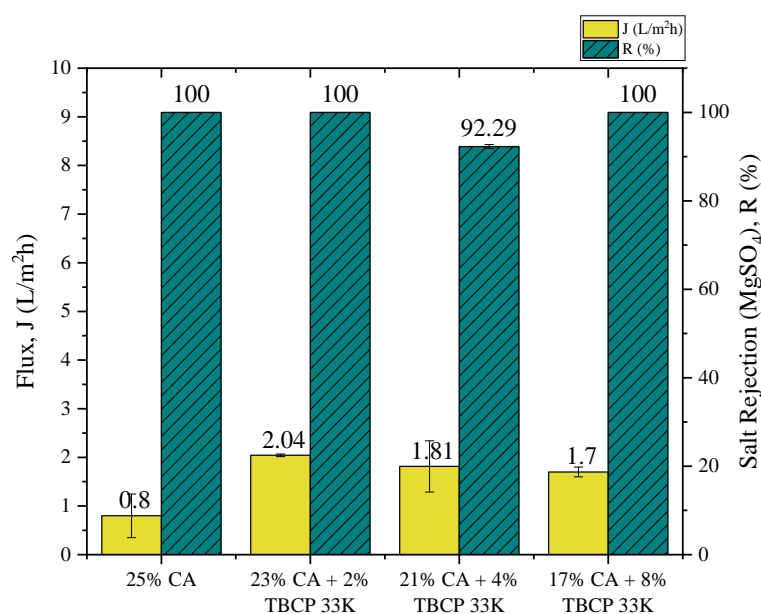


Figure 3.24 25 % (CA+TBCP 33K) membranes $MgSO_4$ filtration results

- 25% CA+TBCP 65K membranes:

To compare the molecular weight effect on the resulting membranes' nanofiltration performance, a higher molecular weight TBCP was synthesized with a molar ratio of 200:1 [Monomer]: [AIBN]. As in the case of membranes produced using TBCP with lower molecular weights, it was observed that flux values generally increased as the TBCP content in the casting composition increased. As can be seen from the results summarized in Table 3.22 and Figure 3.25, the salt rejection values remained at 100% except for the 17%CA+8% TBCP 65K membrane. The flux was increased up to 218% by adding 8% TBCP (%w/w) to the casting solution compared to the 25%CA membrane. Although the

salt rejection value for 17%CA+8% TBCP 65K was slightly reduced, it is still found to be sufficient for nanofiltration membranes with 97.62%.

Table 3.22 25% (CA+TBCP 65K) membranes MgSO₄ filtration results

No	Casting soln. composition	Membrane code	15 Bar 2000 ppm NaCl soln. filtration	
			Flux, <i>J</i> (L/m ² h)	Salt Rejection, <i>R</i> (%)
18	CA (25%) Acetone (16%) Dioxane (40%) Acetic acid (7%) Methanol (12%)	25%CA	0.8 ± 0.45	100
19	CA (23%) TBCP (2%) 65K Acetone (16%) Dioxane (40%) Acetic acid (7%) Methanol (12%)	23%CA+2%TBCP 65K	1.19±0.26	100
20	CA (21%) TBCP (4%) 65K Acetone (16%) Dioxane (40%) Acetic acid (7%) Methanol (12%)	21%CA+4%TBCP 65K	1.85±0.22	100
21	CA (17%) TBCP (8%) 65K Acetone (16%) Dioxane (40%) Acetic acid (7%) Metanol (12%)	17%CA+8%TBCP 65K	2.55±0.44	97.62 ±2.72

2000 ppm MgSO₄ salt of deionized water solutions were prepared, and desalination performance tests were applied at room temperature in the dead-end filtration system under 15 bar pressure nitrogen gas.

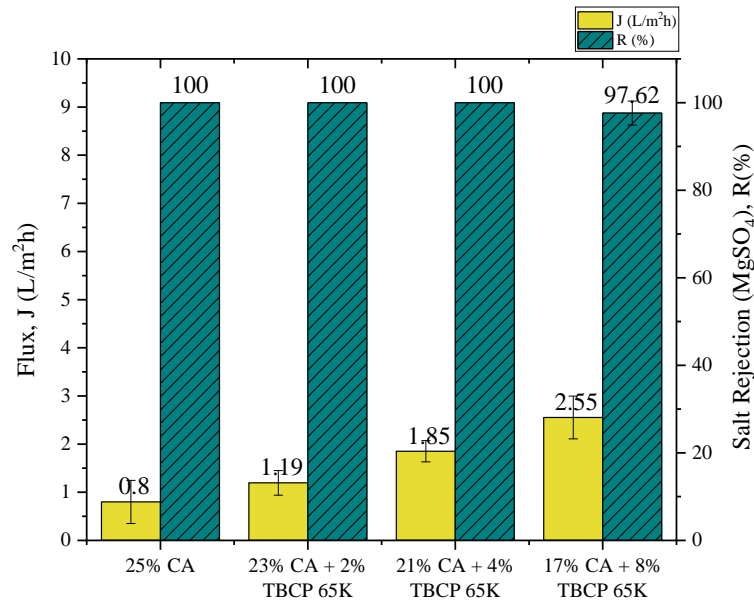
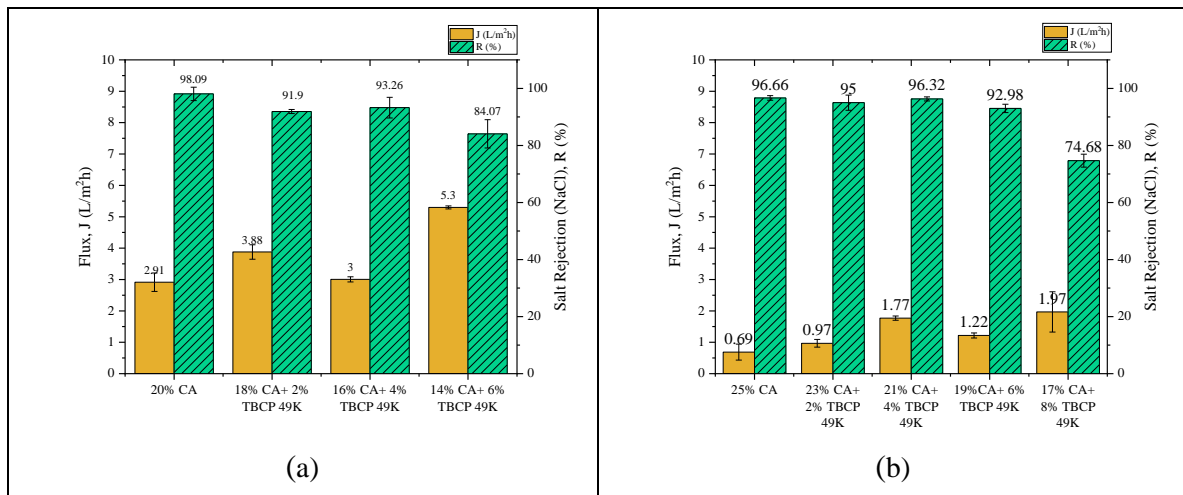


Figure 3.25 25 % (CA+TBCP 65K) membranes MgSO₄ filtration results

3.2.6.1. Casting solution viscosity effect on desalination performance

In order to investigate the effect of membrane casting solution viscosity on membrane performance, membrane casting solutions were prepared with a polymer mixture of 20% (CA+TBCP 49K) and 25% (CA+TBCP 49K) by weight. By increasing the polymer content in the casting solution from 20% to 25%, denser (more compact) membranes were obtained. When the solid content increases in the casting solution the porous structure of the membrane becomes tighter (Wang et al., 2022), which might be useful to achieve higher salt rejection values.



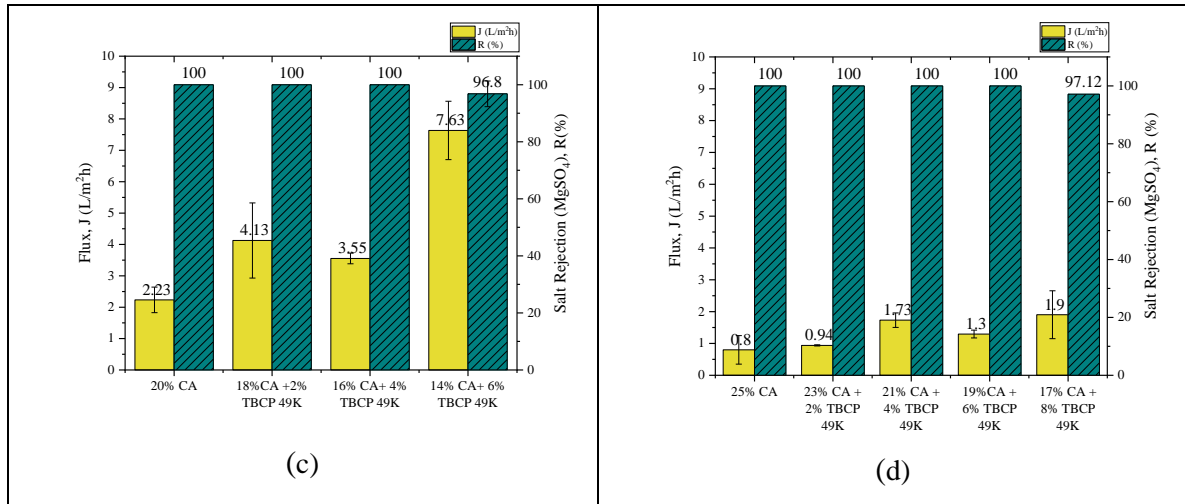


Figure 3.26 Desalination performance comparison of 20% and 25% CA+TBCP 49K (a) 20% CA+TBCP 49K NaCl filtration performance, (b) 25% CA+TBCP 49K NaCl filtration performance, (c) 20% CA+TBCP 49K membranes MgSO₄ filtration performance, (d) 25% CA+TBCP 49K membranes MgSO₄ filtration performance

As shown in Figure 3.26, in the series of membranes prepared from casting solutions with two different polymer concentrations or in different viscosities, it was observed that with the increasing polymer content in the casting solution, the salt rejection values increased while flux values decreased for both NaCl and MgSO₄ filtration tests. The viscosity increases with the increase of the polymer ratio in the membrane casting solution. The viscosity of 16%CA + 4% TBCP 49K and 21%CA + 4% TBCP 49K membrane was found to be 847 and 1283 mPa*s, respectively. Increasing the viscosity results in a tighter membrane, which improves the salt rejection performance. Therefore, it is expected that the performance results of membranes containing a 25% (CA+TBCP) mixture will be more suitable for RO applications.

3.2.6.2. TBCP molecular weight effect on desalination performance

The effect of TBCP molecular weight on desalination performance was investigated by comparing the 17% CA+ 8% TBCP membranes prepared from different molecular weights of TBCP as 33K, 49K, and 65K. As depicted in Figure 3.27, the highest salt rejection performance is obtained from 17% CA + 8% TBCP 33K membrane, which might be attributed to the shorter chain lengths of TBCP since synthesized TBPC 33K has the lowest molecular weight. It can be concluded that the salt rejection performance tended to decrease as the polymer molecular weight increased. As the higher molecular weight TBCP has longer polymer chains, they are expected to create bigger voids in the porous

membranes. This results in higher flux, yet lower salt rejection performance. Although the size of the voids in the porous membrane layer increases with the increasing molecular weight of TBCP, the number of voids per unit surface area of membranes decreases. This may explain the fluctuations in the flux performance.

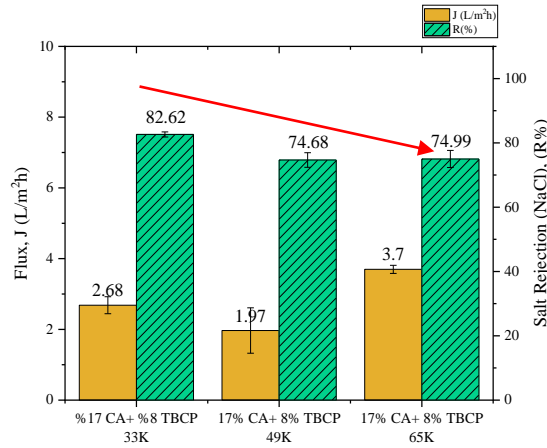


Figure 3.27 Performance comparison of 2000 ppm NaCl filtration 17% CA+ 8% TBCP 33K, 49K, and 65K membrane

3.2.6.3. Stability analysis of the composite membranes

The stability of 20%CA and CA+TBCP membranes was evaluated by the filtration of 2000 ppm MgSO₄ solution for 2 hours under 15 bar trans-membrane pressure. After the first 40 minutes, it was observed that the flux value did not change, showing that the membranes were stable under these conditions, including the pressure applied. The stability analysis of the CA/TBCP blend composite membranes was shown in Figure 3.28.

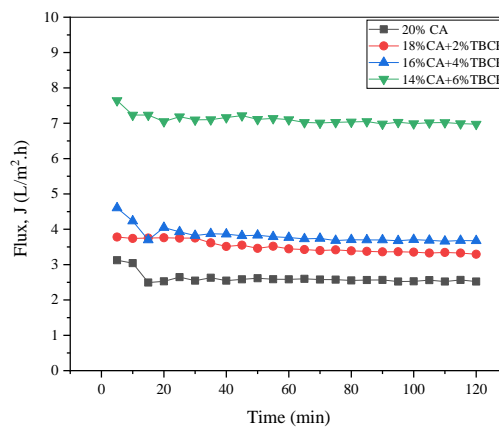


Figure 3.28 Stability analysis of the CA/TBCP blend composite membranes (15 bar 2000 ppm MgSO₄ water solution filtration)

3.3. Conclusions

Tert-butyl alpha-hydroxymethyl acrylate (TBHMA) ether dimer was synthesized and characterized structurally, according to the literature procedure (Erkoc et al., 2006). *Tert*-butyl cyclopolymer (TBCP) was synthesized by free radical polymerization from TBHMA ether dimer monomer. NMR and FTIR analysis were used to confirm the final structure of the resulting cyclopolymers.

In order to incorporate membrane structures and investigate the effect of the molecular weight of TBCP on the resulting membrane performance, TBCP was synthesized at different molecular weights by changing the monomer: initiator ratio. Gel permeation chromatography was used to determine the molecular weight and polydispersity values of synthesized cyclopolymers in molar ratios of 200:1, 100:1, and 50:1 [TB monomer]: [AIBN]. As a result, the highest molecular weight was achieved by 200:1 [TB monomer]: [AIBN] mol ratio cyclopolymer as 65K, while the lowest one was achieved by 50:1 [TB monomer]: [AIBN] mol ratio as 33K, as expected.

Cellulose acetate/*tert*-butyl cyclopolymer (CA/TBCP) blend composite membranes were fabricated by the non-solvent induced phase separation (NIPS) method. The effect of the CA/TBCP blend ratio on the morphology, porosity, hydrophobicity, and desalination performance of the resulting membranes was investigated. Morphological analysis of CA/TBCP composite membranes showed that with the addition of TBCP to the casting solution, macro voids were formed in the porous sub-layer of the membranes. When amorphous TBCP was added to the semi-crystalline CA matrix, it was observed that the flux values increased significantly. The reason for this increase was attributed to the loosely packed nature of the amorphous polymer in the membrane matrix, resulting in higher void content and porosity, through which the transportation occurs (Maheswari et al., 2013).

The performance evaluations of fabricated membranes with NaCl solution filtrations demonstrated that the addition of TBCP to the casting solution tends to decrease the salt rejection values, whereas the flux performance tends to increase. An optimum trade-off between the flux increase and little or no change in the salt rejection values for fabricated membranes offers great potential for these membranes in RO applications of CA-based membranes.

The performance evaluations of fabricated membranes with MgSO_4 water solution filtrations showed that the CA/TBCP composite membranes also offer great potential as nanofiltration membranes. It was demonstrated that until 8% TBCP addition blend membranes the salt rejections remained the same as 25%CA membranes, at 100%. Upon 8% TBCP addition, the salt rejections were decreased slightly, but the flux values were increased significantly. For instance, for 17%CA+8% TBCP 49K membrane, the salt rejection value slightly decreased from 100% to 97.12%; however, the flux performance improved by 200% compared to 25% CA containing control membrane. The stability of the membranes was also investigated, and it was demonstrated that CA/TBCP composite membranes were quite stable within 120 minutes of filtration under high pressure.

Water contact angle analysis of fabricated membranes showed that the hydrophobicity of CA membranes increased upon the incorporation of TBCP addition, due to the hydrophobic nature of TBCP, which is thought to be helpful for the prevention of membrane fouling.

Two different membrane casting compositions were prepared 20%(CA+TBCP 49K) and 25% (CA+TBCP 49K) for the investigation of the effect of casting solution concentration on the structure and performance of resulting membranes. With the higher concentration of the polymer blend in the casting solution, higher salt rejection values were obtained, although a decrement in flux values was observed. This is because denser membranes were obtained by increasing the polymer content in the casting solution.

Finally, the effect of the molecular weight of TBCP on the desalination performance of resulting membranes was also investigated. For this purpose, 17% CA+ 8% TBCP membranes were prepared from TBCP 33K, TBCP 49K, and TBCP 65K. When the molecular weight of the TBCP component increased, the porosity of the membrane sub-layer also increased, which resulted in higher flux and lower salt rejection values. Since TBCP 33K has shorter polymer chains, it created smaller pores in the CA/TBCP matrix, yet the number of pores per unit area was higher than the TBCP 49K and 65K CA/TBCP membranes. And for the TBCP 65K membranes, longer polymer chains created bigger pores, but the number of pores per unit area decreased compared to TBCP 33K, which explains the fluctuations in salt rejection rates and flux performance of membranes depending on the molecular weight of TBCP component.

CHAPTER 4

4. IONICALLY CROSSLINKED CARBOXYLIC ACID FUNCTIONAL CYCLOPOLYMER MEMBRANES

4.1. Materials and Methods

4.1.1. Materials

Cellulose acetate (average $M_n \approx 30,000$ by GPC), paraformaldehyde (reagent grade, crystalline), 1,4-diazabicyclo[2.2.2]octane (DABCO, $\geq 99.5\%$), *tert*-butyl acrylate, (98%), *tert*-butanol, ($\geq 99.5\%$), 2,2'-azobis(2-methylpropionitrile) (AIBN) (0.2 M toluene solution), toluene ($\geq 99.5\%$), methylene chloride (anhydrous $\geq 99.8\%$), methanol ($\geq 99\%$), acetic acid (glacial, 100%), sodium chloride ($\geq 99.5\%$), magnesium sulfate ($\geq 99\%$), calcium chloride (CaCl_2), 1,4- dioxane (anhydrous, 99.8%), were purchased from Sigma-Aldrich (St. Louis, MO, ABD). Acetone (for analysis), trifluoroacetic acid (for synthesis), and sodium hydroxide (0.1 N, volumetric solution) were purchased from Merck & Co., Inc. (USA). Hydrochloric acid, fuming (37%), iron (III) chloride ($\text{FeCl}_3 \cdot 6\text{H}_2\text{O}$), zinc chloride (ZnCl_2), and cobalt (II) chloride ($\text{CoCl}_2 \cdot 6\text{H}_2\text{O}$) were purchased from ISOLAB GmbH. Aluminum nitrate-9-hydrate ($\text{AlCl}_3 \cdot 6\text{H}_2\text{O}$) purchased from Honeywell (Morriston, NJ, USA.) JQM-PS-500 model polysulfone (0.05-micron pore size) from abroad was used as membrane backing material. All glassware, needles, and stirring bars were dried overnight in an oven at 120 °C. Deionized (DI) water obtained from Merck Millipore Direct-Q 3UV ultrapure water system was used in filtration experiments and analysis.

4.2. Experimental

4.2.1.1. Synthesis of carboxylic acid functional cyclopolymers

Carboxylic acid functional cyclopolymers were synthesized by acid hydrolysis of *tert*-butyl cyclopolymers. *Tert*-butyl groups from the polymer chain were converted to carboxylic acid groups by hydrolysis reaction as shown in Figure 4.1 (Rikkou-Kalourkoti et al., 2012a; Tsuda & Mathias, 1994).

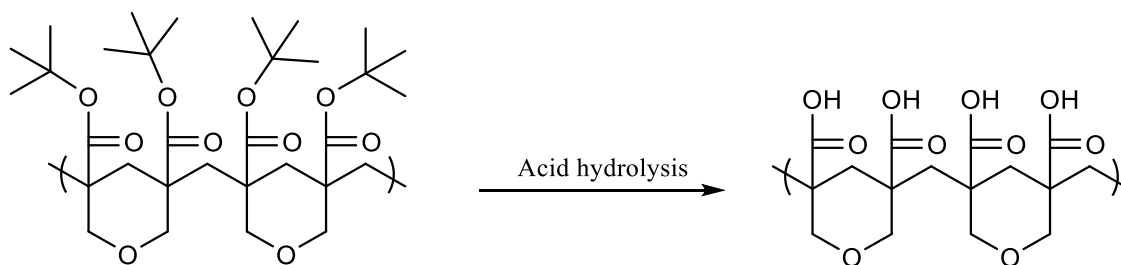


Figure 4.1 Acid hydrolysis of *tert*-butyl cyclopolymer

The carboxylic acid cyclopolymer was obtained by hydrolysis of TBCP with trifluoroacetic acid. A 12 % (w/v) methylene chloride solution of *tert*-butyl cyclopolymer was prepared, and TFA equivalent to 5 moles of *tert*-butyl ester groups was added to the solution. The reaction mixture was stirred at room temperature for 24h. The acid cyclopolymer formed as a precipitate was filtered and washed with methylene chloride and then dried in a vacuum oven. The synthesis of carboxylic acid cyclopolymers were shown in Figure 4.2.

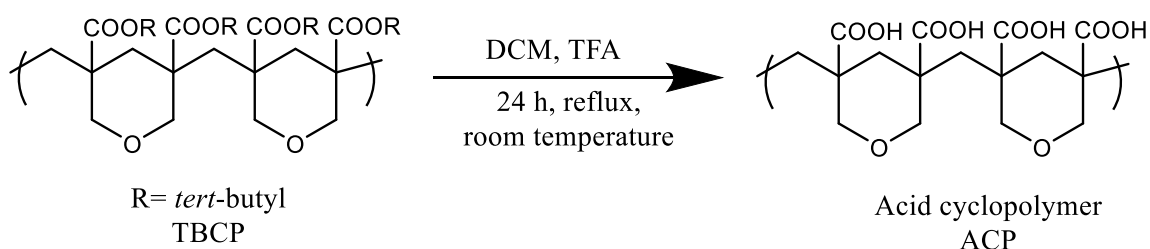


Figure 4.2 Synthesis of carboxylic acid cyclopolymer

4.2.1.2. Degree of carboxylic acid groups by titration

The hydrolysis degree of carboxylic acid groups was calculated by acid-base titration using NaOH as a titrant and bromothymol blue as a pH indicator. A 0.1% (w/v) methanol solution of the acid cyclopolymer was prepared and a few drops of bromothymol blue were added to the solution. Titration was performed with 0.1N NaOH standard volumetric solution until the equivalence point was reached. The volume of the spent NaOH solution

was converted to NaOH moles. Since the acid polymer solution was neutralized with NaOH, the mole amount of NaOH consumed is equal to the mole amount of -COOH groups. The weight of 1 repeating unit of the acid cyclopolymer was calculated as 186.16 grams. Each repeating unit has 2 -COOH groups. In this case, there should be 1.08 mmol -COOH group in 0.1 g of 100% hydrolyzed TBCP. Accordingly, the percent degree of hydrolysis was calculated by proportioning the mole amount of COOH of the titrated acid cyclopolymer solution to the mole amount of COOH in the 100% hydrolyzed TBCP.

4.2.1.3. Fabrication of ionically crosslinked carboxylic acid cyclopolymer membranes

For the fabrication of ionically crosslinked carboxylic acid cyclopolymer membranes, the studies of Habert et al. were taken as a reference. Habert et al. worked on ionically crosslinked polyacrylic acid membranes. They applied two different techniques, wet and dry, in the production of membranes (Habert, Burns, et al., 1979; Habert, Huang, et al., 1979). Since acid cyclopolymer contains carboxylic acid groups like polyacrylic acid, dry and wet techniques were likewise adapted for the fabrication of ionically crosslinked carboxylic acid cyclopolymers. Figure 4.3 shows the metal ion coordination crosslinking reaction in the carboxylic acid cyclopolymer membrane.

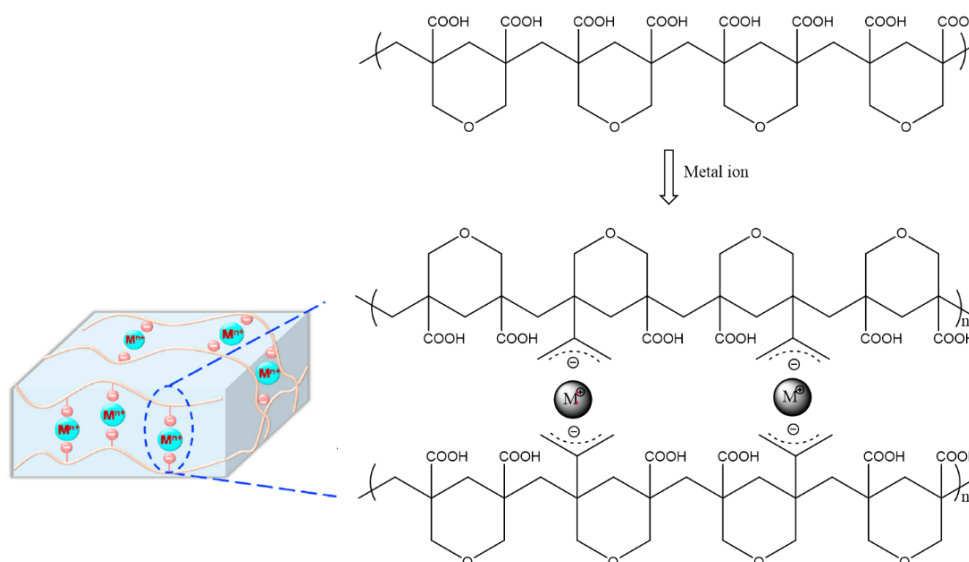


Figure 4.3 Schematic diagram of the metal ion coordination crosslinking reaction in carboxylic acid cyclopolymer membrane.

For the fabrication of ionically crosslinked carboxylic acid cyclopolymer thin film composite membranes, PSF UF membranes were used as a support layer. The technical specifications of the commercially available UF PSF membrane are given in Table 4.1.

Table 4.1 Technical properties of UF PSF membrane.

Model: JQM-PS-500	Technical properties
Pore (micron)	0.05
Retention rate	% 100, 10^7 cfu/cm ²
Maximum operating temperature	125 °C
Maximum temperature tolerance	185 °C
Sterilization condition	121 °C, 30 min
Flux	0.15 t/m ² .h

4.2.1.3.1. Fabrication of ionically crosslinked carboxylic acid cyclopolymer membranes: wet technique

In the wet technique, the acid cyclopolymer was first dissolved in methanol and its solution was prepared. After the polysulfone support layer was wetted with the prepared solution, the membrane was immersed in a solution in which metal ions were dissolved. Metal ions were expected to interact with the carboxylic acid cyclopolymer phase on the surface and form ionic crosslinking with existing carboxylic acid groups. The formation of a metal ion cross-linked active layer was observed after the membrane was kept in a metal ion solution for an appropriate time. In the composite membranes produced with the wet technique, the temperature of the metal ion solution, the duration of the membrane to stay in the metal ion solution, and the valence number of the metal salt used are the factors affecting the degree of crosslinking. At the same time, the crosslinking density can be changed by adding a base such as sodium hydroxide to the membrane polymer solution (Habert, Huang, et al., 1979). The wet technique for the production of ionically crosslinked ACP membranes was shown schematically in Figure 4.4.

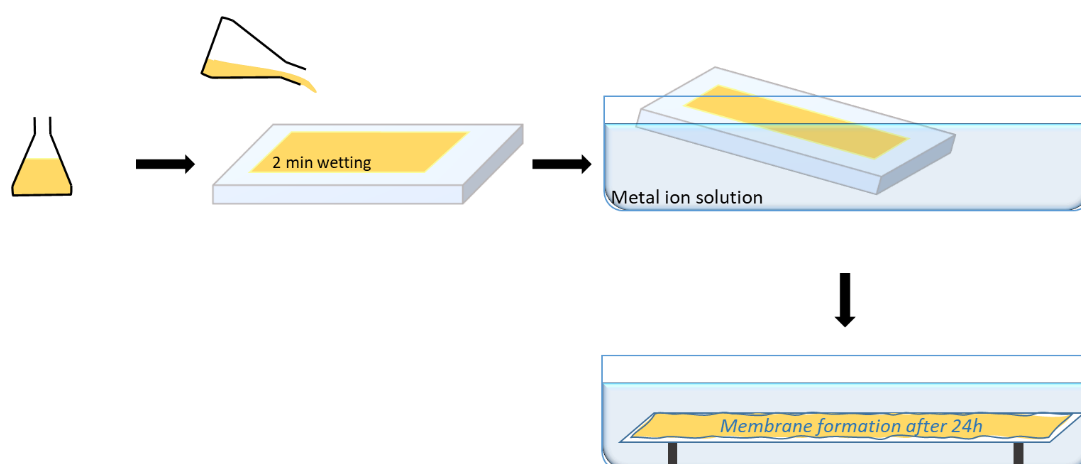


Figure 4.4 Schematic representation of wet technique for the production of ionically crosslinked ACP membranes

For the production of ionically crosslinked carboxylic acid cyclopolymer membranes by the wet technique, three different membranes were produced under different conditions. An acid cyclopolymer methanol solution of 5%(w/v) was prepared and poured onto the polysulfone support layer. It was allowed for 2 minutes for the acid polymer solution to be absorbed by the polysulfone support layer and penetrate the pores, and then the excess solution was poured off. Then, the air drying was done for 5 minutes. The resulting film was immersed in a 10% iron metal ion solution and left overnight at room temperature for the formation of membrane. The casting solution composition and metal ion solutions were prepared differently to see their effect on membrane formation and performance. The membranes produced by the wet technique are given in Table 4.2.

Table 4.2 The composition of the casting solutions prepared in the production of metal ion cross-linked ACP membranes by wet technique and the parameters in membrane production

Membrane code	Casting Solution Composition	Preparation conditions	Metal ion solution	Metal ion bath temperature/ duration
Wet-1	ACP in MeOH 5% w/v	2 min wetting then draining, 5 min air drying	10% FeCl ₃ in water solution	24°C, overnight
Wet-2	ACP in MeOH 5% w/v	2 min wetting then draining, 5 min air drying	10% FeCl ₃ in MeOH solution	24°C, overnight
Wet-3	ACP in water 5% w/v +0.34 g NaOH (1 eq. COOH)	2 min wetting then draining, 5 min air drying	10% FeCl ₃ in MeOH solution	24°C, overnight

4.2.1.3.2. Fabrication of ionically crosslinked carboxylic acid cyclopolymer membranes: dry technique

In the dry technique, the polymer solution and the metal ion solution were prepared separately. A 20% acid polymer methanol solution was mixed with a metal ion methanol solution. The prepared membrane solution was poured onto the polysulfone support layer and waited for 2 minutes for the solution to be absorbed. Then the membrane was squeezed with a roller to obtain a thin film layer and put in the oven. The membrane was dried(cured) at 80 °C for 2 hours. It was aimed to increase the acid cyclopolymer-metal ion

crosslinking density by curing the membranes produced by the dry technique under heat in the oven (Habert, Burns, et al., 1979). After that, membranes were left at room temperature until cooled down. Each membrane was kept in deionized water until performance testing. The production scheme of membranes by the dry technique was given in Figure 4.5.

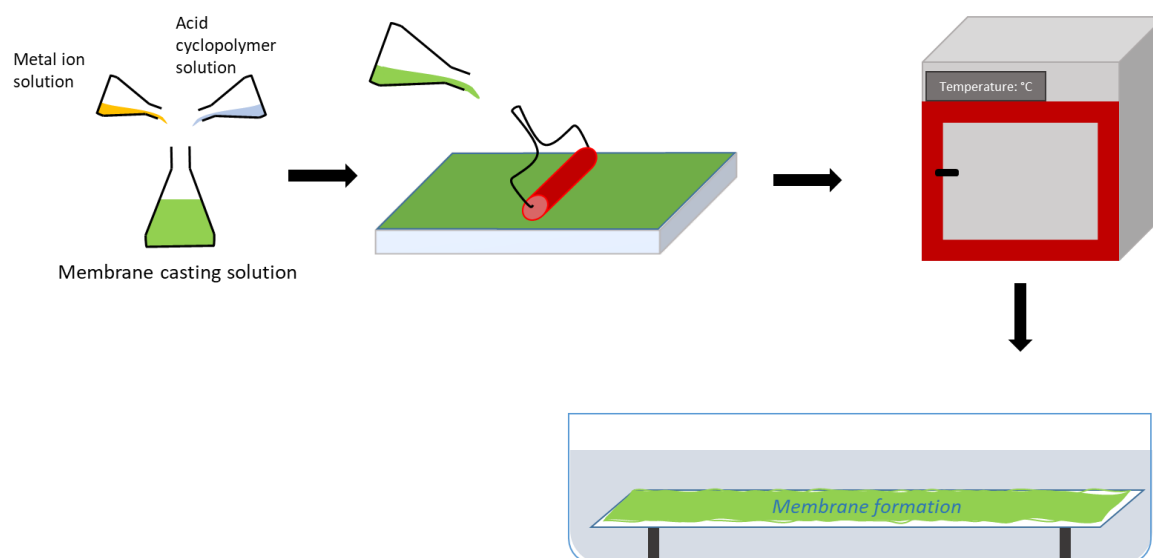


Figure 4.5 Schematic representation of dry technique for the production of ionically crosslinked ACP membranes

For the dry technique, 5 different metal salts were used for ionically crosslinked carboxylic acid cyclopolymer membranes. The used metal salts and their molecular weights are given in Table 4.3.

Table 4.3 Metal salts used for crosslinking and their molecular weights

Metal Salt	MW (g/mol)
FeCl ₃ .6H ₂ O	270.30 g/mol
CoCl ₂ .6H ₂ O	237.90 g/mol
ZnCl ₂	136.30 g/mol
AlCl ₃ .6H ₂ O	241.43 g/mol
CaCl ₂	110.98 g/mol

For the production of Fe metal ion cross-linked membranes by the dry technique, the casting solutions with different [COOH: Metal ion] mole ratios were prepared and the effect of the amount of metal ion on crosslinking and membrane performance was investigated. The preparation conditions of the ionically crosslinked acid cyclopolymer membranes were given in Table 4.4.

Table 4.4 The composition of the casting solutions prepared in the production of metal ion cross-linked ACP membranes by dry technique and the parameters in membrane production

Membrane code	Solution composition	[COOH: Metal ion] mole ratio	Preparation	Membrane curing temperature and duration
Fe (7:1)	2 g ACP in 10 mL MeOH (20%) + 0.00307 mol Fe in 10 mL MeOH	7:1	2 mins wetting then squeezing	80°C, 2 hours then cooled in RT.
Fe (15:1)	2 g ACP in 10 mL MeOH (20%) + 0.00143 mol Fe in 10 mL MeOH	15:1	2 mins wetting then squeezing	80°C, 2 hours then cooled in RT.
Al	2 g ACP in 10 mL MeOH (20%) + 0.00307 mol Al in 10 mL MeOH	7:1	2 mins wetting then squeezing	80°C, 2 hours then cooled in RT.
Zn	2 g ACP in 10 mL MeOH (20%) + 0.00307 mol Zn in 10 mL MeOH	7:1	2 mins wetting then squeezing	80°C, 2 hours then cooled in RT.
Co	2 g ACP in 10 mL MeOH (20%) + 0.00307 mol Co in 10 mL MeOH	7:1	2 mins wetting then squeezing	80°C, 2 hours then cooled in RT.
Ca	2 g ACP in 10 mL MeOH (20%) + 0.00307 mol Ca in 10 mL MeOH	7:1	2 mins wetting then squeezing	80°C, 2 hours then cooled in RT.

All membrane casting compositions were prepared at room temperature according to described conditions. Then all the membranes were kept in distilled water until use.

4.2.2. Characterization

The characterization techniques (NMR, FT-IR, TGA, SEM) described in section 3.1.3 were applied to ionically crosslinked carboxylic acid cyclopolymer membranes. Additionally, Energy Dispersive X-ray (EDS) is applied.

4.2.2.1. Energy Dispersive X-ray Analysis (EDS)

In order to examine the elemental analysis of the membrane surface Bruker Nano GmbH Berlin, Germany Esprit 2.0 was used for EDS analysis.

4.2.3. Membrane Filtration Performance

4.2.3.1. Desalination performance

The desalination performance of the produced metal ion crosslinked ACP membranes was investigated by filtration of 2000 ppm NaCl or MgSO₄ aqueous solutions. The calibration curves and equations shown in sections 0 and 3.1.4.3 were used to determine the membrane performance.

4.3. Results and Discussion

4.3.1. Synthesis of carboxylic acid functional cyclopolymers

Carboxylic acid functional cyclopolymers were synthesized by acid hydrolysis of *tert*-butyl cyclopolymers with trifluoroacetic acid for 24 hours, as shown in Figure 4.6.

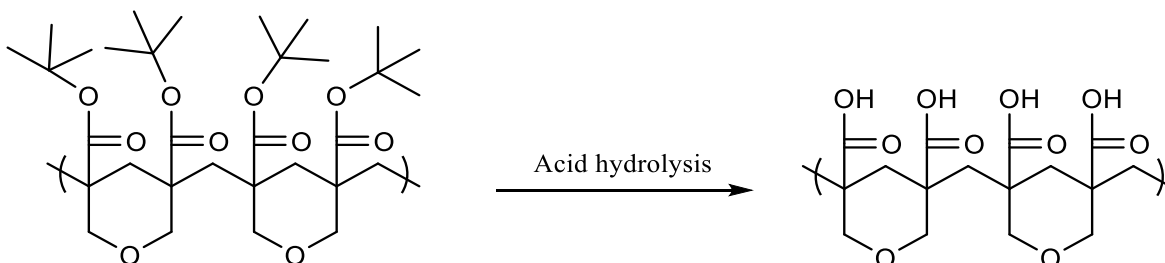


Figure 4.6 Synthesis of carboxylic acid cyclopolymer

The change of the hydrolysis degree depending on the reaction time was investigated. In the hydrolysis reaction, the molar amount of TFA was used about 5 times the molar amount of ester groups. The polymer concentration was also about 12% (w/v). It was observed that the degree of hydrolysis increased rapidly until the second hour but slowed down, especially after the eighth hour as can be seen from Figure 4.7.

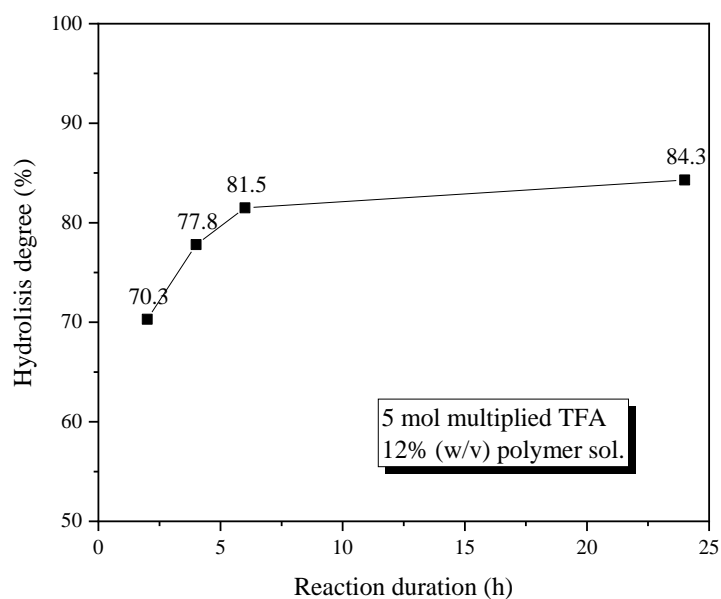


Figure 4.7 Graph of the degree of hydrolysis over time (TFA/ester molar ratio: 5, polymer concentration: 12%, solvent: DCM)

After the synthesis of carboxylic acid cyclopolymer (ACP), ^{13}C NMR analysis was applied at 500 MHz, in DMSO-d_6 to confirm the structure. The ^{13}C NMR spectrums of TBCP and ACP were compared to see the differences in the peaks.

^{13}C NMR spectrum of ACP was shown in Figure 4.8 with the peak of f,d δ : 40.12 (backbone C), the peak of g at δ : 45.3 ppm (backbone C_q), the peak of e at δ : 71.0 ppm (OCH_2C_q), the peak of c at δ : 174.2 ppm ($\text{C}_q\text{COOC}(\text{CH}_3)_3$) (Tsuda & Mathias, 1994).

^{13}C NMR spectrum of TBCP was shown in Figure 4.9 with the peak of a at δ : 28.1 ppm ($\text{OC}(\text{CH}_3)_3$), the peak of g at δ : 45.3 ppm (backbone C_q), the peak of e at δ : 71.0 ppm (OCH_2C_q), the peak of b at δ : 82.1 ppm ($\text{OC}(\text{CH}_3)_3$), the peak of c at δ : 174.2 ppm ($\text{C}_q\text{COOC}(\text{CH}_3)_3$).

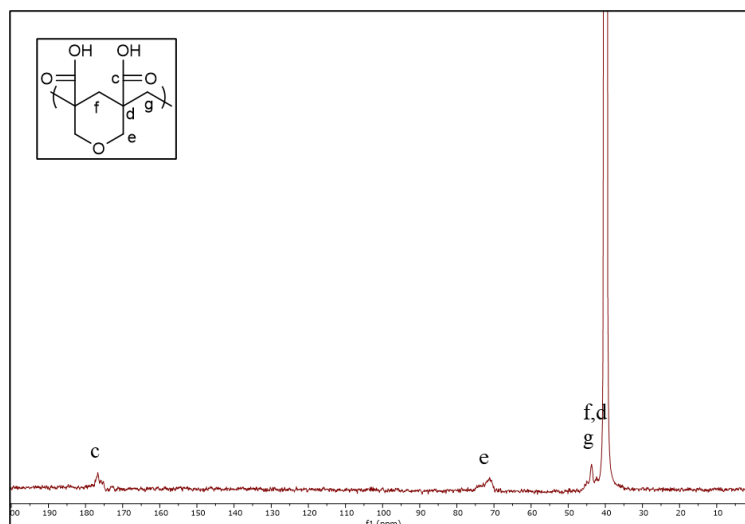


Figure 4.8 ^{13}C NMR spectrum for ACP

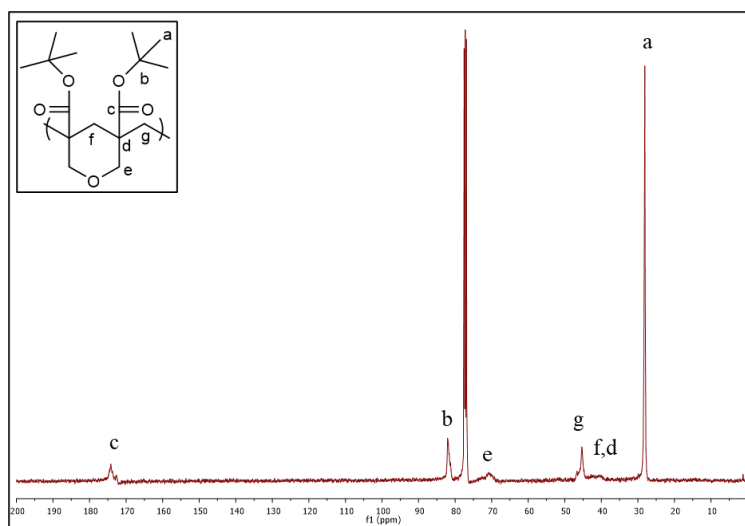


Figure 4.9 ^{13}C NMR of TBCP

When the ^{13}C NMR spectrums of TBCP and ACP were compared, it was seen that the peak of a at δ : 28.1 ppm ($\text{OC}(\text{CH}_3)_3$) and the peak of b at δ : 82.1 ppm ($\text{OC}(\text{CH}_3)_3$) in the ^{13}C NMR spectrum of TBCP disappeared in the ^{13}C NMR spectrum of ACP. This indicated the loss of the *tert*-butyl groups in TBCP and confirmed the chemical structure of ACP (Tsuda & Mathias, 1994).

Thermal gravimetric analysis (TGA) was performed to determine the thermal stability of carboxylic acid cyclopolymers. In ACP, the mass reduction below 110-120 $^\circ\text{C}$ is due to the loss of water adsorbed in the ACP. The second decomposition started around 180-200 $^\circ\text{C}$, which may be due to the elimination of the remaining *tert*-butyl ester groups in the ACP. The basic decomposition started around 350 $^\circ\text{C}$ and continued up to 500 $^\circ\text{C}$, which was caused by the decomposition of carboxylic acid and cyclic structures

(depolymerization)(Bavisotto et al., 2021). In TBCP, two decomposition temperatures were detected. The initial thermal decomposition temperature was 180-200 °C. It is known that tertiary-alkyl ester groups generally dissociate olefinically when heated to this temperature (Mathias et al., 1991). The basic decomposition started around 350 °C and continued up to 500 °C, which was caused by the decomposition of carbonyl (-COO-) and cyclic structures (depolymerization). Figure 4.10 and Table 4.5 shows the TGA results of ACP and TBCP 49K.

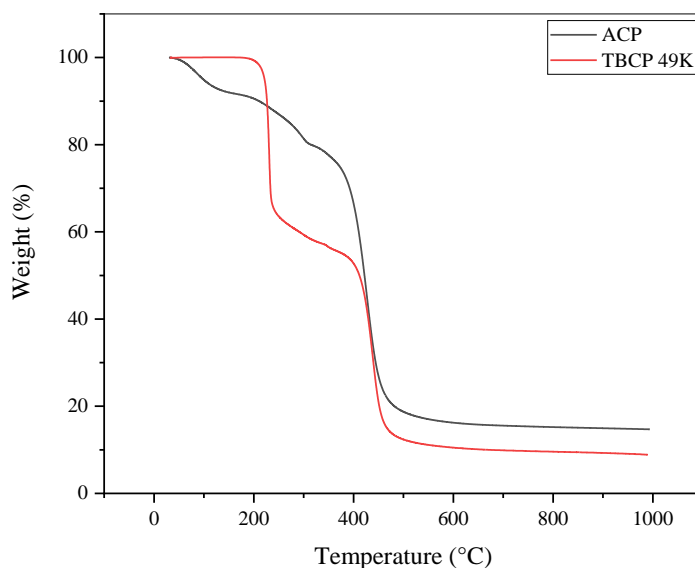


Figure 4.10 TGA results of ACP and TBCP 49K

Table 4.5 TGA results of ACP and TBCP 49K

Sample	Decomposition temperatures (°C)	5% Decomposition temperature	The residue (%)
ACP	91.60°C, (T_{d1}) 265.27 °C, (T_{d2}) 424.78 °C, (T_{d3})	98.51	12%
TBCP 49K	180 °C (T_{d1}) 280 °C (T_{d2})	221	9%

TGA analysis was also applied to ACPs having different hydrolysis degrees. As can be seen from Figure 4.11, the weight loss decreases as the degree of hydrolysis increases. The calculated hydrolysis degrees are consistent with the TGA thermograms.

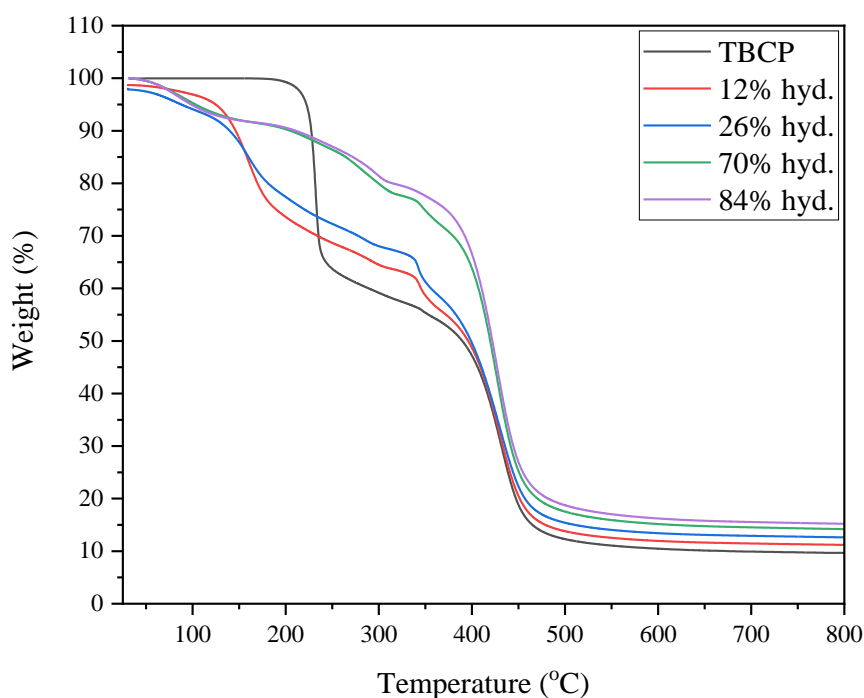


Figure 4.11 TGA thermogram comparison of carboxylic acid cyclopolymers having different hydrolysis degrees

FTIR spectrometry was used to examine the chemical structure of the carboxylic acid cyclopolymer. The ACP was synthesized by the hydrolysis reaction of TBCP 49K synthesized with a mole ratio of 100:1 [M]: [I]. FTIR curves of both polymers (ACP and TBCP 49K) were given in Figure 4.12 to compare their chemical structures. The C-H bond peaks were observed at 2913 cm^{-1} and 1368 cm^{-1} in the FTIR spectrum of TBCP, and the intensity of these peaks decreased in the spectrum of ACP. A peak around 2580 cm^{-1} appeared due to the carboxylic acid groups formed by the hydrolysis of TBCP. The intensity of this peak increases with increasing degree of hydrolysis. It was observed that the peaks of C=O and C-O in the spectrum of TBCP were around 1700 cm^{-1} and 1240 cm^{-1} , respectively, and these peaks shifted in the FTIR spectrum of ACP.

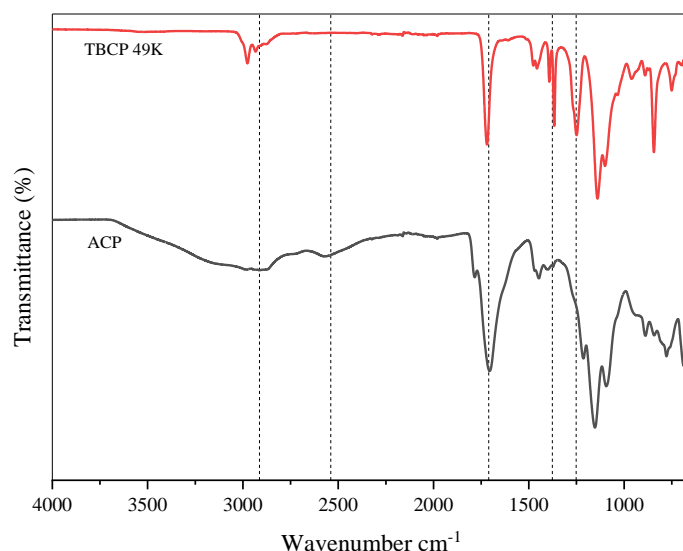


Figure 4.12 FTIR spectrum of TBCP and ACP

4.3.2. Preparation of metal ion crosslinked acid cyclopolymer membranes

Ionically crosslinked acid cyclopolymer membranes with metal ions were prepared by the wet or dry technique according to the procedure described in sections 4.2.1.3.1 and 4.2.1.3.2.

Since a homogeneous film could not be obtained from Wet-2 and Wet-3 coded membranes, performance tests could not be applied to these membranes. Wet-1 coded membrane was used in performance tests.

Table 4.6 The composition of the casting solutions and preparation conditions of produced metal ion cross-linked ACP membranes by wet technique and resulting membrane properties

Membrane code	Casting Solution Composition	Preparation conditions	Metal ion solution	Metal ion bath temperature/duration	Result
Wet-1	ACP in MeOH 5% w/v	2 min wetting then draining, 5 min air drying	10% FeCl ₃ in water solution	24°C, overnight	A homogeneous film formed on the surface of PSF.
Wet-2	ACP in MeOH 5% w/v	2 min wetting then draining, 5 min air drying	10% FeCl ₃ in MeOH solution	24°C, overnight	A non- homogeneous film formed on the surface of PSF.

Wet-3	ACP in water 5% w/v +0.34 g NaOH (1 eq. COOH)	2 min wetting then draining, 5 min air drying	10% FeCl ₃ in MeOH solution	24°C, overnight	A non- homogeneous film formed on the surface of PSF.
-------	--	--	---	--------------------	---

4.3.3. Characterization

The FTIR spectra of the membranes were examined for bonding information on the membrane surface. When the FTIR spectrums given in Figure 4.13 are examined, the peaks around 400-800 cm⁻¹ wavenumber can be defined as the metal-oxygen stress peaks of the metal-carboxyl bond. There is an OH peak around 3260 cm⁻¹ due to carboxylic acid. This peak is not present in the PSF neat membrane. The strong peaks were seen around 1150-1085 cm⁻¹ corresponding to C-O stretching. The peaks around 1700 cm⁻¹ belonging C=O bonds and around 1275-1200 cm⁻¹ peaks representing strong C-O stretching were seen in the FTIR spectrum (Köse & Necefoglu, 2008). There is a strong peak around 1350-1300 cm⁻¹ due to S=O stretching of the PSF support layer (Kumari et al., 2013).

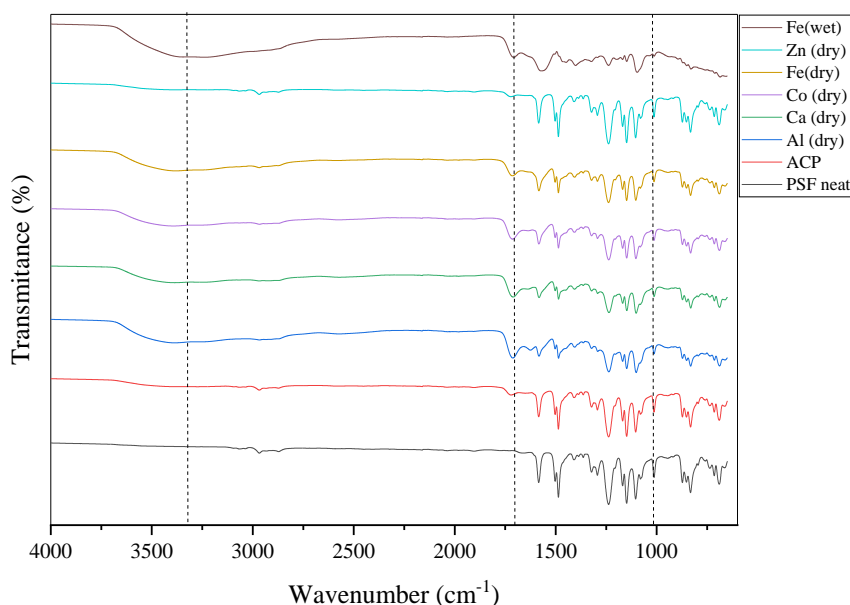


Figure 4.13 FTIR spectrum of the ionically crosslinked ACP membranes

TGA analysis was applied to ionically crosslinked ACP membranes for the investigation of thermal stabilities. As can be seen from Table 4.7 and Figure 4.14, a 5% thermal decomposition temperature was increased in metal ion crosslinked membranes. Higher

residues in metal ion crosslinked membranes compared to ACP neat membrane are due to remaining metal ions. It was observed that the highest metal ion content was in the ionically crosslinked ACP membranes produced with Fe metal salt.

Table 4.7 TGA analysis results of ionically crosslinked ACP membranes

Sample	Decomposition Temperature T_d (°C)	5% Decomposition Temperature T_d (°C) 5%	The residue (%)
Control ACP	431 606	383	7.89
Fe (dry)	433 530	394	20.99
Fe (wet)	433 530	390	21.74
Al (dry)	433 530	398	18.69
Zn (dry)	433 530	396	17
Co (dry)	433 528	397	18.08

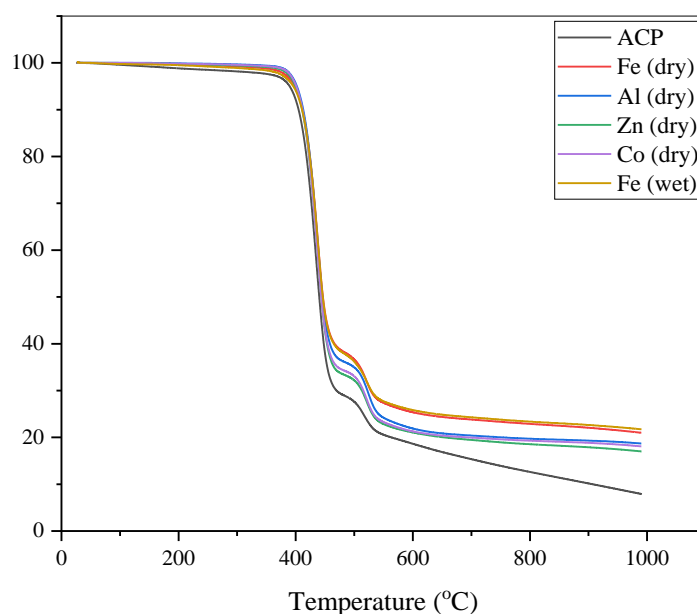
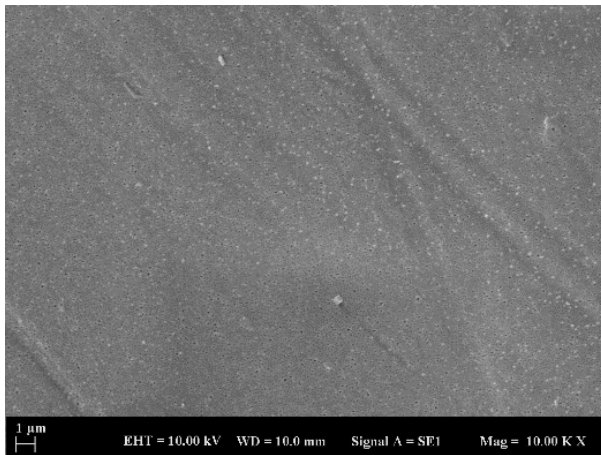
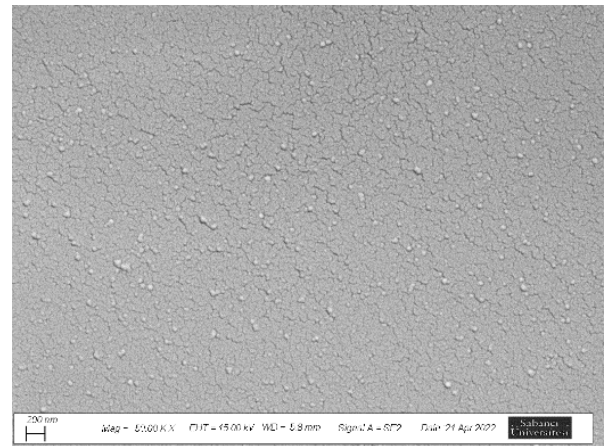


Figure 4.14 TGA thermogram of ionically crosslinked ACP membranes

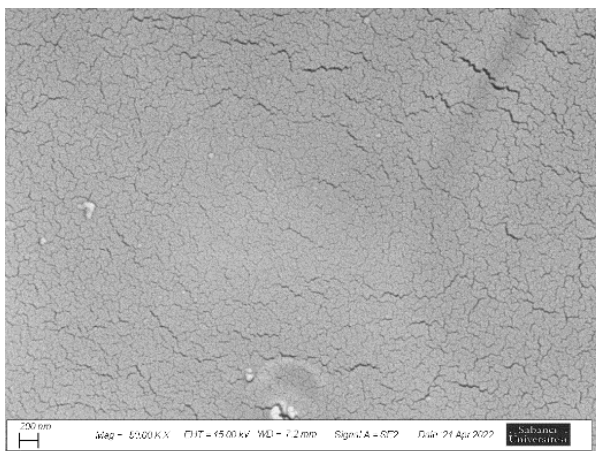
Scanning electron microscopy (SEM) was used for cross-sectional and surface morphology analysis of the produced membranes and the SEM images were shown in Figure 4.15 and Figure 4.16. The surface and cross-section SEM images of the produced TFC membranes were compared with the surface and cross-section images of the neat PSF membrane to see the morphological changes. The PSF UF membrane surface has a porous structure as can be seen in Figure 4.15 (a). The distribution of pores appears homogenous. The cross-section thickness of the PSF membrane was measured as $36.51 \pm 1.36 \mu\text{m}$ and a sponge-like structure was observed at the cross-section as can be seen in Figure 4.16 (a). In the produced membranes, it was seen that the pores on the surface of the PSF membrane were closed by a film formed by metal-ion crosslinking reactions of acid cyclopolymer as can be seen from the Figure 4.15 (b), (c), (d) and (e). In the cross-sectional analysis, it was observed that the ionically crosslinked acid cyclopolymer membrane solution formed a thin film on the surface of the PSF membrane as can be seen from the Figure 4.16 (b), and (c).



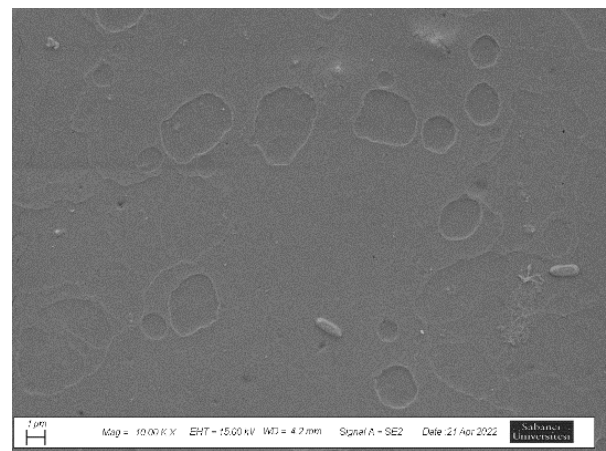
(a) PSF



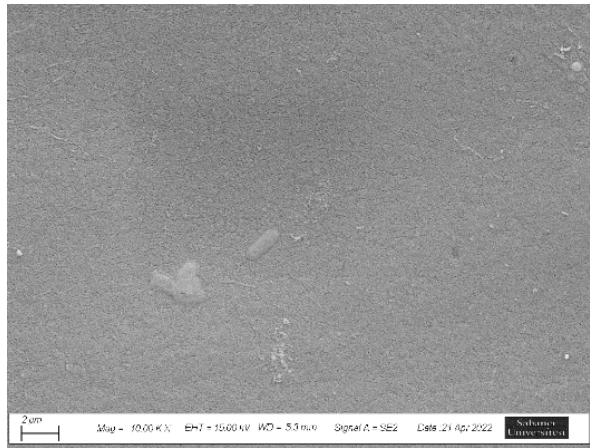
(b) Fe (wet)



(c) Fe (dry)

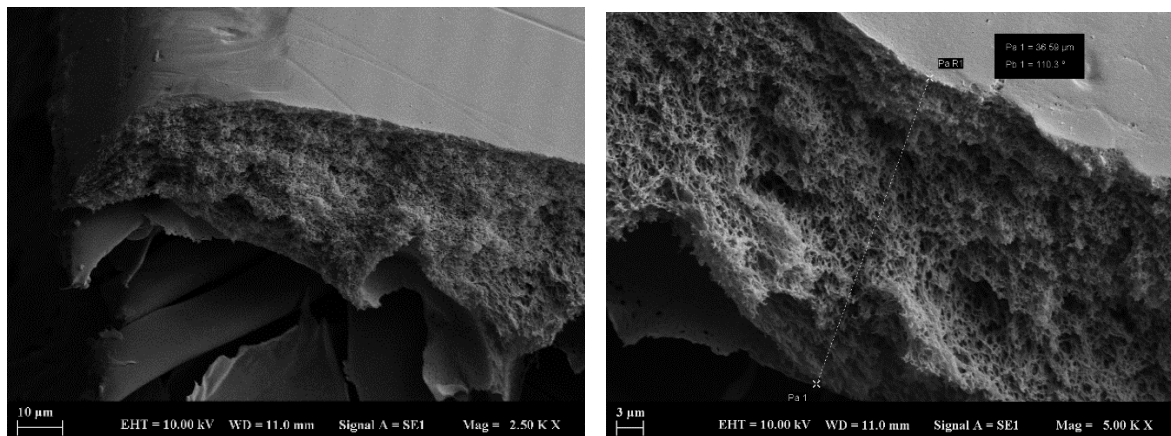


(d) Al (dry)

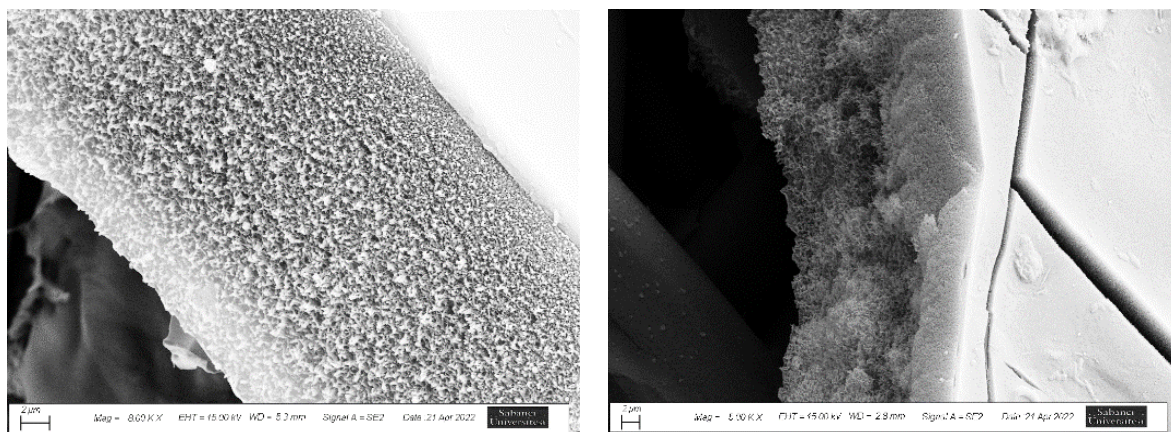


(e) Zn (dry)

Figure 4.15 SEM images of the surface of ionically crosslinked ACP membranes and PSF UF membrane



(a) PSF cross-section



(b) Fe (wet)

(c) Fe (dry)

Figure 4.16 Cross-sectional SEM images of the ionically crosslinked ACP membranes and PSF UF membrane

SEM-EDS characterization was applied for the surface elemental analysis of the membranes. Table 4.8 and Figure 4.17 give the metal atom percentages on the surfaces of

the membranes according to the SEM-EDS analysis. The highest metal contents were observed in the membranes produced by the wet and dry technique using Fe metal salt, which are 48.7% and 44.08% respectively. Therefore, these membranes are considered to have the highest crosslinking density. The metal contents in the membranes produced by the crosslinking reaction of Zn and Al salts with ACP are 6.01% for Zn and 6.96% for Al.

Table 4.8 EDS analysis results as atomic percentages of the elements

Element	Atom [%]
Fe (dry)	44.08
Fe (wet)	48.7
Zn (dry)	6.01
Al (dry)	6.96

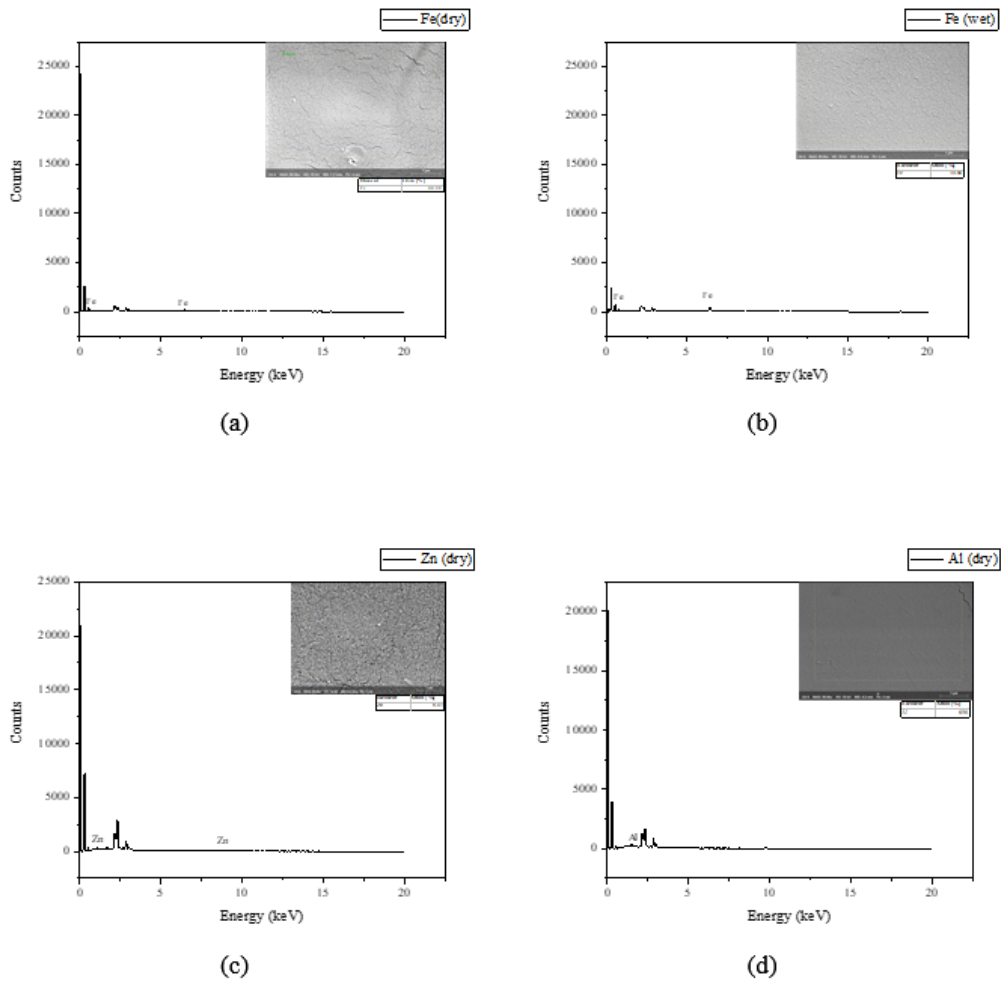


Figure 4.17 EDS analysis results of the ionically crosslinked ACP membranes. (a) Fe(dry); (b) Fe (wet); (c) Zn (dry); (d) Al (dry).

4.3.4. Filtration performance

4.3.4.1. Desalination

- Dry technique membranes NaCl filtration performance:

2000 ppm of NaCl aqueous solution filtration test was applied to the membranes for investigation of desalination performance. The performance results were given in Table 4.9 and Figure 4.18.

Table 4.9 Dry technique metal ion crosslinked ACP membranes 2000 ppm of NaCl aqueous solution filtration performance results

Membrane code	Solution composition	[COOH: Metal ion] mole ratio	Preparation	Membrane curing temperature and duration	Flux, J (L/m ² h)	Salt Rejection, R (%) 2000 ppm NaCl 15 bar filt.
Fe 15:1 (dry)	2 g ACP in 10 mL MeOH (20%) + 0.00143 mol Fe in 10 mL MeOH	15:1	2 mins wetting then squeezing	80°C, 2 hours then cooled in RT.	7.15±2.84	59.49±6.54
Fe 7:1 (dry)	2 g ACP in 10 mL MeOH (20%) + 0.00307 mol Fe in 10 mL MeOH	7:1	2 mins wetting then squeezing	80°C, 2 hours then cooled in RT.	8 ± 1.6	64.2 ± 0.2
Al (dry)	2 g ACP in 10 mL MeOH (20%) + 0.00307 mol Al in 10 mL MeOH	7:1	2 mins wetting then squeezing	80°C, 2 hours then cooled in RT.	11.2 ± 2.4	64.1 ± 2.9
Zn (dry)	2 g ACP in 10 mL MeOH (20%) + 0.00307 mol Zn in 10 mL MeOH	7:1	2 mins wetting then squeezing	80°C, 2 hours then cooled in RT.	16.41±1.27	47.56±0.1

Co (dry)	2 g ACP in 10 mL MeOH (20%) + 0.00307 mol Co in 10 mL MeOH	7:1	2 mins wetting then squeezing	80°C, 2 hours then cooled in RT.	55.6± 19.1	9.1±3.6
Ca (dry)	2 g ACP in 10 mL MeOH (20%) + 0.00307 mol Ca in 10 mL MeOH	7:1	2 mins wetting then squeezing	80°C, 2 hours then cooled in RT.	49.6 ± 6.7	13.3 ± 0.4

2000 ppm NaCl salt of deionized water solution was prepared, and desalination performance tests were applied at room temperature in the dead-end filtration system under 15 bar pressure nitrogen gas.

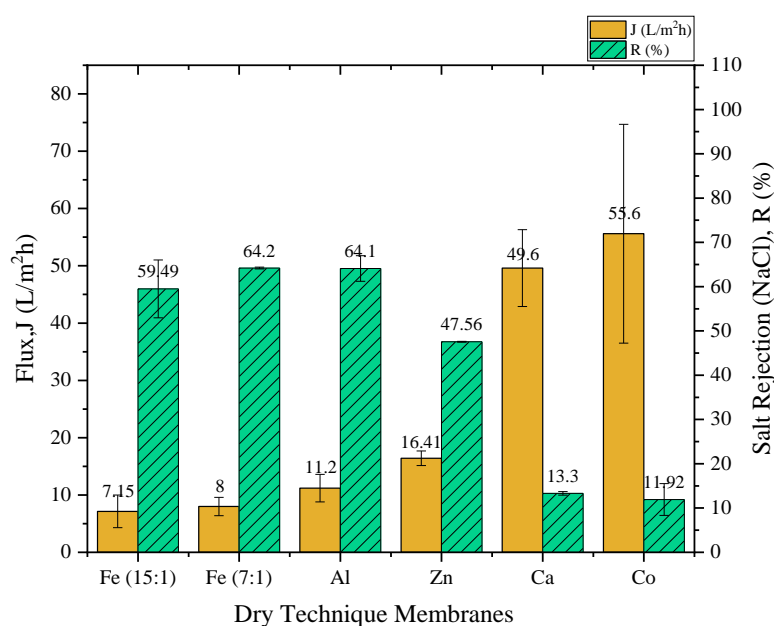


Figure 4.18 Dry technique metal ion crosslinked ACP membranes 2000 ppm of NaCl aqueous solution filtration performance results

It can be seen from Figure 4.18 that the membrane produced by the dry technique using Fe salt with a mole ratio of 7:1 [COOH: Metal ion] has higher salt rejection values than the membrane produced with a mole ratio of 15:1 [COOH: Metal ion]. This may be due to increased crosslinking ratio with increasing mole content of Fe metal ion in the membrane production. Since the membrane produced with 7:1 [COOH:Fe] mole ratio has a higher crosslinking density, its salt rejection performance is better than that of the membrane produced with 15:1 [COOH:Fe] mole ratio.

The highest NaCl salt rejection performance was observed in Fe (7:1) and Al (7:1) dry technique membranes with 64.2% and 64.1% salt rejections, respectively. Compared with the Fe and Al metal ion crosslinked membranes, the salt rejection performance results of the membranes crosslinked with other metal ions (Zn, Ca, and Co) were lower. The reason for that may be that Fe and Al had higher crosslinking density due to their higher metal ion valence (3+). It can be thought that the reason for the high standard deviation values in the Ca and Co metal ion crosslinked membranes is that the stability of the membranes was not very good and/or that the metal ion was lost over time.

- Wet technique membranes NaCl filtration performance:

2000 ppm of NaCl aqueous solution filtration test was applied to the metal (Fe) ion crosslinked membranes produced by the wet technique for the investigation of desalination performance. Table 4.10 shows the performance results of the wet technique membrane in the NaCl salt solution filtration and Figure 4.19 shows the comparison of the performance results of dry and wet technique membranes with Fe metal salt.

When the Fe (wet) technique membrane was compared to Fe (7:1) (dry) membrane and Fe (15:1) (dry) membrane, it can be seen that the salt rejection performance of it is lower. While Fe (7:1) (dry) membrane has a 64.2 % salt rejection value, Fe (wet) membrane has a 31.4% salt rejection value, which means that the salt rejection performance is halved. Additionally, the flux performance of the Fe (7:1) (dry) membrane is higher than that of the Fe (wet) membrane. The Fe (7:1) (dry) membrane has a flux value of 8.0 L/m²h while the flux value of Fe (wet) membrane was 6.2 L/m²h.

Table 4.10 Wet technique metal ion crosslinked ACP membrane 2000 ppm of NaCl aqueous solution filtration performance result

Membrane code	Casting Solution Composition	Metal ion solution	Metal ion bath temperature/ duration	Flux, J (L/m ² h)	Salt Rejection, R (%) 2000 ppm NaCl 15 bar filt.
Wet-1 Fe (wet)	ACP in MeOH 5% w/v	10% FeCl ₃ in water solution	24°C, overnight	6.2±1	31.4 ±13.5

2000 ppm NaCl deionized aqueous solution was prepared, and desalination performance tests were applied at room temperature in the dead-end filtration system under 15 bar pressure nitrogen gas.

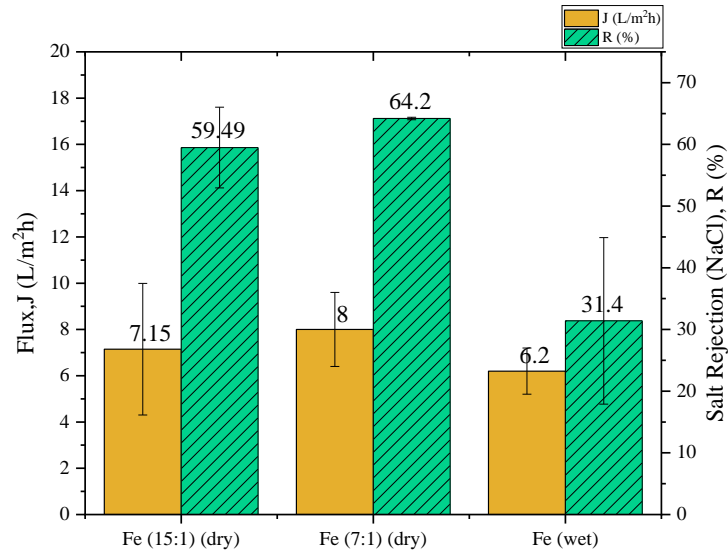


Figure 4.19 Wet technique metal ion crosslinked ACP membrane 2000 ppm of NaCl aqueous solution filtration performance result comparison with Fe (dry) technique membranes

- Dry technique membranes MgSO₄ filtration performance:

2000 ppm of MgSO₄ aqueous solution filtration test was applied to the ionically crosslinked ACP membranes produced by dry technique for the investigation of desalination performance. The performance results are given in Table 4.11.

Table 4.11 Dry technique metal ion crosslinked ACP membranes 2000 ppm of MgSO₄ aqueous solution filtration performance results

Membrane code	Solution composition	[COO H: Metal ion] mole ratio	Preparation	Membrane curing temperature and duration	Flux, J (L/m ² h)	Salt Rejection, R (%) 2000 ppm MgSO ₄ 15 bar filt.
Fe (15:1) (dry)	2 g ACP in 10 mL MeOH (20%) + 0.00307 mol Fe in 10 mL MeOH	15:1	2 mins wetting then squeezing	80°C, 2 hours then cooled in RT.	2.9 ± 0.1	93.4 ± 3.5
Fe (7:1) (dry)	2 g ACP in 10 mL MeOH (20%) + 0.00307 mol Fe in 10 mL MeOH	7:1	2 mins wetting then squeezing	80°C, 2 hours then cooled in RT.	4.6 ± 0.4	97.8 ± 1.3

Al (dry)	2 g ACP in 10 mL MeOH (20%) + 0.00307 mol Al in 10 mL MeOH	7:1	2 mins wetting then squeezing	80°C, 2 hours then cooled in RT.	6.5 ± 2.0	81.2 ± 6.5
Zn (dry)	2 g ACP in 10 mL MeOH (20%) + 0.00307 mol Zn in 10 mL MeOH	7:1	2 mins wetting then squeezing	80°C, 2 hours then cooled in RT.	6.58±0.19	59.01±2.05
Co (dry)	2 g ACP in 10 mL MeOH (20%) + 0.00307 mol Co in 10 mL MeOH	7:1	2 mins wetting then squeezing	80°C, 2 hours then cooled in RT.	26.2±9.9	29.7± 25.5
Ca (dry)	2 g ACP in 10 mL MeOH (20%) + 0.00307 mol Ca in 10 mL MeOH	7:1	2 mins wetting then squeezing	80°C, 2 hours then cooled in RT.	23.7 ± 3.6	25.19 ± 10.58

2000 ppm MgSO₄ salt of deionized water solution was prepared, and desalination performance tests were applied at room temperature in the dead-end filtration system under 15 bar pressure nitrogen gas.

As can be seen from Figure 4.20, the Fe (7:1) (dry) membrane has higher salt rejection and flux values than the Fe (15:1) (dry) membrane. The highest salt rejection performance in all dry technique membranes was obtained with Fe (7:1) (dry) membrane that has a 97.8 ± 1.3 % salt rejection which is quite enough for nanofiltration desalination applications. Al (7:1) (dry) membrane had relatively high salt rejection with 81.2 ± 6.5 %. While the salt rejection of Al (7:1) (dry) membrane was lower than the Fe (dry) membranes, the flux value of it was higher than the Fe (dry) membranes, which is an expected result. Zn, Ca, and Co (7:1) (dry) membranes' salt rejection performances were lower compared to Fe and Al dry technique membranes, which may be due to lower crosslinking density or lower stability in these membranes.

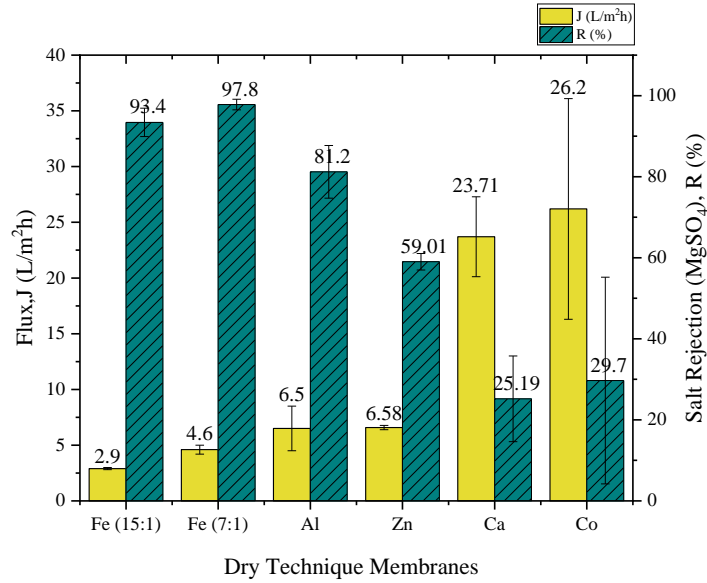


Figure 4.20 Dry technique metal ion crosslinked ACP membranes 2000 ppm of MgSO₄ aqueous solution filtration performance results

- Wet technique membranes MgSO₄ filtration performance:

The Fe wet technique membranes have higher salt rejection performance than the Zn, Co, and Ca dry technique membranes. This shows that the Fe (wet) membranes have a higher ionic crosslinking degree, and the stability of these membranes is better. When Fe dry technique and Fe wet technique membranes were compared, it was seen that Fe (wet) membrane had 71.3% salt rejection, while Fe (15:1) (dry) and Fe (7:1) (dry) membranes had 93.4% and 97.8% salt rejections, respectively as can be seen from Figure 4.21. This means that the dry technique provides better salt rejection performance than the wet technique. In the dry technique, the curing of membranes at 80°C for 2 hours was thought to provide better crosslinking.

Table 4.12 Wet technique metal ion crosslinked ACP membrane 2000 ppm of MgSO₄ aqueous solution filtration performance result

Membrane code	Casting Solution Composition	Metal ion solution	Metal ion bath temperature/duration	Flux, J (L/m ² h)	Salt Rejection, R (%) 2000 ppm MgSO ₄ 15 bar filt.
Wet-1 Fe (wet)	ACP in MeOH 5% w/v	10% FeCl ₃ in water solution	24°C, overnight	4.4±0.9	71.3±4.4

2000 ppm MgSO₄ salt of deionized water solution was prepared, and desalination performance tests were applied at room temperature in the dead-end filtration system under 15 bar pressure nitrogen gas.

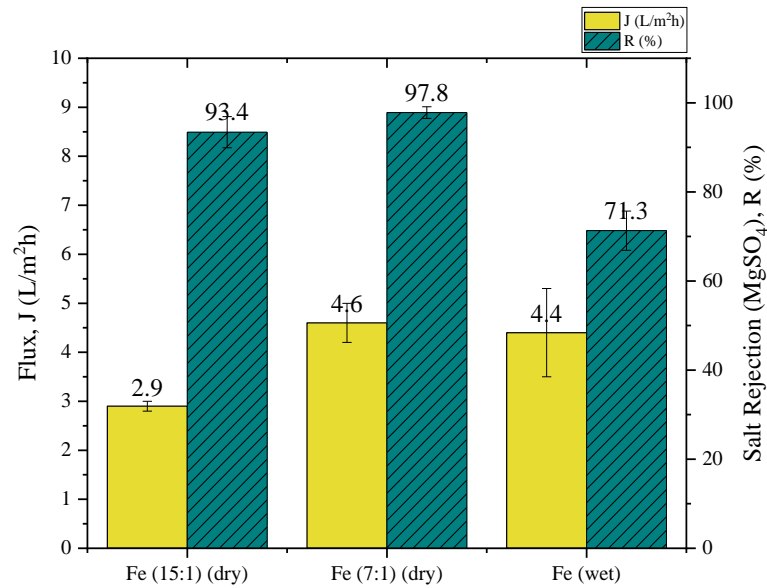
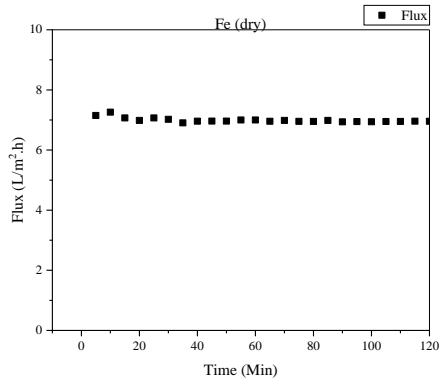


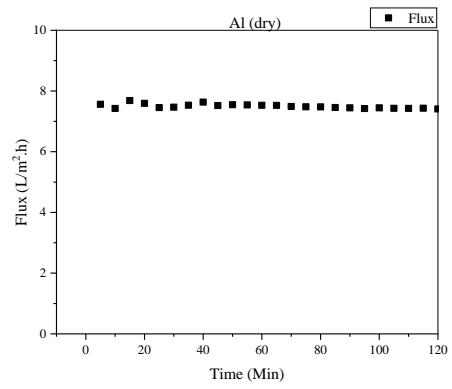
Figure 4.21 Wet technique metal ion crosslinked ACP membrane 2000 ppm of MgSO₄ aqueous solution filtration performance result comparison with Fe (dry) technique membranes

4.3.4.2. Stability analysis of the membranes

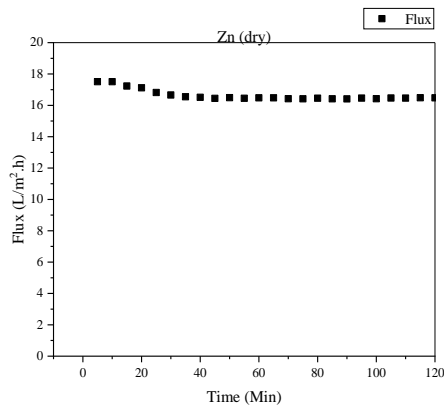
Dynamic stability of the ionically crosslinked ACP membranes was evaluated by the filtration test of 2000 ppm NaCl aqueous solution for 2 hours under 15 bar trans-membrane pressure. As summarized in Figure 4.22, it was observed that the flux values in the Fe (dry), Al (dry), and Zn (dry) and Fe (wet) membranes were quite stable over time. It was observed that the flux values in the Ca (dry) and Co (dry) membranes increased over time, so the membranes were not stable because the flux-time graph did not follow a linear trend. Instability in the flux is thought to be due to the loss of insufficiently cross-linked Ca and Co metal ions during filtration, resulting in an increase in the flux over time. The instability of the membranes caused changes in salt retention and flux values and resulted in high standard deviation values.



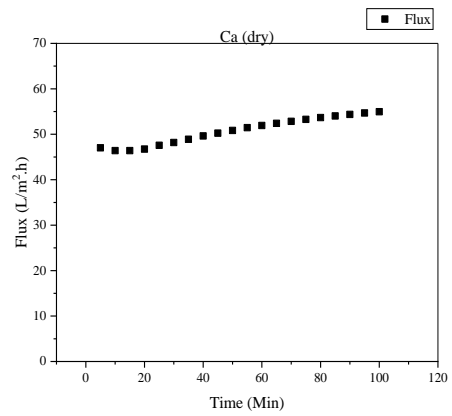
(a) Fe (dry)



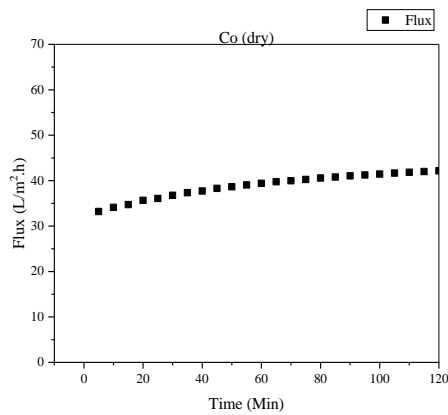
(b) Al (dry)



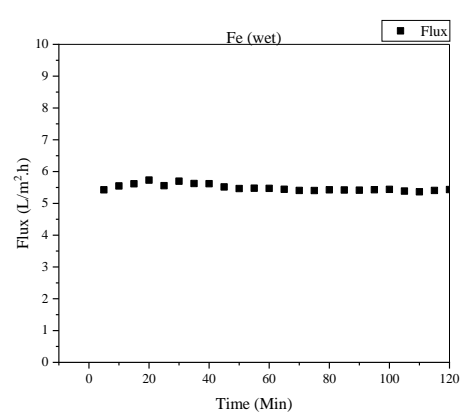
(c) Zn (dry)



(d) Ca (dry)



(e) Co (dry)



(f) Fe (wet)

Figure 4.22 2000 ppm NaCl solution filtration tests for stability analysis. (a) Fe (dry); (b) Al (dry); (c) Zn (dry); (d) Ca (dry); (e) Co (dry); (f) Fe (wet).

4.4. Conclusions

Carboxylic acid cyclopolymer (ACP) was synthesized by acid hydrolysis of *tert*-butyl cyclopolymer and its chemical structure was confirmed by NMR and FTIR spectroscopy

analysis. The degree of hydrolysis of the synthesized ACP was calculated from titration studies with 0.1N standard NaOH solution. The calculated hydrolysis degrees were consistent with the TGA curves of the synthesized acid cyclopolymers.

Ionically crosslinked acid cyclopolymer thin film composite membranes were produced with two techniques, dry and wet. Five different metal salts were used for ionic crosslinking: $\text{FeCl}_3 \cdot 6\text{H}_2\text{O}$, $\text{CoCl}_2 \cdot 6\text{H}_2\text{O}$, ZnCl_2 , $\text{AlCl}_3 \cdot 6\text{H}_2\text{O}$, and CaCl_2 . The desalination performance of the membranes was evaluated by filtering 2000 ppm NaCl or MgSO_4 aqueous solution through the membranes in a dead-end membrane filtration system at room temperature and under 15 bar pressure. It has been observed that the use of high-valence metal salts results in better crosslinking and desalination performance. The best membrane performance was observed in the membranes obtained with $\text{FeCl}_3 \cdot 6\text{H}_2\text{O}$ metal salt. In the production of ionically crosslinked thin film composite membranes using the dry method with Fe metal ion, two different [COOH: Metal ion] mol ratios (7:1 and 15:1) were used for the production. It was observed that the membrane produced with a 7:1 (COOH: Metal ion) mol ratio had a higher salt rejection value than the membrane produced with a 15:1 (COOH: Metal ion) mol ratio. It can be thought that the reason for this is the increasing crosslinking ratio with increasing metal ion concentration in the dry method.

The performance results of the metal ion-carboxylic acid cyclopolymer crosslinked thin film composite membranes obtained by the dry technique were better than the performance results of the membranes obtained by the wet technique. For example, the membranes obtained by the dry method with Fe metal salt have 97.8% MgSO_4 salt rejection, while the membranes obtained by the wet method with Fe metal salt have 71.3% MgSO_4 salt rejection. In the dry technique, other than Fe metal ion crosslinked membranes, Al metal ion crosslinked membranes also showed relatively high performance with 64.1% NaCl and 81.2% MgSO_4 salt rejection.

EDS analysis of the membranes showed that the membranes produced with Fe metal salt had the highest metal atomic percentages on the surface of the membrane with 44.08% in the dry technique and 48.7% in the wet technique. SEM analysis showed that a thin film was formed on the surface of PSF UF membranes and the pores on the surface of PSF UF membranes were closed with ionic cross-linking of ACP.

REFERENCES

- Abdelkareem, M. A., El Haj Assad, M., Sayed, E. T., & Soudan, B. (2018). Recent progress in the use of renewable energy sources to power water desalination plants. *Desalination*, 435(September 2017), 97–113. <https://doi.org/10.1016/j.desal.2017.11.018>
- Andrade, M. C., Pereira, J. C., de Almeida, N., Marques, P., Faria, M., & Gonçalves, M. C. (2021). Improving hydraulic permeability, mechanical properties, and chemical functionality of cellulose acetate-based membranes by co-polymerization with tetraethyl orthosilicate and 3-(aminopropyl)triethoxysilane. *Carbohydrate Polymers*, 261(November 2020). <https://doi.org/10.1016/j.carbpol.2021.117813>
- Andrews, D. H. (1959). The Infra-red Spectra of Complex Molecules. In *Journal of the American Chemical Society* (Vol. 81, Issue 9). <https://doi.org/10.1021/ja01518a076>
- Anis, S. F., Hashaikeh, R., & Hilal, N. (2019). Microfiltration membrane processes: A review of research trends over the past decade. *Journal of Water Process Engineering*, 32(June). <https://doi.org/10.1016/j.jwpe.2019.100941>
- Arthanareeswaran, G., Thanikaivelan, P., Raguime, J. A., Raajenthiren, M., & Mohan, D. (2007). Metal ion separation and protein removal from aqueous solutions using modified cellulose acetate membranes: Role of polymeric additives. *Separation and Purification Technology*, 55(1), 8–15. <https://doi.org/10.1016/j.seppur.2006.10.014>
- Arthanareeswaran, G., Thanikaivelan, P., Srinivasn, K., Mohan, D., & Rajendran, M. (2004). Synthesis, characterization and thermal studies on cellulose acetate membranes with additive. *European Polymer Journal*, 40(9), 2153–2159. <https://doi.org/10.1016/J.EURPOLYMJ.2004.04.024>
- Ashfaq, M. Y., Al-Ghouti, M. A., & Zouari, N. (2020). Functionalization of reverse osmosis membrane with graphene oxide and polyacrylic acid to control biofouling and mineral scaling. *Science of the Total Environment*, 736, 139500. <https://doi.org/10.1016/j.scitotenv.2020.139500>
- Ayyavoo, J., Nguyen, T. P. N., Jun, B. M., Kim, I. C., & Kwon, Y. N. (2016). Protection of polymeric membranes with antifouling surfacing via surface modifications. *Colloids and Surfaces A: Physicochemical and Engineering Aspects*, 506, 190–201. <https://doi.org/10.1016/j.colsurfa.2016.06.026>

- Barud, H. S., Ribeiro, C. A., Crespi, M. S., Martines, M. A. U., Dexpert-Ghys, J., Marques, R. F. C., Messaddeq, Y., & Ribeiro, S. J. L. (2007). Thermal characterization of bacterial cellulose-phosphate composite membranes. *Journal of Thermal Analysis and Calorimetry*, 87(3), 815–818. <https://doi.org/10.1007/s10973-006-8170-5>
- Bavisotto, R., Rana, R., Hopper, N., Hou, K., & Tysoe, W. T. (2021). Influence of the terminal group on the thermal decomposition reactions of carboxylic acids on copper: Nature of the carbonaceous film. *Physical Chemistry Chemical Physics*, 23(32), 17663–17671. <https://doi.org/10.1039/d1cp02078a>
- Bolto, B., Tran, T., Hoang, M., & Xie, Z. (2009). Crosslinked poly(vinyl alcohol) membranes. *Progress in Polymer Science (Oxford)*, 34(9), 969–981. <https://doi.org/10.1016/j.progpolymsci.2009.05.003>
- Cadotte, J. E., Petersen, R. J., Larson, R. E., & Erickson, E. E. (1980). A new thin-film composite seawater reverse osmosis membrane. *Desalination*, 32(C), 25–31. [https://doi.org/10.1016/S0011-9164\(00\)86003-8](https://doi.org/10.1016/S0011-9164(00)86003-8)
- Cao, S., Shi, Y., & Chen, G. (2000). Influence of acetylation degree of cellulose acetate on pervaporation properties for MeOH/MTBE mixture. *Journal of Membrane Science*, 165(1), 89–97. [https://doi.org/10.1016/S0376-7388\(99\)00222-7](https://doi.org/10.1016/S0376-7388(99)00222-7)
- Chen, L., Tian, Y., Cao, C. qing, Zhang, J., & Li, Z. neng. (2012). Interaction energy evaluation of soluble microbial products (SMP) on different membrane surfaces: Role of the reconstructed membrane topology. *Water Research*, 46(8), 2693–2704. <https://doi.org/10.1016/j.watres.2012.02.030>
- Choi, H. G., Yoon, S. H., Son, M., Celik, E., Park, H., & Choi, H. (2016). Efficacy of synthesis conditions on functionalized carbon nanotube blended cellulose acetate membrane for desalination. *Desalination and Water Treatment*, 57(16), 7545–7554. <https://doi.org/10.1080/19443994.2015.1025582>
- Drioli, E., & Giorno, L. (2016). Encyclopedia of Membranes. In *Springer Reference*. Springer Berlin Heidelberg. https://doi.org/10.1007/978-3-662-44324-8_1789
- Duarte, A. P., & Bordado, J. C. (2016). Smart composite reverse-osmosis membranes for energy generation and water desalination processes. In *Smart Composite Coatings and Membranes: Transport, Structural, Environmental and Energy Applications*. Elsevier Ltd. <https://doi.org/10.1016/B978-1-78242-283-9.00012-9>

- Duarte, A. P., Cidade, M. T., & Bordado, J. C. (2006). *Cellulose Acetate Reverse Osmosis Membranes: Optimization of the Composition*. <https://doi.org/10.1002/app.23237>
- El-Dessouky, H. T., & Ettouney, H. M. (2002). *Fundamentals of Salt Water Desalination*. Elsevier.
- El-Gendi, A., Abdallah, H., Amin, A., & Amin, S. K. (2017). Investigation of polyvinylchloride and cellulose acetate blend membranes for desalination. *Journal of Molecular Structure*, *1146*, 14–22. <https://doi.org/10.1016/j.molstruc.2017.05.122>
- Erkoc, S., & Acar, A. E. (2008). Controlled/living cyclopolymerization of tert-butyl α -(hydroxymethyl) acrylate ether dimer via reversible addition fragmentation chain transfer polymerization. *Macromolecules*, *41*(23), 9019–9024. <https://doi.org/10.1021/ma801492a>
- Erkoc, S., Mathias, L. J., & Ersin Acar, A. (2006). Cyclopolymerization of tert-Butyl α -(Hydroxymethyl) Acrylate (TBHMA) ether dimer via Atom Transfer Radical Polymerization (ATRP). *Macromolecules*, *39*(26), 8936–8942. <https://doi.org/10.1021/ma061876e>
- Esmaeilion, F. (2020). Hybrid renewable energy systems for desalination. In *Applied Water Science* (Vol. 10, Issue 3). Springer International Publishing. <https://doi.org/10.1007/s13201-020-1168-5>
- Everaerts, A. I., & Clemens, L. M. (2002). Pressure sensitive adhesives. In *Adhesion Science and Engineering* (pp. 465–534). Elsevier. <https://doi.org/10.1016/B978-044451140-9/50011-1>
- Fikar, M. (2014). Modelling, control, and optimisation of membrane processes. *Proceedings of the 2014 15th International Carpathian Control Conference, ICCC 2014, March*, 109–114. <https://doi.org/10.1109/CarpathianCC.2014.6843579>
- Fritzmann, C., Löwenberg, J., Wintgens, T., & Melin, T. (2007). State-of-the-art of reverse osmosis desalination. *Desalination*, *216*(1–3), 1–76. <https://doi.org/10.1016/j.desal.2006.12.009>
- Ghosh, A. K., & Sirkar, K. K. (1979). Low-pressure reverse osmosis desalination with improved cellulose acetate membranes. *Journal of Applied Polymer Science*, *23*(5), 1291–1307. <https://doi.org/10.1002/app.1979.070230503>

- Glater, J. (1998). The early history of reverse osmosis membrane development. *Desalination*, 117(1–3), 297–309. [https://doi.org/10.1016/S0011-9164\(98\)00122-2](https://doi.org/10.1016/S0011-9164(98)00122-2)
- Greenlee, L. F., Lawler, D. F., Freeman, B. D., Marrot, B., & Moulin, P. (2009). Reverse osmosis desalination: Water sources, technology, and today's challenges. *Water Research*, 43(9), 2317–2348. <https://doi.org/10.1016/j.watres.2009.03.010>
- Guillen, G. R., Pan, Y., Li, M., & Hoek, E. M. V. (2011). Preparation and characterization of membranes formed by nonsolvent induced phase separation: A review. *Industrial and Engineering Chemistry Research*, 50(7), 3798–3817. <https://doi.org/10.1021/ie101928r>
- Habert, A. C., Burns, C. M., & Huang, R. Y. M. (1979). Ionically crosslinked poly(acrylic acid) membranes. II. Dry technique. *Journal of Applied Polymer Science*, 24(3), 801–809. <https://doi.org/10.1002/app.1979.070240316>
- Habert, A. C., Huang, R. Y. M., & Burns, C. M. (1979). Ionically crosslinked poly(acrylic acid) membranes. I. Wet technique. *Journal of Applied Polymer Science*, 24(2), 489–501. <https://doi.org/10.1002/app.1979.070240216>
- Hailemariam, R. H., Woo, Y. C., Damtie, M. M., Kim, B. C., Park, K. D., & Choi, J. S. (2020). Reverse osmosis membrane fabrication and modification technologies and future trends: A review. *Advances in Colloid and Interface Science*, 276, 102100. <https://doi.org/10.1016/j.cis.2019.102100>
- Han, B., Zhang, D., Shao, Z., Kong, L., & Lv, S. (2013). Preparation and characterization of cellulose acetate/carboxymethyl cellulose acetate blend ultrafiltration membranes. *Desalination*, 311, 80–89. <https://doi.org/10.1016/j.desal.2012.11.002>
- Huang, R. Y. M., Gao, C. J., & Kim, J. J. (1983). Ionically crosslinked poly(acrylic acid) membranes. IV. Composite reverse osmosis membranes. *Journal of Applied Polymer Science*, 28(10), 3063–3073. <https://doi.org/10.1002/app.1983.070281006>
- Hunger, K., Schmeling, N., Jeazet, H. B. T., Janiak, C., Staudt, C., & Kleinermanns, K. (2012). Investigation of cross-linked and additive containing polymer materials for membranes with improved performance in pervaporation and gas separation. *Membranes*, 2(4), 727–763. <https://doi.org/10.3390/membranes2040727>
- Idarraga-Mora, J. A., Childress, A. S., Friedel, P. S., Ladner, D. A., Rao, A. M., & Husson,

- S. M. (2018). Role of nanocomposite support stiffness on TFC membrane water permeance. *Membranes*, 8(4), 3–5. <https://doi.org/10.3390/membranes8040111>
- Jazini, F., Karimi, M., & Azari, S. (2021). Tuning the pore features of cellulose acetate/cellulose triacetate membranes via post-casting solvent treatment for forward osmosis. *Carbohydrate Polymers*, 255(October 2020), 117348. <https://doi.org/10.1016/j.carbpol.2020.117348>
- Kahrs, C., & Schwellenbach, J. (2020). Membrane formation via non-solvent induced phase separation using sustainable solvents: A comparative study. *Polymer*, 186(November 2019), 122071. <https://doi.org/10.1016/j.polymer.2019.122071>
- Kim, J. H., & Lee, K. H. (1998). Effect of PEG additive on membrane formation by phase inversion. *Journal of Membrane Science*, 138(2), 153–163. [https://doi.org/10.1016/S0376-7388\(97\)00224-X](https://doi.org/10.1016/S0376-7388(97)00224-X)
- Köse, D. A., & Necefoğlu, H. (2008). Synthesis and characterization of bis(nicotinamide) m-hydroxybenzoate complexes of Co(II), Ni(II), Cu(II) and Zn(II). *Journal of Thermal Analysis and Calorimetry*, 93(2), 509–514. <https://doi.org/10.1007/s10973-007-8712-5>
- Koyuncu, I. (2018). Su/Atıksu Arıtılması ve Geri Kazanılmasında Membran Teknolojileri ve Uygulamaları cilt1. *Tüçev*, 588.
- Kumari, A., Sarkhel, G., & Choudhury, A. (2013). Effect of polyvinylpyrrolidone on separation performance of cellulose acetate-polysulfone blend membranes. *Journal of Macromolecular Science, Part A: Pure and Applied Chemistry*, 50(7), 692–702. <https://doi.org/10.1080/10601325.2013.792200>
- Kunst, R. (1970). Performance membranes desalination. *Water*, 8(I 970).
- Lalia, B. S., Kochkodan, V., Hashaikeh, R., & Hilal, N. (2013). A review on membrane fabrication: Structure, properties and performance relationship. *Desalination*, 326, 77–95. <https://doi.org/10.1016/j.desal.2013.06.016>
- Lau, W. J., Ismail, A. F., Misdan, N., & Kassim, M. A. (2012). A recent progress in thin film composite membrane: A review. *Desalination*, 287, 190–199. <https://doi.org/10.1016/j.desal.2011.04.004>
- Lee, K. P., Arnot, T. C., & Mattia, D. (2011). A review of reverse osmosis membrane

- materials for desalination-Development to date and future potential. *Journal of Membrane Science*, 370(1–2), 1–22. <https://doi.org/10.1016/j.memsci.2010.12.036>
- Liu, S., Hu, L. F., Zhang, W. C., & Ma, H. Y. (2019). Cellulose Acetate Reverse Osmosis Membranes for Desalination: A Short Review. *Non-Metallic Material Science*, 1(2), 14–24. <https://doi.org/10.30564/omms.v1i2.1143>
- Loeb, S., & Sourirajan, S. (1963). Sea Water Demineralization by Mean of an Osmotic Membrane. *Soil Science Society of America Journal*, 27(2), 117–132. <https://doi.org/10.2136/sssaj1963.03615995002700020008x>
- Lonsdale, H. K. (1982). The growth of membrane technology. *Journal of Membrane Science*, 10(2–3), 81–181. [https://doi.org/10.1016/S0376-7388\(00\)81408-8](https://doi.org/10.1016/S0376-7388(00)81408-8)
- Lu, X., & Elimelech, M. (2021). Fabrication of desalination membranes by interfacial polymerization: History, current efforts, and future directions. *Chemical Society Reviews*, 50(11), 6290–6307. <https://doi.org/10.1039/d0cs00502a>
- Luo, X., Wang, Z., Wu, S., Fang, W., & Jin, J. (2021). Metal ion cross-linked nanoporous polymeric membranes with improved organic solvent resistance for molecular separation. *Journal of Membrane Science*, 621(July 2020), 119002. <https://doi.org/10.1016/j.memsci.2020.119002>
- Macedonio, F., & Drioli, E. (2017). *Sustainable Membrane Technology for Water and Wastewater Treatment*. Springer. https://doi.org/10.1007/978-981-10-5623-9_8
- Maheswari, P., Barghava, P., & Mohan, D. (2013). Preparation, morphology, hydrophilicity and performance of poly (ether-ether-sulfone) incorporated cellulose acetate ultrafiltration membranes. *Journal of Polymer Research*, 20(2), 5550–5564. <https://doi.org/10.1007/s10965-013-0074-z>
- Mathias, L. J., Michael Warren, R., & Huang, S. (1991). tert-Butyl α -(Hydroxymethyl)acrylate and Its Ether Dimer: Multifunctional Monomers Giving Polymers with Easily Cleaved Ester Groups. *Macromolecules*, 24(8), 2036–2042. <https://doi.org/10.1021/ma00008a050>
- Mohammed Ali, A. S., Fadl, E. A., Soliman, M. M., & Kandil, S. H. (2020). Optimization of the evaporation step in cellulose acetate membranes preparation by dry–wet phase inversion technique for water desalination applications. *Desalination and Water*

- Treatment*, 174, 63–70. <https://doi.org/10.5004/dwt.2020.24862>
- Mohanty, K., & Purkait, M. K. (2011). Membrane technologies and applications. In *Membrane Technologies and Applications*. <https://doi.org/10.1002/0470020393>
- Nasser, R. (2020). Separation processes with (bio)membranes: Overview and new phenomenological classification. In *Biopolymer Membranes and Films*. Elsevier Inc. <https://doi.org/10.1016/b978-0-12-818134-8.00005-5>
- Nguyen, T. P. N., Yun, E. T., Kim, I. C., & Kwon, Y. N. (2013). Preparation of cellulose triacetate/cellulose acetate (CTA/CA)-based membranes for forward osmosis. *Journal of Membrane Science*, 433, 49–59. <https://doi.org/10.1016/j.memsci.2013.01.027>
- Nicolaisen, B. (2003). Developments in membrane technology for water treatment. *Desalination*, 153(1–3), 355–360. [https://doi.org/10.1016/S0011-9164\(02\)01127-X](https://doi.org/10.1016/S0011-9164(02)01127-X)
- Pageau, L., & Sourirajan, S. (1972). Improvement of porous cellulose acetate reverse osmosis membranes by change of casting conditions. *Journal of Applied Polymer Science*, 16(12), 3185–3206. <https://doi.org/10.1002/app.1972.070161212>
- Peter, S., Hese, N., & Stefan, R. (1976). Phenol-selective, highly resistant RO-membranes made from PVA for the purification of toxic industrial wastes. *Desalination*, 19(1–3), 161–167. [https://doi.org/10.1016/S0011-9164\(00\)88026-1](https://doi.org/10.1016/S0011-9164(00)88026-1)
- Peters, T. (2010). Membrane technology for water treatment. *Chemical Engineering and Technology*, 33(8), 1233–1240. <https://doi.org/10.1002/ceat.201000139>
- Qasim, M., Badrelzaman, M., Darwish, N. N., Darwish, N. A., & Hilal, N. (2019). Reverse osmosis desalination: A state-of-the-art review. *Desalination*, 459(December 2018), 59–104. <https://doi.org/10.1016/j.desal.2019.02.008>
- Reid, C. E., & Breton, E. J. (1959). Water and ion flow across cellulosic membranes. *Journal of Applied Polymer Science*, 1(2), 133–143. <https://doi.org/10.1002/app.1959.070010202>
- Ribba, L. G., Cimadoro, J. D., D'Accorso, N. B., & Goyanes, S. N. (2017). Removal of Pollutants Using Electrospun Nanofiber Membranes. In *Industrial Applications of Renewable Biomass Products* (Issue August, pp. 301–324). Springer International Publishing. https://doi.org/10.1007/978-3-319-61288-1_12

- Rikkou-Kalourkoti, M., Kassi, E., & Patrickios, C. S. (2012a). Synthesis and characterization of rigid functional anionic polyelectrolytes: Block copolymers and star homopolymers. *Journal of Polymer Science, Part A: Polymer Chemistry*, 50(4), 665–674. <https://doi.org/10.1002/pola.25076>
- Rikkou-Kalourkoti, M., Kassi, E., & Patrickios, C. S. (2012b). Synthesis and characterization of rigid functional anionic polyelectrolytes: Block copolymers and star homopolymers. *Journal of Polymer Science Part A: Polymer Chemistry*, 50(4), 665–674. <https://doi.org/10.1002/pola.25076>
- Sagle, A., & Freeman, B. (2004). Fundamentals of membranes for water treatment. *The Future of Desalination in Texas*, 1–17. http://www.twdb.state.tx.us/publications/reports/numbered_reports/doc/R363/C6.pdf
- Salt Water and Freshwater Distribution on Earth*. (n.d.). <https://www.pbslearningmedia.org/resource/buac17-35-sci-ess-waterdistribute/saltwater-and-freshwater-distribution-on-earth/>
- Selatile, M. K., Ray, S. S., Ojijo, V., & Sadiku, R. (2018). Recent developments in polymeric electrospun nanofibrous membranes for seawater desalination. *RSC Advances*, 8(66), 37915–37938. <https://doi.org/10.1039/C8RA07489E>
- Shenvi, S. S., Isloor, A. M., & Ismail, A. F. (2015). A review on RO membrane technology: Developments and challenges. *Desalination*, 368, 10–26. <https://doi.org/10.1016/j.desal.2014.12.042>
- Shieh, J. J., Chung, T. S., Wang, R., Srinivasan, M. P., & Paul, D. R. (2001). Gas separation performance of poly(4-vinylpyridine)/polyetherimide composite hollow fibers. *Journal of Membrane Science*, 182(1–2), 111–123. [https://doi.org/10.1016/S0376-7388\(00\)00560-3](https://doi.org/10.1016/S0376-7388(00)00560-3)
- Strathmann, H., Scheible, P., & Baker, R. W. (1971). A rationale for the preparation of Loeb-Sourirajan-type cellulose acetate membranes. *Journal of Applied Polymer Science*, 15(4), 811–828. <https://doi.org/10.1002/app.1971.070150404>
- Tomczak, W., & Gryta, M. (2022). The Application of Cellulose Acetate Membranes for Separation of Fermentation Broths by the Reverse Osmosis: A Feasibility Study. *International Journal of Molecular Sciences*, 23(19). <https://doi.org/10.3390/ijms231911738>

- Tsuda, T., & Mathias, L. J. (1994). Cyclopolymerization of ether dimers of α -(hydroxymethyl)acrylic acid and its alkyl esters: substituent effect on cyclization efficiency and microstructures. *Polymer*, 35(15), 3317–3328. [https://doi.org/10.1016/0032-3861\(94\)90141-4](https://doi.org/10.1016/0032-3861(94)90141-4)
- UNESCO. (2019). *The United Nations World Water Development Report 2019: Leaving No One Behind*.
- Vatanpour, V., Pasaoglu, M. E., Barzegar, H., Teber, O. O., Kaya, R., Bastug, M., Khataee, A., & Koyuncu, I. (2022). Cellulose acetate in fabrication of polymeric membranes: A review. *Chemosphere*, 295(January). <https://doi.org/10.1016/j.chemosphere.2022.133914>
- Wang, Lawrence K.; Chen, Jiaping Paul; Hung, Yung-Tse; Shammam, N. K. (2011). Membrane and Desalination Technologies. In L. K. Wang, J. P. Chen, Y.-T. Hung, & N. K. Shammam (Eds.), *Membrane and Desalination Technologies*. Humana Press. <https://doi.org/10.1007/978-1-59745-278-6>
- Wang, J., Song, H., Ren, L., Talukder, M. E., Chen, S., & Shao, J. (2022). Study on the preparation of cellulose acetate separation membrane and new adjusting method of pore size. *Membranes*, 12(1). <https://doi.org/10.3390/membranes12010009>
- Wu, S., Qin, X., & Li, M. (2014). The structure and properties of cellulose acetate materials: A comparative study on electrospun membranes and casted films. *Journal of Industrial Textiles*, 44(1), 85–98. <https://doi.org/10.1177/1528083713477443>
- Xu, J., & Xu, Z. L. (2002). Poly(vinyl chloride) (PVC) hollow fiber ultrafiltration membranes prepared from PVC/additives/solvent. *Journal of Membrane Science*, 208(1–2), 203–212. [https://doi.org/10.1016/S0376-7388\(02\)00261-2](https://doi.org/10.1016/S0376-7388(02)00261-2)
- Yang, Z., Zhou, Y., Feng, Z., Rui, X., Zhang, T., & Zhang, Z. (2019). A review on reverse osmosis and nanofiltration membranes for water purification. *Polymers*, 11(8). <https://doi.org/10.3390/polym11081252>
- Zhao, S., Liao, Z., Fane, A., Li, J., Tang, C., Zheng, C., Lin, J., & Kong, L. (2021). Engineering antifouling reverse osmosis membranes: A review. *Desalination*, 499(October 2020), 114857. <https://doi.org/10.1016/j.desal.2020.114857>
- Zhou, J., Chen, J., He, M., & Yao, J. (2016). Cellulose acetate ultrafiltration membranes

reinforced by cellulose nanocrystals: Preparation and characterization. *Journal of Applied Polymer Science*, 133(39), 1–7. <https://doi.org/10.1002/app.43946>